

Migration of plasticisers from PVC and other polymers

UNDERSTANDING OF ADDITIVE
MIGRATION AND DIFFUSION IN
POLYVINYL CHLORIDE (PVC) AND POLYOLEFINS



RASMUS LUNDSGAARD
OCTOBER 15, 2010

Migration of plasticisers from PVC and other polymers

PROJECT PERIOD: 1/7-2007 - 30/9-2010

PHD THESIS

SUPERVISORS: GEORGIOS M. KONTOGEORGIS (CERE, DTU CHEMICAL ENGINEERING),
BJARNE NIELSEN (DANISCO A/S)
& ULRIK AUNSKJÆR (DANISCO A/S)

CENTER FOR ENERGY RESSOURCES ENGINEERING (CERE)
DEPARTMENT OF CHEMICAL AND BIOCHEMICAL ENGINEERING
TECHNICAL UNIVERSITY OF DENMARK

RASMUS LUNDSGAARD

 **DTU Chemical Engineering**
Department of Chemical and Biochemical Engineering

 **CERE**
Center for Energy Resources Engineering

 **DANISCO**
First you add knowledge...

Preface

This thesis is submitted in partial fulfillment of the requirements to obtain the Doctor of Philosophy degree at the Technical University of Denmark (DTU). The work has been carried out at the CERE-DTU (Center for Energy Resources Engineering, formerly known as IVC-SEP) at the Department of Chemical and Biochemical Engineering, DTU, under the supervision of Professors Georgios M. Kontogeorgis from CERE-DTU and Bjarne Nielsen and Ulrik Aunskjær, both from Danisco A/S.

The project was financially supported by 1/3 from the Technical University of Denmark, 1/3 from the Graduate School in Chemical Engineering and finally 1/3 by Danisco A/S. The author gratefully acknowledges their support.

I would like to express my deepest gratitude to my main supervisor Prof. Georgios M. Kontogeorgis for his endless support and encouragement over the last four years since he accepted to be my supervisor on my master project. He is truly my scientific adviser and mentor, and has always shown support and genuine interest in my project. Also I am deeply grateful to Prof. Georgios M. Kontogeorgis for introducing me to the vast network of great Greek scientists in the international community.

One of these is Prof. Ioannis G. Economou of the National Center for Scientific Research "Demokritos" in Athena, Greece, who soon also became an important adviser to me. I am deeply grateful to him for always finding time to discuss and advise me in the problems I encountered during my work on molecular simulations. Moreover I would very much like to thank him and his co-workers (Niki, Zoe, George and Eleni) at N.C.S.R. Demokritos to find space and time to have me visiting the research center in Athens. My two long visits at the research center in Athens have given me an opportunity to learn the greek way of living, and Athens will for always be my second home.

I would also like to thank Nuno Garrido from the Chemical Engineering Department at University of Porto, Portugal, for our sharing of knowledge and code for molecular simulation with the GROMACS software, and Søren Enemark from Department of Chemical and Biomolecular Engineering at the National University of Singapore sharing of code and testing of the developed hydrogen bond cluster counting code.

I would also like to express my gratitude to Danisco A/S and especially Bjarne Nielsen, Ulrik

Aunskjær, Torkil F. Jensen and Jørgen K. Kristiansen for finding time for me in their always busy schedule at Danisco. It was really a valuable experience to me to become a full member of the development team at Danisco on the new antistatic additive project, and through this project learn how my knowledge through the PhD project directly could get to use.

I am also deeply honored that Dr. Otto G. Piringer has taken time to discuss with me on the migration of plasticisers in highly plasticised PVC, and moreover that he has shown personal interest in this project and its progress.

To the colleagues at KT and especially in the CERE group I would like to express my gratitude to the many joyful moments I have shared with you over the last four years. I would especially like to thank Ane S. Avlund for our many discussions on our projects and of course for her company during our professional trips together. Also I am deeply grateful to the guidance and help by Philip L. Fosbøl on Matlab programming, and our many discussions on understanding of the acetic acid data and the development of the antistatic additive migration model.

Lastly I would like to thank my family and friends for nodding and smiling understandingly when I explained you in many details on the complex problems in this project I was trying to solve, and for moments together with reminding me that there are other things in life than molecular dynamics and migration modeling.

Rasmus Lundsgaard
Søborg, Denmark
October 15, 2010

I would like to devote this thesis to my father, who has always encouraged me to be curious and question the world around me. You were always willing to answer my numerous questions, and always in the most truthful way...

Summary

The main purpose of this thesis is to investigate, from a modeling point of view, the migration of GRINDSTED® SOFT-N-SAFE (SNS) and other plasticisers from polyvinyl chloride (PVC) and polyolefin food package materials and into foodstuff (specifically the four food simulants set by EU legislation). In this work it is shown how diffusion coefficients can be obtained by regression of experimental migration data plotted as the square root of time. This was done from plasticiser migration data of GRINDSTED® SOFT-N-SAFE, GRINDSTED® ACETEM 95 CO (Acetem) and Epoxidised Soybean Oil (ESBO) migrating from Polyvinyl Chloride (PVC) and into iso-octane at 20°C, 40°C and 60°C. Using these experimentally obtained diffusion coefficients the migration was modeled using two analytical models with relatively good accuracy. The diffusion coefficient in highly plasticised PVC should, however, not be considered uniform over the whole polymer layer when the migrant is the plasticiser itself.

It was attempted to predict the diffusion coefficient of SNS in highly plasticised PVC from pure component data alone, using the model by Vrentas and Vrentas, which is based on the free volume theory. The results, however, showed that the model under-predicts the experimental diffusion coefficient values. These experimentally obtained values should be regarded as average diffusion coefficient values of the whole polymer and lower than the diffusion coefficient of the fully plasticised PVC. Instead of using this elaborated complex model, it was decided to use the much simpler semi-empirical model by Piringer. Using this simple model, with a polymer-specific parameter obtained from ESBO migration data alone, it was possible to estimate diffusion coefficients for Acetem and SNS. The results were close to the experimentally obtained diffusion coefficients at 20°C, except at higher temperatures.

Using the finite element mesh method in Matlab and COMSOL environments the migration was modeled with a diffusion coefficient able to change with local plasticiser concentration. Three different models for this plasticiser concentration dependence of the diffusion coefficient were evaluated. All models performed similarly, with better predicting ability compared to modeling with a static diffusion coefficient.

This numerical solution by the finite element mesh method has also been used to model the migration of an antistatic additive to the surface of Low Density Polyethylene (LDPE) and Poly Propylene (PP). It was possible with a newly developed model to estimate the migration with very high accuracy. This result leads to the somewhat surprising conclusion that the controlling step in the migration of the additive to the surface was not the migration within the polymer bulk. Migration is probably due to a temperature dependent partitioning of the additive between the polymer bulk and the surface layer.

The possibility of using molecular dynamics calculations to estimate the partition coefficients of additives between polymers and foodstuff was also investigated. The development of the methodology was done against experimental data of a system composed of a hydrophilic or a hydrophobic additive between LDPE and different ethanol/water mixtures. The calculated partition coefficients of different additives between LDPE and ethanol/water were correlated with high accuracy against experimental data. To extend the methodology to acetic acid

systems (food simulant B), it was chosen firstly to investigate the predictive capabilities of the TraPPE, OPLS-AA and CHARMM27 force fields for pure acetic acid and acetic acid / water mixtures. None of the three force fields was able to predict satisfactorily the density of acetic acid / water mixtures. Only the CHARMM27 force field was able to predict the local density maxima of the system.

A hydrogen bond connectivity counting code was developed for investigating the clustering of acetic acid. Statistics using the cluster counting code showed that the acetic acid molecules in the liquid phase mostly formed chain-like structures, with chains of 2 and 3 molecules in size to be the most predominant ones. Furthermore, the ability of the force fields to predict the enthalpy of vaporization was tested. All three force fields over-predict this property, resulting to a value about twice the experimental one ($\approx 50\text{kJ/mol}$ compared to 23.7kJ/mol). The gas phase consisted almost entirely of monomers, where experimental Pressure-Volume data of the gas phase at 298K and 1 bar give a dimer fraction of around 80-90%. This dimer fraction in the gas phase was elevated using higher atomic charges as shown by Chocholousova et al.[J. Chocholousova, J. Vacek, and P. Hobza; J. Phys. Chem. A; 107, 17, (2003), 3086-3092], but the calculated enthalpy of vaporization was still almost twice as high. It was shown that most literature data listing a value of $\approx 50\text{kJ/mol}$ originate from the work by Konicek and Wadsö[J. Konicek and I. Wadsö; Acta Chem. Scand.; 24, 7, (1970), 2612-2616] from 1970. In the same work is explained how the enthalpy of vaporization of acetic acid theoretically can be seen as consisting of two contributions, the "pure" enthalpy of vaporization of the monomer and the enthalpy of dissociation. It is important that this theoretically-derived "pure" enthalpy of vaporization (which is $\approx 50\text{kJ/mol}$) is not confused with the experimentally obtained enthalpy of vaporization (23.7kJ/mol). The OPLS-AA force field is parameterized towards the theoretical "pure" enthalpy of vaporization in a correct way, by only calculating the energy difference for the single acetic acid monomer molecule between the two phases. However simulations in this work have shown that these parameters do not allow the force field to predict the gas phase dimer fraction accurately.

Overall from this work it can be concluded that a full prediction of migration in polyolefins can be obtained using the numerical solution by finite element mesh together with diffusion coefficients obtained from the Piringer model and partition coefficient by molecular dynamics. For the complex system of migration of plasticisers in highly plasticised PVC, a full predictive model was not obtained. A model was, however, developed for this system that predicts satisfactorily with only 1 or 2 adjustable parameters to plasticiser migration from PVC.

Resumé

(Summary in Danish)

Hovedformålet med denne afhandling er at undersøge, fra et modelleringssynspunkt, migrationen af GRINDSTED[®] SOFT-N-SAFE (SNS) og andre blødgørere fra fødevareemballager af polyvinylchlorid (PVC) og polyolefiner og ind i fødevarer (specielt de fire fødevarer simulanter fastsat i EU's lovgivning). I dette arbejde er det vist, hvordan diffusionskoefficienter kan fås ved regression af eksperimentelle migration data plottet som funktion af kvadratroden af tid. Dette blev gjort i dette arbejde med data fra migrationen af blødgørerne SNS GRINDSTED[®] ACETEM 95 CO (Acetem) og Epoxideret sojaolie (ESBO) fra polyvinylchlorid (PVC) og ud i iso-oktan ved 20°C, 40°C og 60°C. Ved hjælp af disse eksperimentelt opnåede diffusionskoefficienter, blev migrationen modelleret ved hjælp af to analytiske modeller med relativt god nøjagtighed. Diffusionskoefficienten i blødgjort PVC bør dog ikke betragtes som ensartet over hele polymeren hvis migrationen netop er af blødgøreren selv.

Det blev forsøgt at estimere diffusionskoefficienten af SNS i blødgjort PVC fra ren komponent data alene, ud fra modellen af Vrentas og Vrentas, som er baseret på den frie volume teori. Resultaterne viste imidlertid, at modellen underestimerer de eksperimentelle diffusionskoefficientværdier. Disse beregnede diffusionskoefficienter fra eksperimentelle data, bør betragtes som en gennemsnitsdiffusionskoefficient for hele polymeren og dermed lavere end diffusionskoefficienten i den fuldt blødgjorte PVC. I stedet for at bruge denne komplekse model, blev det besluttet at anvende den enklere semi-empiriske model af Piringer. Ved at bruge denne simple model, med en polymer-specifik parameter kun fra ESBO data, var det muligt at estimere diffusionskoefficienter for Acetem og SNS. Resultaterne var tæt på de eksperimentelt opnåede diffusionskoefficienter ved 20°C, men ikke ved højere temperaturer.

Ved brug af finite element mesh metoden i Matlab og COMSOL, blev migrationen modelleret med en koncentrationsafhængig diffusionskoefficient, der ændrer sig med den lokale blødgørerkoncentration. Tre forskellige modeller for denne blødgørerkoncentrationsafhængighed af diffusionskoefficienten blev evalueret. Alle modeller var ca. lige succesfulde, med generelt bedre resultater end modellering med en statisk diffusionskoefficient.

Den numeriske løsning med finite element mesh metoden er også blevet brugt til at modellere et antistatisk additivs migration til overfladen af Low Density Polyethylen (LDPE) og Poly Propylen (PP). Det var muligt med en nyudviklet model at estimere migration med meget stor nøjagtighed. Dette resultat førte til den lidt overraskende konklusion, at det kontrollerende led i migrationen af additivet til overfladen ikke var migration i selve polymeren. Migration er sandsynligvis kontrolleret af en temperatur afhængig partititionskoefficient for additivet imellem polymer og overfladelaget.

Muligheden for at anvende molekyle simuleringer ved "Molecular dynamics" beregninger til estimering af partititionskoefficienter for additiver i de forskellige polymerer og fødevarer blev også undersøgt. Udvikling af metoden blev gjort mod eksperimentelle data af et system bestående af et hydrofilt og et hydrofobt additiv imellem LDPE og forskellige ethanol/vand blandinger. De beregnede partititionskoefficienter for forskellige additiver imellem LDPE og

ethanol/vand var korreleret med stor nøjagtighed til eksperimentelle data. For at udvide denne metode til også eddikesyre systemer (fødevarer simulat B), blev det valgt først at undersøge hvor godt de tre force fields (Trappe, OPLS-AA og CHARMM27) virker for simuleringer af eddikesyre og eddikesyre/vand blandinger alene. Ingen af de tre force fields kunne forudsige densiteten af eddikesyre/vand blandingerne tilfredsstillende. Kun CHARMM27 force fieldet var i stand til at forudsige det lokale densitetsmaksimum.

En kode blev udviklet til at tælle størrelsen eddikesyre klynger defineret ud fra hydrogenbinding imellem enkelte eddikesyre molekyler. Statistik fra koden viste at eddikesyre molekyler i væskefasen mest forefindes som kæde strukturer, med kæder af 2 og 3 molekyler i størrelse som værende den mest fremherskende størrelse. Derudover blev det også undersøgt hvor godt de enkelte force fields kunne forudsige fordampningsenthalpien. Alle tre force fields overestimerede denne egenskab til en værdi omkring det dobbelte af den eksperimentelle værdi ($\approx 50^{\text{kJ/mol}}$ sammenlignet med $23.7^{\text{kJ/mol}}$). Det viste sig at gasfasen næsten udelukkende bestod af monomerer, hvor eksperimentelle data af gasfasen på 298K og 1 bar giver en dimer andel på omkring 80-90%. Dimer andelen i gasfasen blev forhøjet v.h.a. højere atomare ladninger, som beskrevet af Chocholousova et al. [J. Chocholousova, J. Vacek, and P. Hobza; J. Phys. Chem. A; 107, 17, (2003), 3086-3092], men fordampningsenthalpien var stadig næsten dobbelt så høj. Det blev vist, at de fleste data fra litteraturen der referer en værdi $\approx 50^{\text{kJ/mol}}$ stammer fra arbejdet af Konicek og Wadsö [J. Konicek and I. Wadsö; Acta Chem. Scand.; 24, 7, (1970), 2612-2616] fra 1970. I dette arbejde er det forklaret hvordan fordampningsenthalpien af eddikesyre teoretisk kan ses som bestående af to bidrag, den "rene" fordampningsenthalpi af monomer og dissocieringsenthalpien. Det er vigtigt, at denne teoretisk udledte "rene" fordampningsenthalpi ($\approx 50^{\text{kJ/mol}}$) ikke forveksles med den eksperimentelt opnåede fordampningsenthalpi ($23.7^{\text{kJ/mol}}$). OPLS-AA force fieldet er parametriseret imod den teoretiske "rene" fordampningsenthalpi på en korrekt måde, ved kun at beregne energi forskellen for eddikesyre monomeren alene imellem de to faser. Men simuleringer i dette arbejde har dog vist, at molekyle simuleringer med disse parametre ikke vil representere dimer andelen i gasfasen korrekt.

Samlet set ud fra dette arbejde kan det konkluderes, at en komplet estimering af migration i polyolefiner kan opnås ved hjælp af numeriske løsninger ved finite element mesh metoden sammen med diffusionskoefficienter opnået ud fra Piringers model og partitionskoefficienten opnået ved hjælp af molekyle simuleringer. For det komplekse system af migration af blødgørere i blødgjort PVC, blev en komplet prædiktiv model ikke opnået. En model blev imidlertid udviklet til dette system, som forudsiger tilfredsstillende ved fitning af kun 1 eller 2 empiriske parametre til migrationsdata.

Contents

Symbols and abbreviations	3
1 Introduction	6
1.1 Structure of the Thesis	7
2 Plasticisers	9
2.1 The Danisco migration data	9
2.2 GRINDSTED® SOFT-N-SAFE	10
2.2.1 Hansen solubility parameters	11
2.3 GRINDSTED® ACETEM 95 CO	12
2.4 ESBO	13
2.5 DEHP	13
2.5.1 Hansen solubility parameters	15
3 Diffusion coefficient	17
3.1 Vrentas and Vrentas Free Volume theory for Diffusion	19
3.1.1 Calculation of parameters of free volume models	20
3.1.2 Conclusion	24
3.2 Empirical diffusion coefficient estimation	25
3.2.1 A_p by equation 3.27	25
3.2.2 A_p by equation 3.28	26
3.2.3 Estimation of diffusion coefficients by equations 3.27 and 3.28	28
3.2.4 Conclusion	30
3.3 Concentration dependent diffusion coefficient	30
3.3.1 Results	34
3.3.2 Conclusion	42
4 Migration	43
4.1 Modeling of migration in highly plasticised PVC	46
4.1.1 Conclusion	46

4.2	Modeling of antistatic additive migration	47
4.2.1	The antistatic additive project	47
4.2.2	Modelling	49
4.2.3	Conclusion	58
5	Modeling partition coefficients	59
5.1	Molecular Dynamics	60
5.2	Partition coefficients article	63
5.2.1	Abstract	63
5.2.2	Introduction	63
5.2.3	Partition coefficients from thermodynamic integration	65
5.2.4	Force fields	68
5.2.5	Computational details	70
5.2.6	Results and discussion	72
5.2.7	Conclusions	77
5.2.8	Acknowledgement	78
5.3	Modeling Acetic Acid by Molecular Dynamics	79
5.3.1	The true enthalpy of vaporization	90
5.4	Conclusion	93
6	Conclusion and Future work	95
A	Article: Modeling of the Migration in PVC	108
B	XPS measurements	121
B.1	Impact Poly Propylene	122
B.2	Poly Propylene (RB 707)	123
B.3	Poly Propylene (RD 226)	125
B.4	Low Density Poly Ethylene	126
C	Migration of antistatic additive	127
C.1	Low Density Poly Ethylene	128
C.2	Poly Propylene	130
D	Hydrogen bond clustering	131
D.1	hb-dat.sh	131
D.2	Hydrogen_bond_wrap.m	131
D.3	make_clusters.m	135
D.4	find_dimers.m	138

Symbols and abbreviations

Symbol	Description	SI Units
A_p	Empirical polymer specific parameter	
A'_p	Empirical polymer specific parameter ($A_p = A'_p - \frac{\tau}{T}$)	
$C_{1,i}^g$	The C_1 constant from the WLF equation[1] for component i with T_g as the reference temperature	
$C_{2,i}^g$	The C_2 constant from the WLF equation[1] for component i with T_g as the reference temperature	[K]
C_{p0}	Initial concentration of migrant in polymer	[mg/cm ³]
D	Diffusion coefficient	[cm ² /s]
D_0	Constant preexponential diffusion factor from Vrentas original model[2]	[cm ² /s]
\bar{D}_0	Average constant preexponential diffusion factor defined by Vrentas[3] ($-\ln \bar{D}_0 \approx -\ln D_0 + \frac{E_s}{RT}$)	[cm ² /s]
D_{01}	Average constant preexponential diffusion factor defined by Hong[4] ($D_{01} = \bar{D}_0$ when $E_p - E_s = 0$)	[cm ² /s]
D_1	Solvent self diffusion coefficient	[cm ² /s]
$E_p - E_s$	Energy per mole for one molecule to overcome the attractive forces which holds it to its neighbours	[J/mol]
$\Delta_{solvX}G$	Free energy of solvation into component X	[kJ/mol]
K_{1i}	Free-volume parameter for component i	[cm ³ /g·K]
K_{2i}	Free-volume parameter for component i	[K]
K_{ps}	Polymer/solvent partition coefficient of the migrant	
L	Thickness of polymer	[cm]
M_∞	Amount of plasticiser migrated at infinite time	[mg/cm ²]
M_i	The molar weight of component i	[g/mol]
M_r	The molar weight of the migrant	[g/mol]
M_t	Amount of plasticiser migrated at time t	[mg/cm ²]
q_n	Positive roots of $\tan q_n = -\alpha q_n$	

Symbol	Description	SI Units
t	Time	[s]
T	Temperature	[K]
T_{gi}	Glass transition temperature of component i	[K]
u	Mass transfer velocity parameter (agitation parameter)	
\hat{V}_i^*	Specific critical hole free volume required for a jump for a molecule of component i , can be set equal to the specific occupied volume of component i at temperature $0K$ ($(\hat{V}_i^0(O))$)	[cm ³ /g]
$\hat{V}_{FH}(T)$	The specific hole free volume of component i at temperature T	[cm ³ /g]
$\hat{V}_i^0(T)$	The specific volume of component i at temperature T	[cm ³ /g]
$\hat{V}_{c,i}$	The molar volume of component i at its critical temperature T_c	[cm ³ /mol]
α	Ratio of solvent volume over polymer volume times the partition coefficient ($\alpha = \frac{1}{K_{ps}} \frac{V_s}{V_p}$)	
χ	Flory-Huggins polymer-solvent interaction parameter	
η	Viscosity	[pa · s]
λ	Decoupling parameter used in Molecular Dynamics	
ϕ_i	Solvent volume fraction of component i	
γ_i	Overlap factor for the free-volume of component i	
ω_i	Mass fraction of component i	
τ	Polymer specific parameter ($A_p = A'_p - \frac{\tau}{T}$)	[K]
ξ	Ratio of solvent jumping unit critical molar volume over polymer jumping unit critical molar volume	

Abbreviation	Description
--------------	-------------

Acetem	GRINDSTED [®] ACETEM 95 CO
CHARMM27	All Atom force field (Chemistry at HARvard Macromolecular Mechanics)[5]
DEHP	Di-2-ethylhexyl phtalate
DIMODAN HP	GRINDSTED DIMODAN HP, an antistatic additive developed by Danisco A/S

Abbreviation	Description
ESBO	Epoxidised Soybean oil
FEM	numerical solution by Finite Element Mesh
GMS	Glycerol MonoStearate
GROMACS	Software for Molecular Dynamics calculation (GRONingen MACHine for Chemical Simulations)[6]
IPP	Impact Polypropylene
LJ	Lennard-Jones
LDPE	Low Density Polyethylene
OPLS-AA	All Atom force field (Optimized Potentials for Liquid Simulations)[7]
PGE 308	Antistatic additive developed by Danisco A/S
PP	Polypropylene
PVC	Polyvinyl Chloride
SNS	GRINDSTED [®] SOFT-N-SAFE
TraPPE	United atom force field (Transferable Potentials for Phase Equilibria)[8]

Introduction

The process of changing the temperature at which the transition from the glassy state to the rubbery state of polymers by adding adequate chemicals with strong solvent effects on them is called plasticisation. Rather than dissolving the plastic material, the plasticiser causes the polymer structure to swell, which causes increased chain movement, especially locally, giving a softer and more flexible structure. Plasticisers are like a solvent for the polymer where only enough solvent is added to cause some swelling. This leads to disentangling of the molecules and some breaking of secondary intermolecular bonds, but where sufficient intermolecular interactions still exist that the material is not liquid. This more flexible state, still not as flexible as a liquid, is called the rubbery state. The transition from glassy state (rigid and brittle structure) to the rubbery state (flexible state, as rubber) is called the glass transition temperature. Adding plasticiser to a polymer gives the ability to shift the glass transition temperature, and by this "design" the macroscopic structure of the final polymer product.

The most important commercial application for plasticisation is in polyvinyl chloride (PVC) production. PVC is hard and brittle in its non-plasticised state but when plasticised, it is soft and flexible. Plasticisers are added to the polymer PVC (Polyvinyl Chloride) to enhance the flexibility of the polymer by decreasing its glass transition temperature from around 80°C to below 0°C [9]. The plasticiser is not chemically bonded to the polymer, as already mentioned, which means that it can migrate from the polymer depending on the environment surrounding the polymer (hydrophobic/hydrophilic, solvent or air). The most commonly used plasticisers for PVC are the phthalates, especially the plasticiser DEHP (Di-2-ethylhexyl phthalate)[10]. Several phthalates used as PVC- additives are very slow biodegradable and most importantly they are being suspected to be carcinogenic, therefore there is an immediate need to find safe substitutes of these plasticisers in food packaging materials.

The Danish food-additive manufacture Danisco has recently developed such an alternative, the GRINDSTED® SOFT-N-SAFE (SNS) plasticiser which is based on a fully acetylated glycerol monoester on the hardened oil from the castor bean. The product is now approved for use in

the European market while preliminary results show smaller migration to specific food simulants (aqueous acetic acid, water-ethanol and sunflower oil) compared to DEHP[11]. In addition, GRINDSTED[®] SOFT-N-SAFE has shown to be fully biodegradable and a non toxic substitute of phthalates.

The purpose of this thesis is to investigate, from a modelling point of view, the migration of GRINDSTED[®] SOFT-N-SAFE and other plasticisers from PVC and polyolefins into different liquids (specifically the four food simulants set by the European Commission[12]: water, 3% acetic Acid, 10% ethanol and olive oil). While the development of a full migration model is the main aim of this project, a qualitative understanding of the factors controlling the migration, and their quantification, are also of paramount importance.

1.1 Structure of the Thesis

The thesis is structured in the same way as the work progressed throughout the three years of the PhD project. **Chapter 2 - Plasticisers** contains information on the four plasticisers of main interest in this work. The choice of these specific plasticisers is based on a migration experiment Danisco conducted in 2005 (also described in this chapter).

Chapter 3 - Diffusion coefficient it is firstly described how diffusion coefficients have been estimated from the migration data by Danisco. Then it is explained how to model the diffusion coefficients based on the free volume theory by Vrentas and Vrentas[13] and further on with the semi-empirical model by Piringer[14]. The last section in this chapter describes three proposed models for modeling a diffusion coefficient dependent on the local plasticiser concentration in PVC.

Chapter 4 - Migration firstly explains how to model migration from food packaging materials and into foodstuff by numerical and analytical solutions. Then the work on modeling migration of SNS in PVC is presented, which has been published in the article "Modeling of the Migration of Glycerol Monoester Plasticizers in Highly Plasticized Poly(vinyl chloride)"[15] and is available in Appendix A. The last section in the migration chapter describes how the developed numerical solution has been used to model migration of an antistatic additive to the surface of Low Density Polyethylene (LDPE) and Polypropylene (PP), which is part of a product development project at Danisco.

The developed migration model is only as good as the parameters used in the model, i.e. the diffusion and the partition coefficients. The semi-empirical model by Piringer had showed to be successful for the systems in this work, but no model existed for estimation of partition coefficients. For this reason it was chosen to continue the work by developing a consistent way to estimate partition coefficients for the systems of interest in this work. This work, based on molecular dynamics simulation, is presented in **Chapter 5 - Modeling partition coefficients**

in polymer/solvent systems by molecular dynamics. Very little experimental data exist for partition coefficients of small organic molecules between polymers and one of the four food simulants. It was chosen to develop the methodology on a system of LDPE and water/ethanol solvents. The last part of this chapter is testing of the modeling capabilities of molecular dynamics for acetic acid (one of the four food simulants).

Finally **Chapter 6 - Conclusion and Future work** gives the overall conclusions to the presented work, and suggestions to future work.

Common symbols and abbreviations used throughout this work are listed in the front at page 3.

Plasticisers

The most important commercial application for plasticisation is in PVC. Plasticisers are an additive necessary to manufacture flexible PVC products, as PVC alone is hard and brittle. Depending on the final use of the polymer, the plasticiser content in PVC varies between 15 and 60% (by weight), with typical ranges for most flexible applications around 35 to 40%[9]. In Europe alone approximately 1 million tonnes of plasticisers are produced each year, out of which around 90% are added in PVC[9]. Plasticisers for PVC are generally phthalate esters (93% in 1997)[10], among which the most common one by far is Di(2-ethylhexyl) phthalate (DEHP). From the mid 1990's especially DEHP, but also phthalates in general, came under strong suspicion for being carcinogenic and mutagenic, which lead to a EC recommendation on the use of phthalates in toys in 1998[12] and later in 2002 an EU Directive for the use of plastic materials coming in contact with food[16]. Both documents have been updated many times over the years[17–20], while in parallel other plasticisers, in particular adipates, trimellitates, organophosphates and epoxidised soybean oil have been more and more used in PVC[10]. However, these other plasticisers represent still today only a small fraction of total plasticisers in use due to their price (they are more expensive than phthalates) and their lower performance. Danisco, a world leader company in food ingredients, enzymes and bio-based solutions, released in 2006 a new product called GRINDSTED[®] SOFT-N-SAFE which is a fully biodegradable and non-toxic plasticiser for PVC[11].

2.1 The Danisco migration data

In 2005 Danisco conducted a big migration experiment on two new plasticisers for PVC, candidates to replace the widely used ESBO (Epoxidised Soybean oil) in the market of gaskets for jars[21]. The migration experiment was conducted because every polymer used as food contact material sold in the EU or US has to comply with current legislation, which asks from the producer to prove that all additive migration from the polymer to the food stays within the systematic migration limits (SML) set by EU or the FDA in the US. The data from this experiment were made available for this PhD project with the aim to investigate and develop a better un-

derstanding of the migration in the system under study. The three plasticisers (GRINDSTED[®] SOFT-N-SAFE (SNS), GRINDSTED[®] ACETEM 95 CO (Acetem) and Epoxidised Soybean Oil (ESBO)) are described in more detail later in this chapter (section 2.2, 2.3 and 2.4). The total migration experiment was set up by measuring migration of the three plasticisers from three different PVC types at three different temperatures (20°C, 40°C and 60°C) into iso-octane, leading to 27 independent migration measurements. The composition of the three PVC types was the following:

Type 1: 50*phr* plasticiser, 2.5*phr* surfactant and stabiliser.

Type 2: 50*phr* plasticiser, 2.5*phr* surfactant and stabiliser, 7*phr* lubricant.

Type 3: 67*phr* plasticiser, 2.5*phr* surfactant and stabiliser.

(where phr is parts per hundred resin, a concentration term often used in the polymer industry)

A full description of the experimental setup and all migration data can be found in the article: "Modeling of the Migration of Glycerol Monoester Plasticizers in Highly Plasticized Poly(vinyl chloride)"[15] (printed in in appendix A). A good plasticiser candidate should not only give easily controlled property changes in the plastic material over a reasonably wide range of plasticiser concentrations, but it should also have low cost, remain in the polymer, be nontoxic, biodegradable and stable through processing and use. The two new plasticiser candidates are more expensive than ESBO, but superior to ESBO in being nontoxic and biodegradable.

2.2 GRINDSTED[®] SOFT-N-SAFE

GRINDSTED[®] SOFT-N-SAFE [11] (SNS) is a newly developed plasticiser which shows great potential for being a safe alternative to the widely used DEHP plasticiser for PVC polymers[11]. SNS is a fully acetylated glycerol monoester based on fully hydrogenated oil from the castor bean. The oil from the castor bean (castor oil) is known as a liquid used as a cure for constipation and for inducing vomiting, especially adequate for children. The fully hydrogenated castor oil (mainly consisting of 12-hydroxystearic acid) is esterified with excess glycerin to make a product of 95-96% monoglycerides. The free hydroxyl groups on the monoglycerides are then esterified by acetic acid to give the final product (see figure 2.1). As this product is made from a natural product (the castor oil), small deviations within the product are to be expected, fact which means that different isomers and also small amounts of di- and triglycerides can be found in the product[22]. Throughout this work SNS has been modelled as shown in figure 2.1 for simplification reasons.

Table 2.1: Calculated Hansen solubility parameters for the two main components of SNS using the group contribution methods by van Krevelen[25] and Stefanis et al.[26]. Furthermore some experimentally obtained parameters for similar compounds found in the official Hansen database[24] are listed for comparison

[MPa ^(1/2)]	δ_d	δ_p	δ_h	δ
van Krevelen[25]:				
SNS90	17.20	2.11	7.76	18.99
SNS10	17.33	2.00	7.03	18.81
Stefanis[26]:				
SNS90	14.32	4.40	7.13	16.59
SNS10	14.71	3.90	5.03	16.03
Isopropyl palmitate				
	14.30	3.90	3.70	15.28
Dioctyl adipate				
	16.70	2.00	5.10	17.58
Butyl stearate				
	14.50	3.70	3.50	15.08

In table 2.1 the calculated Hansen solubility parameters are listed together with experimentally obtained Hansen solubility parameters of three similar compounds found in the official Hansen database[24]. As it can be seen the estimated parameters from group contribution methodology are fairly close to the parameters from similar compounds.

2.3 GRINDSTED[®] ACETEM 95 CO

GRINDSTED[®] ACETEM 95 CO (Acetem) is a Danisco product normally utilised for moisture coating or as a plasticiser in chewing gum. Acetem is very similar to SNS and is also a fully acetylated glycerol monoester, but instead of being produced from castor oil, it is made from coconut oil. This means that the fatty acid used for Acetem mainly consists of caprylic-, capric- and lauric acid (carboxylic acids with carbon chain lengths of 8, 10 and 12 respectively, see figure 2.2).

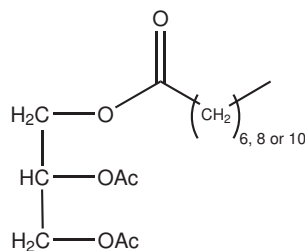


Figure 2.2: The main components of GRINDSTED[®] ACETEM 95 CO. The fatty acids used for Acetem production come from the coconut oil and have a carbon chain length of 8, 10 or 12.

2.4 ESBO

Epoxidised Soybean oil (ESBO, see figure 2.3) is commonly used as the plasticiser for PVC when the latter is destined to be used as the lid of jars. ESBO serves a double purpose when added to the PVC, first of all as plasticiser it makes the polymer more flexible and soft, secondly for binding any hydrogen chloride released from the PVC during heating by ring opening of the epoxide (PVC has a tendency to decompose by giving off HCl gas and forming crosslinks among the polymer chains when HCl leaves. This autocatalytic decomposition occurs at temperatures near the melting point should be prevented).[9]. ESBO is known for its low migration compared to other plasticisers, and for this reason it is used in food packaging films and other PVC products in direct contact with food. The reason for this is to keep the migration of the plasticisers in the polymer and into the food product within the maximum migration limit of additives[9]. The migration limits set by the European Commission for the use of ESBO is 60mg/kg, and furthermore there is a limit of 30mg/kg specifically for use in lids of jars containing babyfoods[18].

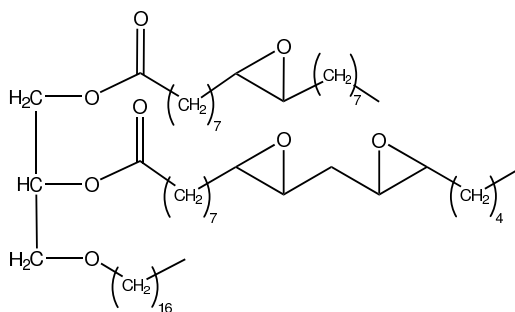


Figure 2.3: The main component of ESBO.

2.5 DEHP

Di-2-ethylhexyl phthalate (DEHP, see figure 2.4), also sometimes named dioctyl phthalate (DOP), is by far the most commonly used PVC plasticiser in the world; in 1997 phthalate production represented 93% of the 900.000 tonnes of plasticisers produced for PVC that year[10]. This is the reason why this plasticiser is the one against which other plasticisers for PVC are compared and measured[9].

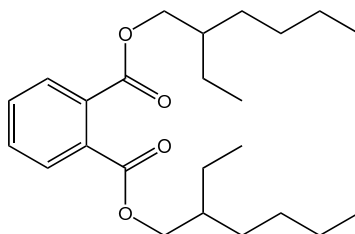


Figure 2.4: Di-2-ethylhexyl phthalate (DEHP)

From the mid 1990's DEHP came under strong suspicion for being carcinogenic and mutagenic, which lead to limitations to its use as plasticiser in babytoys (0.04 mg/cm^2) in 1998[12], and by 2005 close to a total ban of the product (up to 0.1% in the final product)[27] in the EU. From 2002 the migration from packaging and into foodstuff was also limited by EU legislation[16], and in 2007 DEHP was only to be used in foodcontact materials as[19]:

- a:** Plasticiser in repeated use materials and articles contacting non-fatty foods
- b:** Technical support agent in concentrations up to 0.1 % in the final product

The general systematic migration limit (SML) of DEHP is 1.5 mg/kg food simulant (1.5 ppm).

Along with the implementation of these limitations to the use of DEHP in Europe, a thorough investigation was conducted by the EU to evaluate the risks of using DEHP. The final risk assessment report was published in 2008[28] with the following general results:

DEHP will not build up in the body, but will be naturally metabolised to mono(2-ethylhexyl)phthalate (MEHP) and 2 ethylhexanol and excreted from the body mainly through the urine but also faeces. Only very few studies with humans exist. These studies show a somewhat different result, but in general a half-life of DEHP in the human body from 12 to 48 hours is probably a good estimate.

As babies have a smaller body mass than adults and as a result a higher exposure ratio of DEHP, and as they tend to suck and chew on polymer products, many studies have evaluated the exposure of babies to PVC products containing DEHP. In the risk assessment report a general worst case exposure for children is set to $0.2 \text{ mg/kg}\cdot\text{day}$ (sucking and chewing for 3 hours a day). By monitoring the excretion level of DEHP and its metabolites of a big sample of people an estimated median intake level of DEHP has been set to $0.0138 \text{ mg/kg}\cdot\text{day}$.

The LD₅₀ of DEHP (single dose exposure) is estimated to $>10,000 \text{ mg/kg}$ from experiments with mice. Repeated dose toxicity tests (2 years with rats) showed toxicity effects to kidneys (increase of kidney size) which lead to a NOAEL (No Observable Adverse Effect Level) for males at $29 \text{ mg/kg}\cdot\text{day}$ and $36 \text{ mg/kg}\cdot\text{day}$ for females.

Studies with rodents have shown DEHP to be non-mutagenic, but regarding carcinogenicity a relevance to humans can not be ruled out, although the evidence is inconclusive. As for reproduction concerns a very conservative NOAEL has been set to 4.8 mg/kg·day, based on minimal testis atrophy at 14 mg/kg·day and complete testis atrophy at 359 mg/kg·day.

Based on these general results, the general conclusion towards consumer risks are[28]:

There is a need for limiting the risks; risk reduction measures which are already being applied shall be taken into account.

This conclusion is reached because of:

- Concerns for children with respect to testicular effects, fertility and toxicity to kidneys, on repeated exposure, as a consequence of oral exposure from toys and child-care articles, and multiple routes of exposure.
- Concerns for children undergoing long-term blood transfusion and neonates undergoing transfusions with respect to testicular toxicity and fertility, as a consequence of exposure from materials in medical equipment containing DEHP.
- Concerns for adults undergoing long-term haemodialysis with regard to repeated dose toxicity to kidney and testis, fertility, and developmental toxicity, as a consequence of exposure from materials in medical equipment containing DEHP.

2.5.1 Hansen solubility parameters

For comparison reasons to the calculated Hansen solubility parameters calculated for SNS, these were also calculated for DEHP. The parameters have been estimated from the group contribution methodology as proposed by van Krevelen[25] and more recently by Stefanis et al.[26]. The calculated Hansen solubility parameters calculated by group contribution are listed in table 2.2 together with the parameters found in the official Hansen database[24].

Table 2.2: Calculated Hansen solubility parameters for DEHP using the group contribution methods by van Krevelen[25] and Stefanis et al.[26] and parameters from the official Hansen database[24] for comparison

[MPa ^(1/2)]	δ_d	δ_p	δ_h	δ
van Krevelen[25]:	17.71	1.84	6.10	18.82
Stefanis[26]:	17.54	5.85	1.22	18.53
Hansen[24]:	16.60	7.00	3.10	18.28

From table 2.2 it can be seen that the group contribution method captures the dispersive part (δ_d) fairly well. Both group contribution methods show problems in estimating the polar (δ_p) and the hydrogen bonding part (δ_h), with the method of Stefanis et al.[26] showing to be the best of the two for DEHP. The Hansen solubility parameters of DEHP are very similar to the estimated for SNS (table 2.1), as expected because of the similarities of the two solvents. Furthermore is

the method of Stefanis et al.[26] also the one performing best for SNS when comparing to the similar compounds Hansen solubility parameters.

Diffusion coefficient

The quality of the results from migration modeling are only as good as the parameters used in the model, i.e. the diffusion and partition coefficients. If experimental migration data exist for the system of interest, the diffusion coefficient can be obtained by linear regression of the migration data as a function of the square root of time, eq. 3.1. This very simple correlation holds however only when there is a big concentration difference of the migrant in the polymer and the solvent:

$$M_t = 2C_{p0}\sqrt{\frac{Dt}{\pi}} \Leftrightarrow \frac{M_t}{C_{p0}} = \sqrt{D} \cdot 2\sqrt{\frac{t}{\pi}} \quad (3.1)$$

In the linear migration model (eq. 3.1) is M_t [mg/cm²] the migration at time t [s], C_{p0} [mg/cm³] is the initial concentration in the polymer and D [cm²/s] is the diffusion coefficient. The problem with this method for estimating the diffusion coefficient is that there must be sufficient available data points in the early part of the migration, where the concentration difference between the two layers is very big. Only the four first data points of the seven from the experiment with Acetem migrating from PVC compound 3 into iso-octane at 20°C (figure 3.1), clearly lie in the linear part of the migration, whereas the last three data points show a slower migration than the correlation (eq. 3.1) predicts. For the same system with SNS as the migrant, six of the seven data points lie in the linear part.

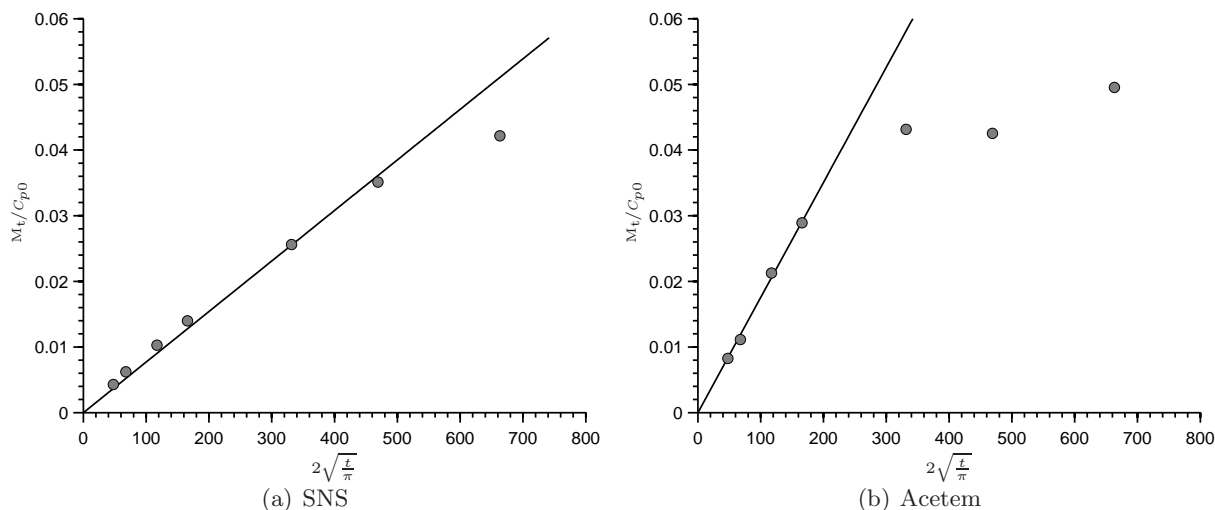


Figure 3.1: Plots of the linear regression of the data points from the migration of SNS and Acetem from PVC compound 3 at 20°C into iso-octane used for the estimation of the diffusion coefficient through equation 3.1. Only the 4 first data points are used for the regression in the right figure, whereas 6 out of the 7 data points are used in the left figure.

One of the purposes of this project was to estimate the diffusion coefficients of SNS at different temperatures, based on the migration data from the Danisco experiment. As the migration experiments conducted by Danisco also included the plasticiser candidate Acetem and the widely used plasticiser ESBO, the diffusion coefficients were calculated for these plasticisers as well. All the estimated diffusion coefficients are listed in table 3.1.

Table 3.1: Estimated diffusion coefficients based on equation 3.1 from the Danisco migration experiment on SNS, Acetem and ESBO from PVC into iso-octane. (data points = data points used for linear regression / total number of data points in the experiment.)

	20°C [cm ² /s] (data points)	40°C [cm ² /s] (data points)	60°C [cm ² /s] (data points)
SNS			
PVC type 1	1,30·10 ⁻⁹ (5/7)	1,10·10 ⁻⁹ (4/7)	2,49·10 ⁻⁹ (5/5)
PVC type 2	5,95·10 ⁻⁹ (5/7)	5,84·10 ⁻⁹ (5/7)	2,67·10 ⁻⁹ (5/5)
PVC type 3	5,93·10 ⁻⁹ (6/7)	5,81·10 ⁻⁹ (4/7)	4,95·10 ⁻⁹ (5/5)
Acetem			
PVC type 1	6,17·10 ⁻⁹ (7/7)	6,42·10 ⁻⁹ (4/7)	1,07·10 ⁻⁹ (5/5)
PVC type 2	1,66·10 ⁻⁸ (5/7)	3,30·10 ⁻⁸ (4/7)	1,49·10 ⁻⁹ (5/5)
PVC type 3	3,07·10 ⁻⁸ (4/7)	6,63·10 ⁻⁸ (4/7)	7,67·10 ⁻⁹ (5/5)
ESBO			
PVC type 1	7,07·10 ⁻¹¹ (5/7)	2,43·10 ⁻¹⁰ (3/6)	6,21·10 ⁻¹⁰ (5/5)
PVC type 2	1,25·10 ⁻¹⁰ (5/7)	7,25·10 ⁻¹⁰ (6/7)	8,59·10 ⁻¹⁰ (4/4)
PVC type 3	3,09·10 ⁻¹⁰ (5/7)	9,47·10 ⁻¹⁰ (5/7)	1,78·10 ⁻⁹ (4/4)

When diffusion coefficients are needed for temperatures or systems where no experimental data exist, a theoretical model is then needed. In this work both the polymer-solvent free volume model of Vrentas and Vrentas[13], and the empirical model by Piringer[14] have been used.

3.1 Vrentas and Vrentas Free Volume theory for Diffusion

For the estimation of diffusion coefficients in polymer-solvent systems, models based on free volume theory are widely used, among which the model by Vrentas and Vrentas[13] is probably the most widely used. This model has shown to be accurate for the estimation of diffusion coefficients of organic solvent molecules in both rubbery and glassy polymers[14]. A complete list of symbols for all the expressions used in this section are provided at the end of this thesis. In all expressions are sub-index 1 used for the solvent and sub-index 2 for the polymer.

By the terminology of Vrentas and Vrentas the solvent self-diffusion coefficient in a rubbery (above T_g) polymer-solvent system, can be calculated by[13]:

$$D_1 = \bar{D}_0 \exp \left[-\frac{E_p - E_s}{RT} \right] \exp \left[-\frac{\omega_1 \hat{V}_1^* + \omega_2 \xi \hat{V}_2^*}{\hat{V}_{FH}/\gamma} \right] \quad (3.2)$$

$$\frac{\hat{V}_{FH}}{\gamma} = \omega_1 \frac{K_{11}}{\gamma_1} (K_{21} + T - T_{g1}) + \omega_2 \frac{K_{12}}{\gamma_2} (K_{22} + T - T_{g2}) \quad (3.3)$$

The model parameters are: $\bar{D}_0, E_p, E_s, \gamma_1, \gamma_2, K_{11}, K_{12}, K_{21}, K_{22}, \omega_1, \omega_2, T_{g1}, T_{g2}, \hat{V}_1^*, \hat{V}_2^*, \xi$

As it can be seen in equation 3.2 the solvent self-diffusion coefficient by Vrentas and Vrentas[13] depends on 16 parameters. Though being a large number of parameters it is stated by the authors that all parameters are physically meaningful (as opposed to the later explained empirical model by Piringer, eq. 3.27 and 3.28).

For systems where the solvent mass fraction is between 0 to 0.9 ($0 < \omega_1 < 0.9$) the polymer molecule overlap is very much predominant, and for this reason E_s can be neglected compared to E_p in the expression $E_p - E_s$ [2]. For simplification reasons and in order to reduce the number of parameters, many researchers have chosen to set the term $E_p - E_s$ equal to zero[4, 29], which can be the case for many polymer - solvent systems especially at lower temperatures, but is far from always the case as stated by Macedo and Litovitz [30]. In this work this simplification has also been used, which means that the expression of the solvent self diffusion coefficient reduces to:

$$D_1 = D_{01} \exp \left(\frac{-(\omega_1 \hat{V}_1^* + \xi \omega_2 \hat{V}_2^*)}{\hat{V}_{FH}/\gamma} \right) \quad (3.4)$$

$$\frac{\hat{V}_{FH}}{\gamma} = \omega_1 \frac{K_{11}}{\gamma_1} (K_{21} - T_{g1} + T) + \omega_2 \frac{K_{12}}{\gamma_2} (K_{22} - T_{g2} + T) \quad (3.5)$$

Parameters: $D_{01}, \omega_1, \gamma_1, \gamma_2, K_{11}, K_{12}, K_{21}, K_{22}, \omega_2, T_{g1}, T_{g2}, \hat{V}_1^*, \hat{V}_2^*, \xi$

In this more simplified expression of the solvent self diffusion coefficient by Hong[4], only 14 parameters are needed. D_{01} in the equation of Hong (Eq. 3.4) is equal to \bar{D}_0 when $E_p - E_s$ is set to 0 in the original expression by Vrentas and Vrentas[13], equation 3.2. The determination of all the parameters needed for the system of SNS in PVC is explained in the following section.

3.1.1 Calculation of parameters of free volume models

\bar{D}_0 and D_{01} can be calculated by a relationship between viscosity and temperature proposed by Vrentas[3] derived from a viscosity/self-diffusion relationship by Dullien[31] (Eq. 3.6) and the solvent self diffusion coefficient expression (eq. 3.2) for the pure solvent, i.e. $\omega_1 = 1$ (Eq. 3.7).

$$\frac{\eta VD}{RT} = 0.124 \cdot 10^{-16} V_c^{2/3} \quad (3.6)$$

$$D_1 = D_0 \exp \left[-\frac{E_s}{RT} \right] \exp \left[-\frac{\hat{V}_1^*}{(K_{11}/\gamma_1)(K_{21} + T - T_{g1})} \right] \quad (3.7)$$

As E_s does not change much with temperature, it was chosen by Vrentas to define a new preexponential diffusion factor in order to decrease the number of parameters $-\ln \bar{D}_0 \approx -\ln D_0 + \frac{E_s}{RT}$ [3]. With this new average preexponential diffusion factor in the equation it is possible to determine \bar{D}_0 , K_{11}/γ_1 and $K_{21} - T_{g1}$ from viscosity/temperature data, by combining eq. 3.6 and eq. 3.7 into eq. 3.8 and using the viscosity/temperature relationship by Vogel[32] (Eq. 3.9).

$$\ln \eta_1 = \ln \left(\frac{0.124 \cdot 10^{-16} \hat{V}_{c,1}^{2/3} RT}{M_1 \hat{V}_1^0} \right) - \ln \bar{D}_0 + \frac{\hat{V}_1^*}{(K_{11}/\gamma_1)(K_{21} + T - T_{g1})} \quad (3.8)$$

$$\ln \eta_i = A_i + \frac{B_i}{C_i + T} \quad (3.9)$$

Hence (K_{11}/γ_1) can be calculated as:

$$K_{11}/\gamma_1 = \frac{\hat{V}_1^*}{B_i} \quad (3.10)$$

and $(K_{21} - T_{g1})$ as:

$$K_{21} - T_{g1} = C_i \quad (3.11)$$

and \bar{D}_0 as:

$$\bar{D}_0 = \left(\frac{0.124 \cdot 10^{-16} \hat{V}_{c,1}^{2/3} RT}{M_1 \hat{V}_1^0} \right) \exp(A_i) \quad (3.12)$$

From viscosity/temperature data of SNS from Danisco it was possible to obtain a fit to the expression by Vogel[32] (Eq. 3.9 as shown in figure 3.2). Danisco had two sets of viscosity/temperature data for SNS, and fitting was done using the *lsqnonlin* function of MATLAB to each set of data separately and both sets combined. The three sets of parameters did not deviate much (see figure 3.2), so it was decided to use the combined data for the subsequent calculations.

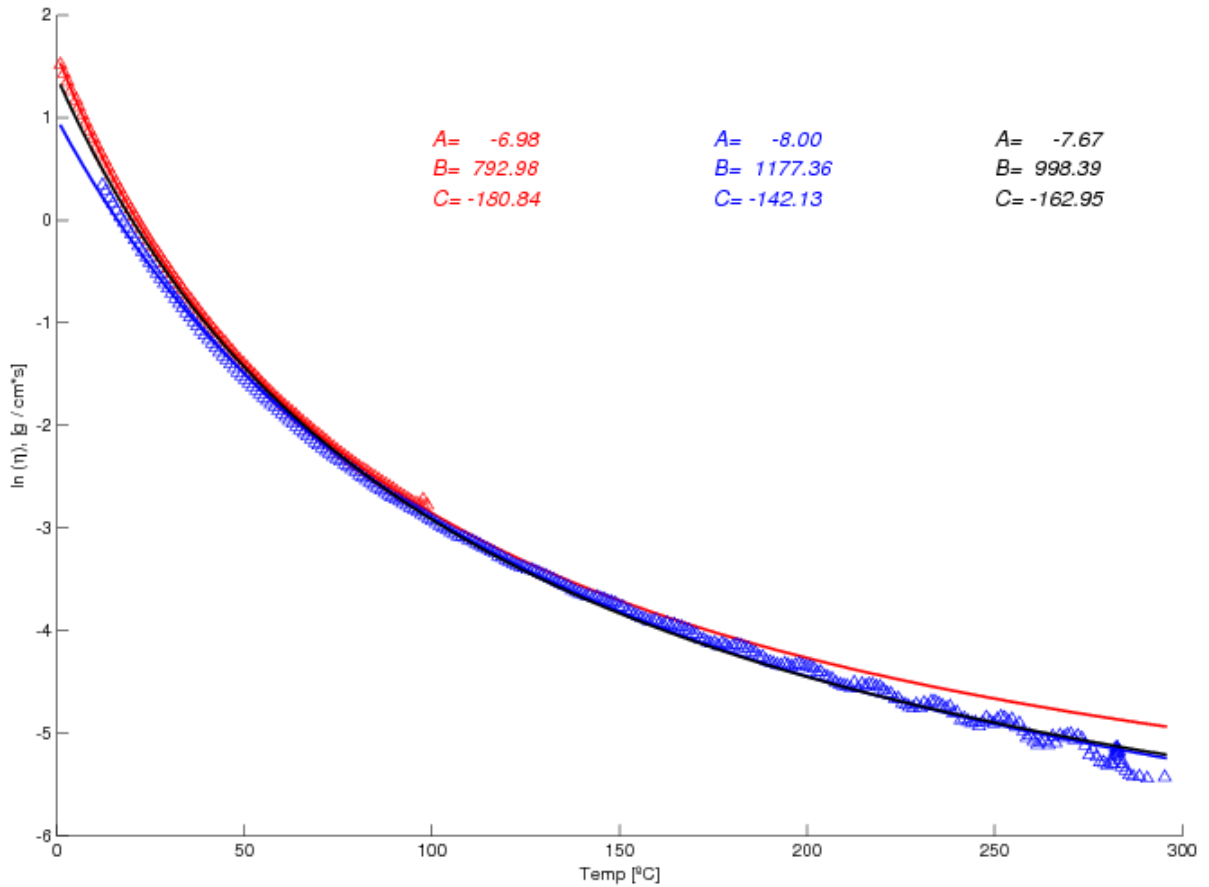


Figure 3.2: The fitting to the viscosity/temperature data of SNS by the model of Vogel (eq. 3.9). Two sets of experimental data was given by Dansico and the three sets of parameters were obtained by using each set of experimental data or the two combined. The fitting is done by the *lsqnonlin* function of MATLAB, which uses a levenberg-marquardt algorithm.

(K_{12}/γ_2) and K_{22} are proposed by Vrentas to be in direct relationship with the WLF constants[1] by equations 3.13 and 3.14 [33].

$$\frac{K_{12}}{\gamma_2} = \frac{\hat{V}_2^*}{2.303 C_{1,2}^g C_{2,2}^g} \quad (3.13)$$

$$K_{22} = C_{2,2}^g \quad (3.14)$$

These relationships are derived from the WLF theory[1] by:

$$\log a_T = \log \left(\frac{\eta}{\eta_g} \right) = \log \left(\frac{D_g}{D} \right) = \frac{-C_1^g(T - T_g)}{C_2^g + T - T_g} \quad (3.15)$$

From the definition of the self diffusion coefficient for one component (the pure polymer) by Vrentas[33], it is given that:

$$\ln D = \ln D_0 - \frac{\gamma \hat{V}_2^*}{K_{12}(K_{22} + T - T_{g2})} \quad (3.16)$$

Thus:

$$\ln \frac{D_g}{D_0} = -\frac{\gamma \hat{V}_2^*}{K_{12}(K_{22} + T_{g2} - T_{g2})} \Leftrightarrow \quad (3.17)$$

$$\ln \frac{D_g}{D_0} = -\frac{\gamma \hat{V}_2^*}{K_{12}K_{22}} \quad (3.18)$$

By combination of (3.16) and (3.18):

$$\ln \frac{D_g}{D_0} + \ln \frac{D_0}{D} = -\frac{\gamma \hat{V}_2^*}{K_{12}K_{22}} + \frac{\gamma \hat{V}_2^*}{K_{12}(K_{22} + T - T_{g2})} \Leftrightarrow \quad (3.19)$$

$$\ln \frac{D_g}{D} = \frac{\gamma \hat{V}_2^* K_{22} - \gamma \hat{V}_2^* (K_{22} + T - T_{g2})}{K_{12}K_{22}(K_{22} + T - T_{g2})} \Leftrightarrow \quad (3.20)$$

$$\ln \frac{D_g}{D} = \frac{-\gamma \hat{V}_2^* (T - T_{g2})}{K_{12}K_{22}(K_{22} + T - T_{g2})} \Leftrightarrow \quad (3.21)$$

$$\ln \frac{D_g}{D} = \frac{-\frac{\gamma \hat{V}_2^*}{K_{12}K_{22}} (T - T_{g2})}{K_{22} + T - T_{g2}} \quad (3.22)$$

By comparing (3.22) to the WLF equation (3.15), it can be seen that:

$$C_2^g = K_{22} \quad \wedge \quad (3.23)$$

$$2.303C_1^g = \frac{\gamma \hat{V}_2^*}{K_{12}K_{22}} \Leftrightarrow \quad (3.24)$$

$$2.303C_1^g C_2^g = \frac{\gamma \hat{V}_2^*}{K_{12}} \quad (3.25)$$

ω_1 is the weight fraction of the solvent in the polymer, hence ω_2 (the weight fraction of the polymer in the solvent) is $(1 - \omega_1)$. This parameter is kept as the one free parameter that the

self diffusion should be dependent on.

T_{g2} is the glass transition temperature of the polymer and can be found for many polymers in the literature f.ex. many data are included in the "Polymer Handbook"[34].

\hat{V}_1^* the specific critical hole free volume, which is the free volume required for a jump of a solvent molecule. It has been argued by e.g. Vrentas[35] that this volume can be set equal to the specific occupied volume of solvent at $0K$, hence $\hat{V}_1^* = \hat{V}_1^0(O)$. This is also the case of the polymer, which means that $\hat{V}_2^* = (\hat{V}_2^0(O))$

Table 3.2: The calculated parameters used for calculation of the solvent self-diffusion coefficient (D_1) of SNS in PVC by equation 3.4. In the reference column is listed how the parameters are calculated and the reference.

Parameter	value	unit	Reference
$E_p - E_s$	0.00	[J/mol]	[4, 29]
K_{11}/γ_1	$9.66 \cdot 10^{-4}$	[cm ³ /g.K]	visc./temp. data (eq. 3.8)[3]
$K_{21} - T_{g1}$	$-1.63 \cdot 10^2$	[K]	visc./temp. data (eq. 3.8)[3]
K_{12}/γ_2	$5.44 \cdot 10^{-4}$	[cm ³ /g.K]	WLF (eq. 3.13)[1, 33, 36]
K_{22}	$3.22 \cdot 10^1$	[K]	WLF (eq. 3.13)[1, 33, 36]
T_{g2}	$3.39 \cdot 10^2$	[K]	[34]
\hat{V}_1^*	$8.22 \cdot 10^{-1}$	[cm ³ /g]	GC model[37]
\hat{V}_2^*	$6.25 \cdot 10^{-1}$	[cm ³ /g]	[34]
$\hat{V}_{c,1}$	$1.61 \cdot 10^3$	[cm ³ /g]	GC model[38]
M_1	$4.95 \cdot 10^2$	[g/mol]	
$\hat{V}_1^0(298K)$	$9.66 \cdot 10^{-1}$	[cm ³ /g]	GC model[37]
\bar{D}_0/D_{01}	$4.68 \cdot 10^{-4}$	[cm ² /s]	visc./temp. data (eq. 3.8)[3]
ω_1	$3.50 \cdot 10^1$		
ξ	$1.31 \cdot 10^0$		from \hat{V}_1^* and \hat{V}_2^* [4]
χ	$3.60 \cdot 10^{-1}$		estimate from data by Wang[29]

From the calculated parameters of table 3.2 it is now possible to calculate the solvent self-diffusion coefficient (D_1) using equation 3.4. For the migration modeling it is the polymer/solvent binary mutual diffusion coefficient that is needed, which can be calculated by equation 3.26[4].

$$D = D_1(1 - \phi_1)^2(1 - 2\chi\phi_1) \quad (3.26)$$

In figure 3.3 an approximated estimate of the Flory-Huggins polymer-solvent interaction parameter has been used ($\chi = 0.36$)[29] for the calculation of the mutual diffusion coefficient by equation 3.26. By this method an estimated diffusion coefficient for SNS with a weight ratio of approximately 0.35 at 298K is $7.0 \cdot 10^{-14}$ cm²/s. The calculated value of SNS from experimental data as shown in table 3.1 is approximately $6.0 \cdot 10^{-9}$ cm²/s.

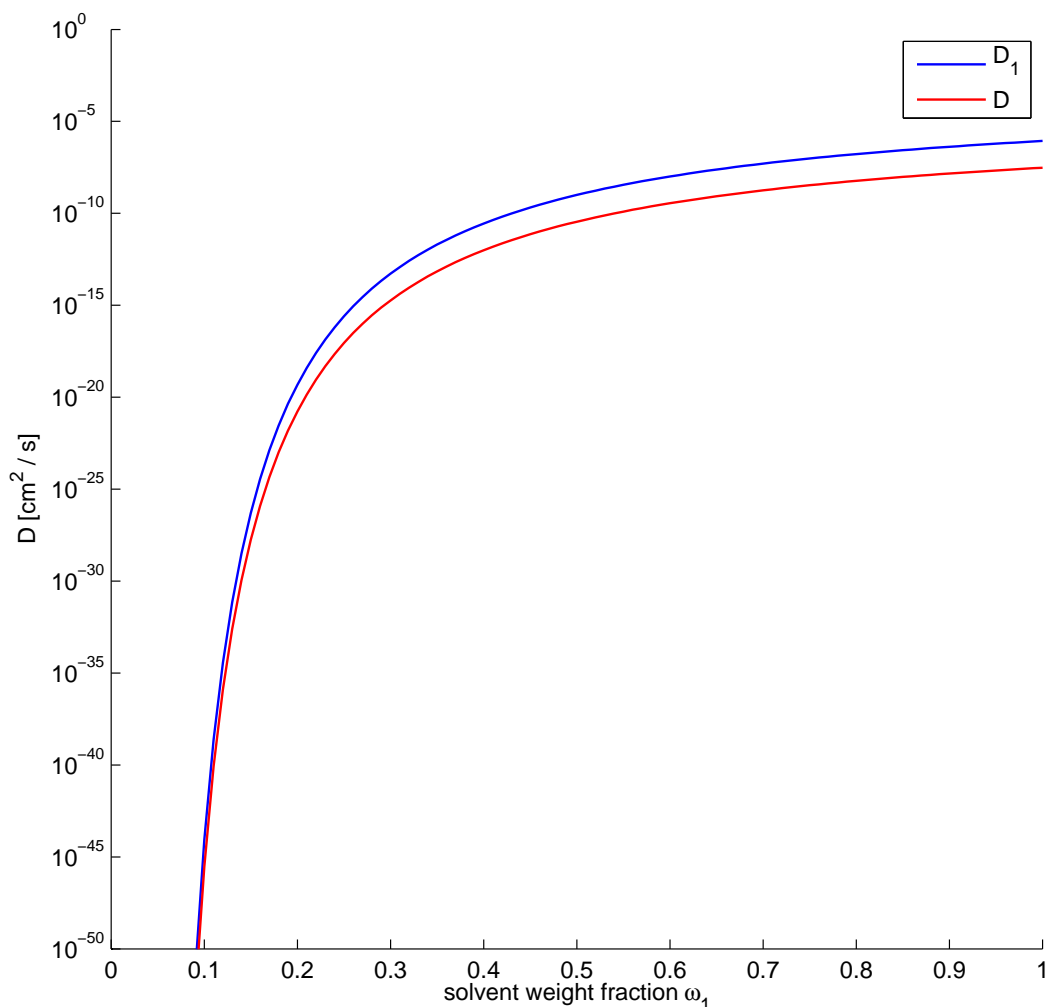


Figure 3.3: Estimated solvent self-diffusion coefficient (D_1 , eq 3.4) and the solvent diffusion coefficient from the Vrentas/Duda free volume model.

3.1.2 Conclusion

This complex model by Vrenta and Vrentas contains 7 to 12 physical parameters depending on how they are defined. The results shows for this specific case that the model under predict the experimentally derived mutual diffusion coefficients of this highly plasticised PVC. As highly plasticised PVC is a complex system, there is no guarantee that the experimentally derived diffusion coefficient is physically meaningful. But a system is never stronger than its weakest point. In this case the model uses up to 12 physically meaningful parameters, but many of these parameters are at best derived from fitting to experimental data and in many cases from group contribution models. This results in low predictive power for the model. Many of these estimated physically meaningful parameters for each of the pure components could just as well be grouped to one or two non-physical meaningful parameters fitted to one set of experimental data. Moreover, the estimated value of ξ is larger than 1, meaning that the jumping unit of the solvent (SNS) is larger than the jumping unit of the polymer for this system. To conclude, this

free volume model does not perform well for systems where ξ is larger than 1, i.e. for diffusion of very large organic molecules. The scope of this work has been to develop a simple method to be used by the industry (in this case specifically by Danisco) able to obtain accurate and reliable migration data, which proved to be very hard with the previously examined free volume model.

3.2 Empirical diffusion coefficient estimation

In 2003 a simplified, empirical approach to obtain diffusion coefficients for the migration modeling was approved in EU, for the cases where only little or none data exist for the system of interest. The model that was approved for this use, was the semi-empirical model proposed by Otto Piringer for safe over estimation of diffusion coefficients[14]. Safe over estimation means that the model is optimized to predict or overpredict at least 95% of the diffusion coefficient data that was used for the development of the model. The aim when developing the specific model has been to make a reliable model with as few as possible parameters, easy to use for industrial applications. The model is only dependent on three parameters: a purely empirical collective polymer specific parameter (A_p), the molecular weight of the migrant (M_r) and the temperature (T).

From the migration experiments of Danisco it was only the data of the ESBO plasticiser that followed the Arrhenius correlation. For this reason it was chosen to use only these data in order to find the polymer specific parameter A_p for the three PVC types in the study. In the book by Piringer[14] two versions of the diffusion coefficient estimation model (3.27 and 3.28) are presented:

$$D_p = 10^4 \exp \left(A_p - 0.01M_r - \frac{10454}{T} \right) \quad (3.27)$$

$$D_p = 10^4 \exp \left(\left(A'_p - \frac{\tau}{T} \right) - 0.1351M_r^{2/3} + 0.003M_r - \frac{10454}{T} \right) \quad (3.28)$$

3.2.1 A_p by equation 3.27

From the experimentally derived diffusion coefficients of ESBO in the three compounds it is possible to get the A_p value for each experiment when the molecular weight of the migrant is known. Table 3.3 shows the values and the mean values for the different PVC types:

Table 3.3: Experimentally derived A_p values for ESBO in PVC by equation 3.27, using the diffusion coefficients from table 3.1, temperature and the molecular weight of ESBO ($M_r = 905\text{g/mol}$)

	20°C	40°C	60°C	Mean A_p
Type 1	12.13	11.09	10.02	11.08
Type 2	12.70	12.18	10.34	11.74
Type 3	13.60	12.44	11.07	12.37

When the diffusion takes place in PVC it is suggested by Piringer to use only equation 3.27, but as it can be seen in figure 3.4, the A_p values seem to be dependent on temperature as well.

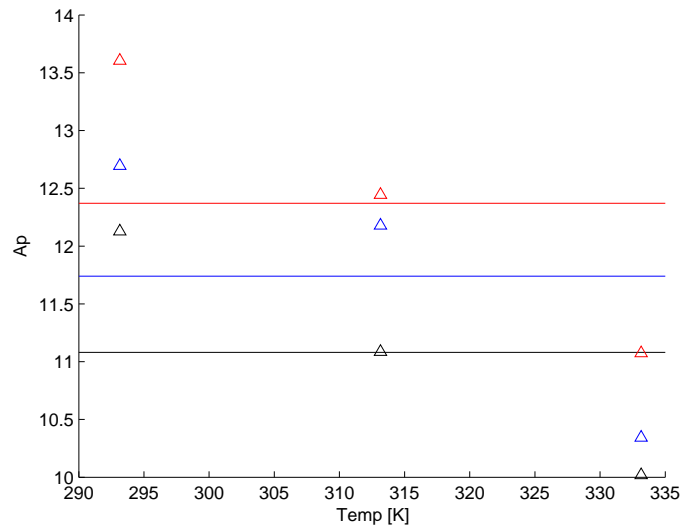


Figure 3.4: A_p mean value for each PVC type by equation 3.27. (black=type 1, red=type 2, blue=type 3)

3.2.2 A_p by equation 3.28

As for equation 3.27 the A_p value can be estimated for all the PVC types and temperatures of ESBO (see table 3.4).

Table 3.4: Experimentally derived A_p values for ESBO in PVC by equation 3.28 using the diffusion coefficients from table 3.1, temperature and the molecular weight of ESBO ($M_r = 905\text{g/mol}$).

	20°C	40°C	60°C
Type 1	13.00	11.96	10.89
Type 2	13.57	13.05	11.22
Type 3	14.48	13.32	11.95

From these A_p values the two polymer parameters of equation 3.28 can be calculated by linear regression ($A_p = A'_p - \frac{\tau}{T}$, see table 3.5). This gives a satisfactory fit of the model to the experimentally derived A_p values (see figure 3.5).

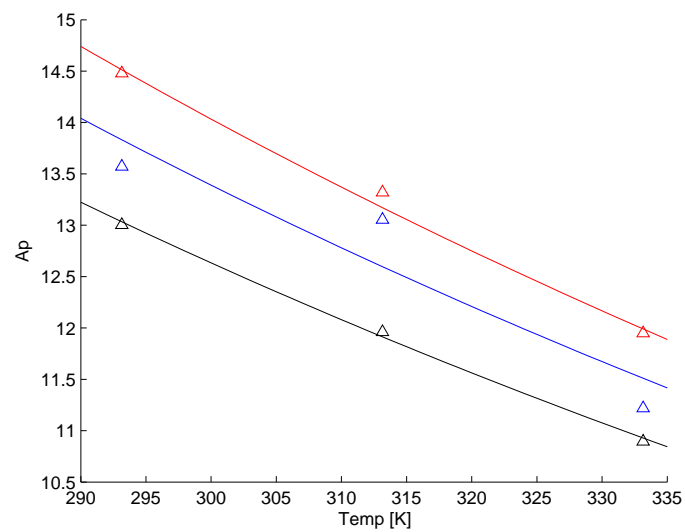


Figure 3.5: A_p now also dependent of temperature ($A_p = A'_p - \frac{\tau}{T}$) for each compound by equation 3.28. (black=type 1, red=type 2, blue=type 3)

The fitted parameters for equation 3.28 are presented in table 3.5:

Table 3.5: The fitted polymer parameters of equation 3.28, and the collected Arrhenius activation energy $E_A = (10454 + \tau)R$.

	A'_p	τ	E_A [kJ/mol]
Type 1	-4.5	-5140	44.16
Type 2	-5.5	-5667	39.78
Type 3	-6.5	-6160	35.68

3.2.3 Estimation of diffusion coefficients by equations 3.27 and 3.28

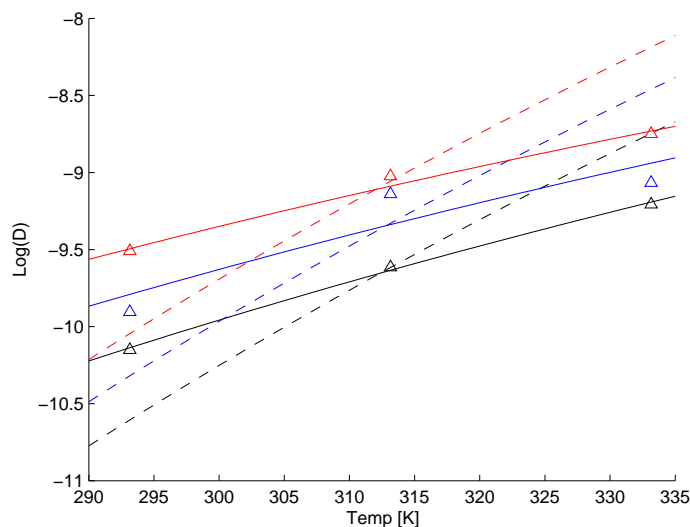


Figure 3.6: Estimation of the diffusion coefficients for ESBO in the three PVC compounds (black=type 1, red=type 2, blue=type 3). The dotted line corresponds to equation 3.27 results, and the filled corresponds to equation 3.28 results .

As it can be seen in figure 3.6 there is no doubt that equation 3.28 correlates more accurately the experimental data. In the book by Piringer[14] the listed A_p value for PVC ($T < 70^\circ C$) has a value of -4, which is very far from the value of A_p estimated here, which is in the area of 11 to 13. This is because the value for PVC in the Piringer book corresponds to empty and very rigid PVC. The "high" loading of plasticiser in the PVC in the experiments performed by Danisco makes the polymer much more flexible, hence a totally different specific polymer parameter is obtained. The results from this work have been confirmed by Otto Piringer himself as being very plausible (by private communications in 2008).

Once these polymer specific parameters have been obtained, it should be possible to estimate the diffusion coefficients for the two other plasticisers (SNS and Acetem), knowing that ESBO has a molecular weight of 905 g/mol, SNS of 500 g/mol and Acetem of 330 g/mol. The estimation for each of the three PVC types can be seen in figures 3.7 and 3.8.

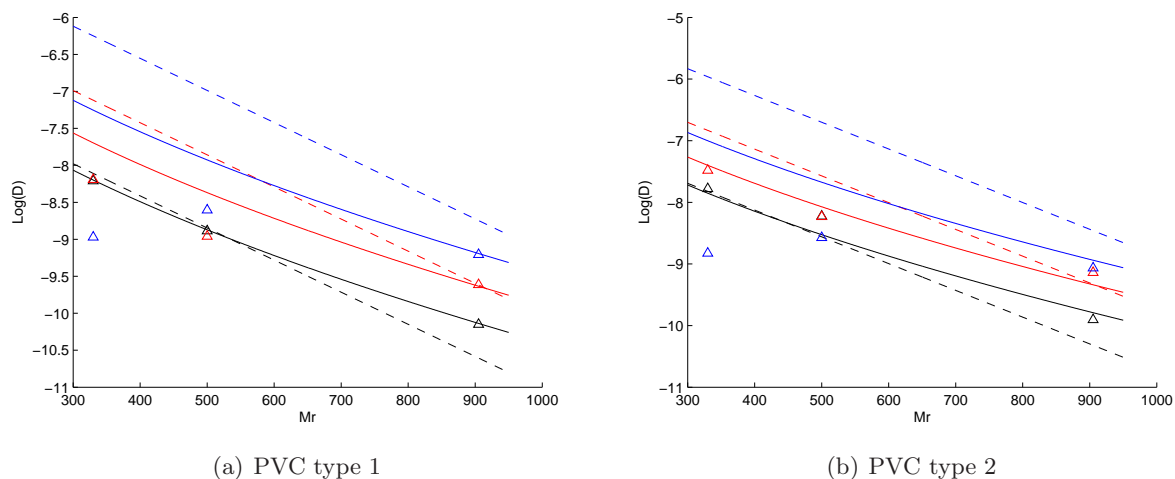


Figure 3.7: The estimation of the diffusion coefficient for **PVC Type 1 and 2**. Dashed line is obtained with eq. 3.27 and solid line is obtained with eq. 3.28. (black=20°C, red=40°C, blue=60°C)

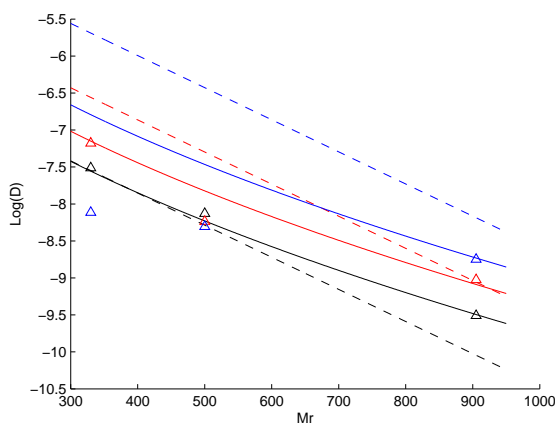


Figure 3.8: The estimation of the diffusion coefficient for **PVC Type 3**. Dashed line is obtained with eq. 3.27 and solid line obtained is with eq. 3.28. (black=20°C, red=40°C, blue=60°C)

From figures (3.7, 3.8) it is clear that the diffusion coefficients obtained experimentally (by the linear model, eq. 3.1) for SNS and Acetem at 40°C and 60°C are not as high as predicted by the Piringer model. This is thought to be because of the fast depletion of plasticisers from the outer area of the polymer, which gives a much lower diffusion through this more rigid PVC area. This partly depleted PVC polymer will then have a much different average mutual diffusion coefficient of the system. This is explained in more detail in section "Diffusion Coefficients from Experimental Data" in the article: "Modeling of the Migration of Glycerol Monoester Plasticisers in Highly Plasticised Poly(vinyl chloride)"[15], printed in appendix A. Moreover, it is clear that equation 3.28 makes the best fit also at higher molecular weights. Table 3.6 lists the estimated diffusion coefficients at 20°C of SNS, Acetem, ESBO and DEHP.

Table 3.6: Diffusion coefficients estimated (D_{calc} by equation 3.28) and from experimentally data (D_{exp}) for SNS, Acetem, ESBO and DEHP in PVC at 20°C. PVC type 1,2,3 are almost the same PVC compound only with minor changes to the ratio of the different additives in the final PVC compound (see section 2.1).

	M_w [g/mol]	PVC type 1		PVC type 2		PVC type 3	
		D_{calc} [cm ² /s]·10 ⁻¹⁰	D_{exp}	D_{calc} [cm ² /s]·10 ⁻¹⁰	D_{exp}	D_{calc} [cm ² /s]·10 ⁻¹⁰	D_{exp}
Acetem	330	62.68	61.66	139.32	166.01	275.71	307.36
DEHP	390	35.10		78.00		154.36	
SNS	500	13.32	13.00	29.59	59.54	58.56	74.30
ESBO	905	0.72	0.71	1.60	1.25	3.18	3.09

This methodology of estimating diffusion coefficients was used for the approval of SNS as plasticiser in Polyethylene terephthalate (PET) polymers by the American Food and Drug Administration (FDA) in 2009. The calculations was done using equation 3.28 with the specific polymer parameters of $A'_p = 6.0$ and $\tau = 1577$ as suggested by Begley et al.[39]. The calculated diffusion coefficients of SNS in PET by this method are: $D_{calc}(20^\circ\text{C}) = 2.53 \cdot 10^{-10} \text{ cm}^2/\text{s}$; $D_{calc}(40^\circ\text{C}) = 17.54 \cdot 10^{-10} \text{ cm}^2/\text{s}$; $D_{calc}(60^\circ\text{C}) = 96.33 \cdot 10^{-10} \text{ cm}^2/\text{s}$.

3.2.4 Conclusion

The fully estimated diffusion coefficients of SNS and Acetem at 20°C are very close to those experimentally derived. This shows the capability of this very simple model to give fairly good estimates of diffusion coefficients of similar migrants in the same polymer. The problem of over prediction of diffusion coefficients at the higher temperatures is probably related to the change of the polymer physics of the system due to fast depletion of plasticisers[15].It seems that the model is very applicable for the specific use of getting good and fast estimates of the diffusion coefficients.

3.3 Concentration dependent diffusion coefficient

Normally for migration modeling the Diffusion coefficient (D) is seen as concentration independent, which in most cases is acceptable. But for highly plasticised Polyvinyl Chloride (PVC), where the plasticisers migrates away from the polymer this concentration independence of the diffusion coefficient is not feasible any more. It is proposed that the diffusion coefficient in PVC can change from $10^{-7} \text{ cm}^2/\text{s}$ in fully plasticised PVC to around $10^{-16} \text{ cm}^2/\text{s}$ in depleted, rigid PVC[14]. This large span has to be implemented in the migration model in some way. As the migration is solved by fem methodology it is proposed to let the diffusion coefficient between each mesh point be a function of the local concentration. Three functions for this dependence is proposed:

Model 1:

$$D = \left(\frac{C_t}{C_0} \right)^w (D_{high} - D_{low}) + D_{low} \quad (3.29)$$

Model 2:

$$\log D = \left(\frac{C_t}{C_0} \right)^w (\log D_{high} - \log D_{low}) + \log D_{low} \quad (3.30)$$

where D is the calculated diffusion coefficient; D_{low} is the diffusion coefficient in rigid PVC; D_{high} is the diffusion coefficient in fully plasticised PVC; C_t is the local concentration of plasticiser at time t ; C_0 is the concentration of plasticiser at the beginning or when fully plasticised and w is the fitting parameter going from 0 to 1000 for model 1 and from 0 to 100 for model 2 (see figure 3.9).

These two models (eq. 3.29 and 3.30) are simply the completely linear relationship between the two outer points of the diffusion coefficient function (D_{low} is rigid and D_{high} fully plasticised PVC). Model 2 is the same as model 1 but the two outer points are represented as the logarithm of the diffusion coefficients. For both models the boundary conditions are fulfilled ($\frac{C_t}{C_0} = 0 \rightarrow D = D_{low}$ and $\frac{C_t}{C_0} = 1 \rightarrow D = D_{high}$). Plots of model 1 and 2 can be seen in figure 3.9, using some arbitrary model parameters covering most of the parameters space.

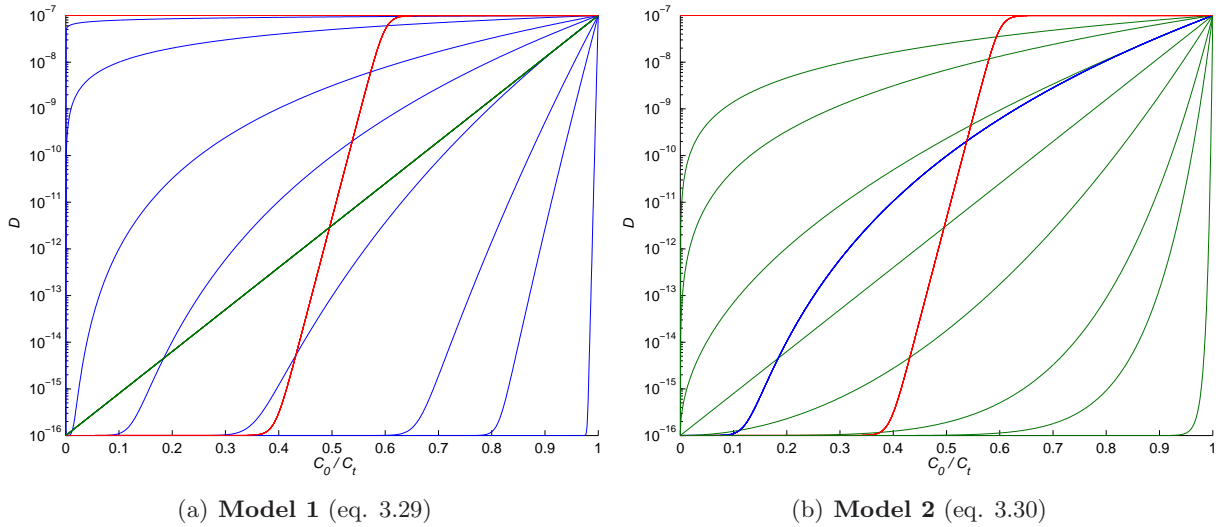


Figure 3.9: Plot of D as function of the local concentration when changing the w parameter for model 1 (left, $w=[0.1, 1, 5, 10, 20, 50, 100, 1000]$) and model 2 (right, $w=[0.1, 0.2, 0.5, 1, 2, 5, 10, 100]$). For reference in all graphs are plotted **model 1** ($w=10$), **model 2** ($w=1$) and **model 3** ($w=0.6$; $p=100$).

Model 3:

$$D = D_{low} + \frac{D_{high}}{1 + \exp\left(p \left(w - \frac{C_t}{C_0}\right)\right)} \quad (3.31)$$

where D is the calculated diffusion coefficient; D_{low} is the diffusion coefficient in rigid PVC;

D_{high} is the diffusion coefficient in fully plasticised PVC; C_t is the local concentration of plasticiser at time t ; C_0 is the concentration of plasticiser at start or when fully plasticised and w and p are fitting parameters going from 0 to 1 or 1 to 1000 respectively.

Model 3 (plotted in figure 3.10) is derived after discussing with professor Ole Hassager from the Danish Polymer Centre, Department of Chemical and Biochemical Engineering, DTU. If the concentration of the plasticiser is lowered in the polymer, then the glass transition temperature (T_g) will rise (the opposite of plasticisation of the polymer). At some stage as the concentration of the plasticiser changes T_g will be equal to the temperature of the system (T), if the system is at ambient temperature. At this point a big change of the diffusion coefficient is expected. Model 3 can mimic such a sudden change between the two outer values. The boundary conditions are not fulfilled as such in model 3, and some further derivations have to be done. Two new terms are introduced, D_{empty} (true diffusion coefficient at empty PVC) and D_{full} (true diffusion coefficient at fully plasticised PVC)

Boundary Condition 1, ($\frac{C_t}{C_0} = 0 \rightarrow D = D_{empty}$):

$$\begin{aligned} D_{empty} &= D_{low} + \frac{D_{high}}{1 + \exp(p(w-0))} \Leftrightarrow \\ D_{low} &= D_{empty} - \frac{D_{high}}{1 + \exp(pw)} \end{aligned} \quad (3.32)$$

Boundary Condition 2, ($\frac{C_t}{C_0} = 1 \rightarrow D = D_{full}$):

$$\begin{aligned} D_{full} &= D_{low} + \frac{D_{high}}{1 + \exp(p(w-1))} \Rightarrow \text{using Boundary Condition 1, eq. 4} \\ D_{full} &= D_{empty} - \frac{D_{high}}{1 + \exp(pw)} + \frac{D_{high}}{1 + \exp(p(w-1))} \Leftrightarrow \\ D_{full} - D_{empty} &= D_{high} \left(\frac{-1}{1 + \exp(pw)} + \frac{1}{1 + \exp(p(w-1))} \right) \Leftrightarrow \\ D_{high} &= \frac{D_{full} - D_{empty}}{\frac{1}{1 + \exp(p(w-1))} - \frac{1}{1 + \exp(pw)}} \end{aligned} \quad (3.33)$$

This means that model 3 (eq. 3.31) with the right boundary conditions (eq. 3.32 and 3.33) will be:

Model 3:

$$\begin{aligned} D &= D_{empty} - \frac{\frac{D_{full} - D_{empty}}{1 + \exp(p(w-1))} - \frac{1}{1 + \exp(pw)}}{1 + \exp(pw)} + \frac{\frac{D_{full} - D_{empty}}{1 + \exp(p(w-1))} - \frac{1}{1 + \exp(pw)}}{1 + \exp\left(p\left(w - \frac{C_t}{C_0}\right)\right)} \Leftrightarrow \\ D &= D_{empty} + \frac{D_{full} - D_{empty}}{\frac{1}{1 + \exp(p(w-1))} - \frac{1}{1 + \exp(pw)}} \left(\frac{1}{1 + \exp\left(p\left(w - \frac{C_t}{C_0}\right)\right)} - \frac{1}{1 + \exp(pw)} \right) \end{aligned} \quad (3.34)$$

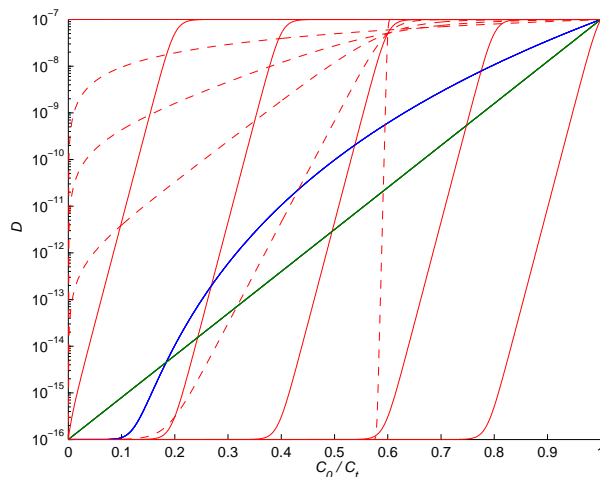


Figure 3.10: Plot of D as function of the local concentration when changing the w parameter ($w=[0.2, 0.4, 0.6, 0.8, 1.0]$, the full line with $p=100$) and the p parameter ($p=[1, 10, 20, 50, 100, 1000]$, broken lines with $w=0.6$) for model 3 (eq. 3.31). For reference in all graphs are plotted model 1 ($w=10$), model 2 ($w=1$) and model 3 ($w=0.6$; $p=100$).

Finally, an analytical model with a concentration independent diffusion coefficient which in earlier investigations showed capabilities to mimic the slower migration along with the depletion of the plasticiser from the polymer was also tested against the migration data[15]. This model was originally developed by Kondyli et al.[40] for migration into more or less agitated solutions. In this model (named model 4) the fitting is done on the agitation parameter "u", and this model is not solved by the `fem` methodology but by calculating the migration as a function of time t .

Model 4:

$$\begin{aligned} \frac{M_t}{M_\infty} &= \frac{ut}{2L} \operatorname{erf}\left(\frac{ut}{2\sqrt{Dt}}\right) - \frac{ut-L}{2L} \operatorname{erf}\left(\frac{L-ut}{2\sqrt{Dt}}\right) + \frac{1}{2} \\ &+ \frac{\sqrt{Dt}}{L\sqrt{\pi}} \left\{ \exp\left[-\frac{(ut)^2}{4Dt}\right] - \exp\left[-\frac{(L-ut)^2}{4Dt}\right] \right\} \end{aligned} \quad (3.35)$$

With the migration data at 20°C it was possible with the normal concentration independent diffusion coefficient to obtain fairly good correlation to the experimental data[15], but this was not possible at 40°C and at 60°C. This investigation around concentration-dependent diffusion coefficient modeling aims at finding better methods for the estimation of migration data at 40°C and 60°C, but of course all available data were used. From the same migration data as used in this investigation the polymer specific parameters for the Piringer model[14] for diffusion coefficient estimation have been found[15]. These parameters can be seen in table 3.4.

In the fitting calculations the diffusion coefficient of the empty, rigid PVC (D_{low} or D_{empty}) was set to the same value calculated by equation 3.27 using the polymer specific parameters given by Piringer for rigid PVC ($A_p = -4$), which give diffusion coefficients in the order of $\sim 10^{-17}$ cm²/s. For the diffusion coefficient of the fully plasticised PVC (D_{high} or D_{full}) three different

values where used.

D_{Ap}	Calculated with eq. 3.27 using an A_p value of 14.
D_{Ap2}	Calculated with eq. 3.28 using an A_p value of 20 and $\tau = 1577$.
D_{est}	Calculated with eq. 3.28 using data from table 3.4.

The fitting was done via the optimisation functions in MatLab (R2008a) called "lsqnonlin" and "fmincon". The objective function used is:

$$f_{eval} = \sum_{t=1}^n \left(\frac{x_t - M_t}{x_t} \right)^2 \quad (3.36)$$

where x_t is migration measured at time t , M_t is the estimated migration at time t , and n is the number of samples (here 7).

3.3.1 Results

SNS

As it can be seen in table 3.7, model 4 (the analytical model by Kondyli et al. eq. 3.35) is not very accurate at 40°C and especially at 60°C. Furthermore, the agreement when using D_{Ap2} or D_{Ap} , which are diffusion coefficients with no use of experimental data, is very poor. When comparing models 1-3 (the models with concentration dependent diffusion coefficient) it is clear that there is no significant difference in the results when using D_{est} , D_{Ap2} or D_{Ap} . Should one be chosen, it must be D_{Ap2} when looking at all three temperatures. In the same way the difference between using models 2 or 3 is very small, although these two models are somewhat better than model 1.

Table 3.7: The optimal value of the objective function (f_{eval} in eq. 3.36) for all the experiments with SNS. The value is multiplied with 100 for easier reading of the table. For each experiment the best fit is indicated with **bold letters**.

Temp	Compound	Model	D_{est}		D_{Ap2}	D_{Ap}
			(lsq)	(fmin)	(fmin)	(fmin)
20°C	1	1	109	109	87	33
		2	110	110	88	35
		3	138	109	63	38
		4	991	995	31	4061
	2	1	505	505	8	26
		2	505	505	8	24
		3	716	508	6	34
		4	882	882	355	163

table 3.7 – continued

Temp	Compound	Model	D_{est}		D_{Ap2}	D_{Ap}	
			(lsq)	(fmin)	(fmin)	(fmin)	
40°C	3	1	75	75	43	13	
		2	75	75	43	12	
		3	160	85	43	22	
		4	654	654	580	47	
	1	1	1	185	185	6958	3364
			2	186	186	121	155
			3	180	179	127	191
			4	141	141	29170	66026
		2	1	96	96	60	194
			2	97	97	50	165
			3	77	77	42	450
			4	472	472	1380	5583
		3	1	204	206	63	107
			2	207	206	63	86
			3	132	132	60	124
			4	304	304	788	3633
60°C	1	1	13	13	4947	173	
		2	13	13	82	132	
		3	15	15	96	140	
		4	91	91	129254	178930	
	2	1	75	76	39	4739	
		2	74	74	36	41	
		3	83	83	41	61	
		4	516	516	75702	103966	
	3	1	57	57	61	4990	
		2	58	58	54	76	
		3	59	59	67	103	
		4	296	296	38900	54820	

With this knowledge when looking at table 3.8 with the optimal parameters of the models, it is clear that by average the optimal p parameters for model 3 is around 20. this means that

the optimal slope of model 3 (see figure 3.10) is almost the same as for models 1 and 2. It was hoped that when making the calculated diffusion coefficient a function of the temperature (D_{est} , D_{Ap2} or D_{Ap}) it would be possible to obtain a good average parameter from the fitting at the different temperatures. But as it can be seen the optimal parameters for models 2 and 3 (the w parameter) are not the same for the three temperatures. This is not even the case within the same temperature where the optimal parameter deviates significantly between the three PVC types.

Table 3.8: The optimal parameters (w and p) for SNS for models 1-3. For model 4 the optimal agitation parameter u is listed in the w column and it is multiplied with 10^5 .

Temp	Compound	Model	D_{est}		D_{Ap2}		D_{Ap}			
			(lsq)		(fmin)		(fmin)			
			w	p	w	p	w	p		
20°C	1	1	0.02		0.02		1.74		4.68	
		2	0.00		0.00		0.11		0.28	
		3	0.03	20	0.00	120	0.55	20	0.77	20
		4	7.23		6.77		0.15		0.00	
	2	1	0.00		0.00		0.10		1.51	
		2	0.00		0.00		0.01		0.09	
		3	0.01	20	0.00	1000	0.00	20	0.64	5
		4	38.68		38.92		36.61		26.80	
	3	1	0.00		0.00		0.00		1.22	
		2	0.00		0.00		0.00		0.07	
		3	0.01	20	0.00	121	0.00	431	0.50	7
		4	39.98		39.96		39.90		34.14	
40°C	1	1	1.58		1.58		72.42		38.69	
		2	0.12		0.12		0.69		1.03	
		3	0.53	20	0.53	20	1.00	15	1.00	22
		4	0.00		0.00		0.00		0.00	
	2	1	0.25		0.25		3.39		6.06	
		2	0.02		0.02		0.22		0.37	
		3	0.13	20	0.13	20	1.00	6	0.82	20
		4	31.59		31.56		0.00		0.00	

table 3.8 – continued

Temp	Compound	Model	D_{est}		D_{Ap2}		D_{Ap}				
			(lsq)		(fmin)		(fmin)				
			w	p	w	p	w	p			
60°C	3	1	0.74		0.74		3.24		5.66		
		2	0.05		0.05		0.21		0.35		
		3	0.32	20	0.32	20	0.85	7	0.89	12	
		4	27.51		27.36		0.15		0.00		
	60°C	1	1	1.79		1.79		72.42		32.09	
			2	0.15		0.15		1.61		1.92	
			3	0.57	20	0.57	20	1.00	31	0.99	40
			4	0.00		0.00		0.00		0.00	
		2	1	2.36		2.38		19.69		65.21	
			2	0.19		0.19		1.30		1.67	
			3	0.63	20	0.63	20	1.00	27	0.99	35
			4	0.00		0.00		0.00		0.00	
3		1	2.20		2.20		14.85		154.03		
		2	0.17		0.17		0.97		1.27		
		3	0.62	20	0.62	20	1.00	21	1.00	27	
		4	0.00		0.00		0.00		0.00		

In figure 3.11 are shown two examples for the best fit of the models to SNS migration from PVC type 3 at 40°C and 60°C. The models are compared to the estimated migration by the analytical solution of Crank[41] with the calculated diffusion coefficient from the first 5 data points (D_{exp}).

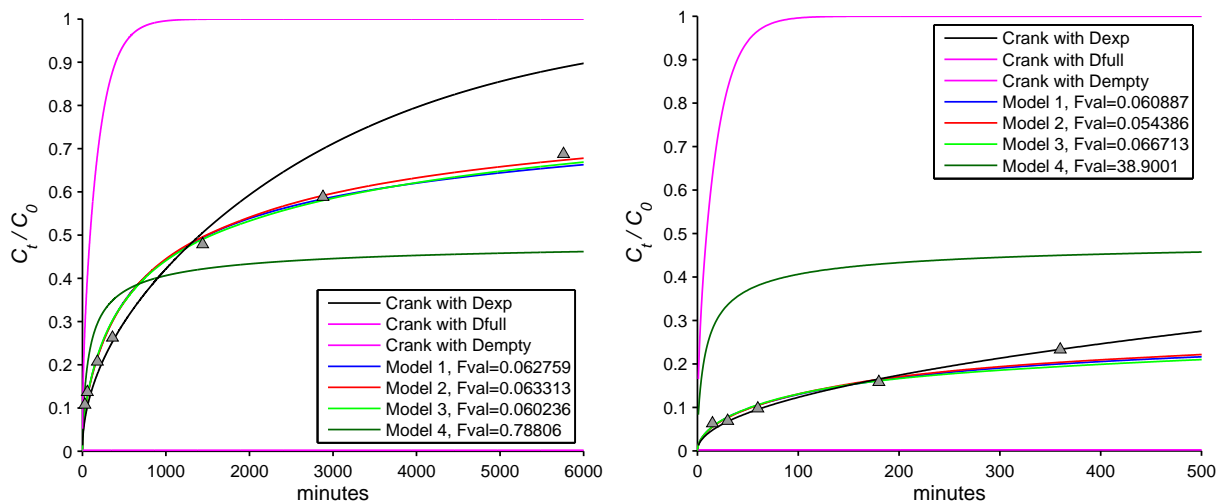


Figure 3.11: Migration estimated with the optimal parameter fitting results (listed in table 3.10) of the 4 models for SNS in PVC type 3 at 40°C (left) and 60°C (right) using D_{Ap2} . Also in the figure is plotted the migration using the analytical migration model of Crank (eq. 4.1) using the three diffusion coefficients D_{empty} , D_{exp} , D_{full} .

Acetem

As for SNS, model 4 performs poorly compared to the other models at 60°C (see table 3.9). When comparing the other three models over all temperatures it is seen that, as for SNS, models 2 and 3 perform somewhat better than model 1. For Acetem using D_{est} and D_{Ap2} in models 1 and 2 the results are overall about equally good.

Table 3.9: The optimal value of the objective function (f_{eval} in eq. 3.36) for all the experiments with Acetem. The value is multiplied with 100 for easier reading of the table. For each experiment the best fit is indicated with **bold letters**.

Temp	Compound	Model	D_{est} fmin	D_{Ap2} fmin	D_{Ap} fmin
20°C	1	1	130	264	617
		2	130	255	585
		3	134	285	631
		4	185	825	7570
	2	1	67	78	284
		2	67	78	261
		3	70	140	236
		4	108	24	1603

table 3.9 – continued

Temp	Compound	Model	D_{est} fmin	D_{Ap2} fmin	D_{Ap} fmin
	3	1	43	38	36
		2	43	38	31
		3	40	31	45
		4	166	141	179
40°C	1	1	165	231	455
		2	170	186	368
		3	102	193	436
		4	153	7061	13533
	2	1	132	128	422
		2	132	105	345
		3	73	83	715
		4	214	1031	2604
	3	1	252	108	152
		2	252	116	136
		3	238	105	131
		4	305	178	394
60°C	1	1	3251	300	186
		2	52	187	1368
		3	51	143	160
		4	37257	658300	768552
	2	1	4647	64	4951
		2	128	56	351
		3	125	68	71
		4	25051	221284	256737
	3	1	405	4658	479
		2	407	444	468
		3	430	473	480
		4	8082	54238	63394

When looking at the optimal parameters found for Acetem (table 3.10) there is no tendency towards one optimal p parameter when looking at D_{Ap2} . When D_{est} is used the value $p=20$ is again the optimal value, as for SNS. As for SNS, there are no overall best w parameters for

models 2 and 3, not even at each temperature.

Table 3.10: The optimal parameters (w and p) for Acetem for models 1-3. For model 4 the optimal agitation parameter u is listed in the w column and is multiplied with 10^5 .

Temp	Compound	Model	D_{est}		D_{Ap2}		D_{Ap}	
			(fmin)		(fmin)		(fmin)	
			w	p	w	p	w	p
20°C	1	1	0.10		1.89		5.56	
		2	0.01		0.12		0.34	
		3	0.00	20	0.73	6	0.94	10
		4	44.98		19.79		0.00	
	2	1	0.00		0.63		2.79	
		2	0.00		0.04		0.17	
		3	0.00	75	0.28	20	1.00	5
		4	116.43		92.85		44.06	
	3	1	0.00		0.05		1.58	
		2	0.00		0.00		0.09	
		3	0.02	638	0.00	20	0.65	6
		4	186.11		183.41		135.27	
40°C	1	1	1.12		7.51		12.19	
		2	0.09		0.50		0.77	
		3	0.42	20	1.00	11	1.00	17
		4	24.00		0.00		0.00	
	2	1	0.30		3.31		6.06	
		2	0.02		0.22		0.37	
		3	0.17	20	1.00	6	0.81	15
		4	159.96		112.19		82.73	
	3	1	0.00		1.85		3.56	
		2	0.00		0.12		0.22	
		3	0.05	20	0.59	9	1.00	7
		4	424.77		261.22		347.51	
60°C	1	1	33.60		42.05		49.85	
		2	0.86		3.61		3.47	
		3	0.92	20	1.00	53	1.00	59
		4	0.00		0.00		0.00	

table 3.10 – continued

Temp	Compound	Model	D_{est}		D_{Ap2}		D_{Ap}	
			(fmin)		(fmin)		(fmin)	
			w	p	w	p	w	p
	2	1	49.85		37.70		109.59	
		2	0.78		2.94		2.95	
		3	0.91	20	1.00	47	1.00	52
		4	0.00		0.00		0.00	
	3	1	6.11		65.21		32.09	
		2	0.50		1.80		2.25	
		3	0.83	20	0.99	35	1.00	40
		4	0.00		0.00		0.00	

In figure 3.12 are shown two examples given for the best fit of the models to Acetem migration from PVC type 3 at 40°C and 60°C. The models are compared to the estimated migration by the analytical solution of Crank[41] with the calculated diffusion coefficient based on the first 5 data points (D_{exp}). As it can be seen the quality of experimental migration data is not very good in all cases, fact which partly explains the somewhat poor performance of the models.

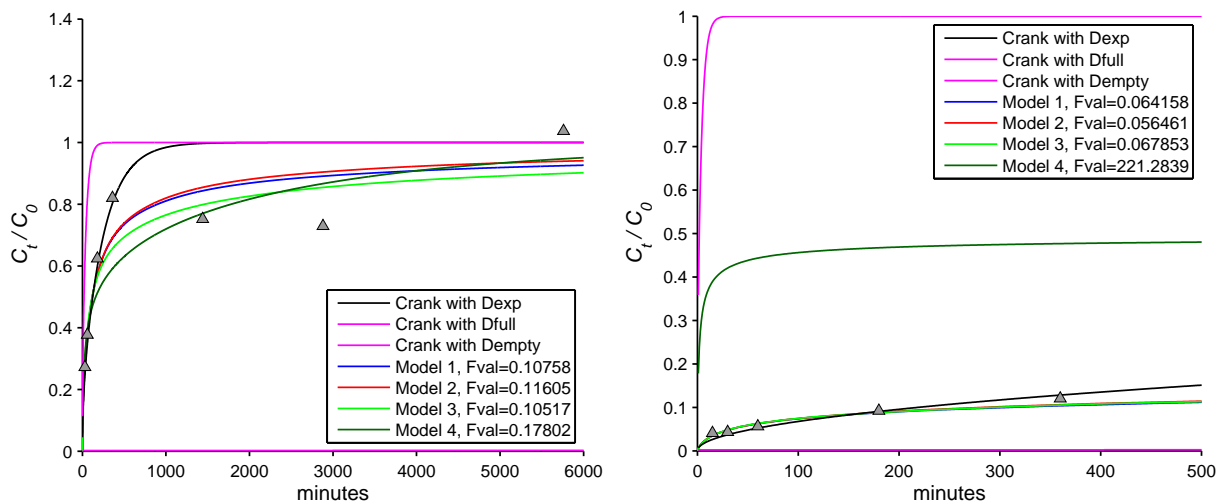


Figure 3.12: Migration estimated with the optimal parameter fittings (listed in table 3.10) of the 4 models for Acetem in PVC type 3 at 40°C (left) and PVC type 2 60°C (right) using D_{Ap2} . Also in the figure is plotted the migration using the analytical migration model of Crank using the three diffusion coefficients D_{empty} , D_{exp} , D_{full} . Especially on the left plot the scattering of the experimental migration data can be clearly seen.

3.3.2 Conclusion

The main conclusion from this investigation is that no new final model with physically meaningful parameters has been found, able to correlate satisfactorily the migration data of the plasticisers in highly plasticised PVC. However, when compared to the proposed best migration model with concentration independent diffusion coefficient (model 4, eq. 3.35), all three new suggested models perform better with optimised parameters. Models 2 and 3 seem to perform overall slightly better than model 1, and D_{Ap2} is the best function to use for calculating the diffusion coefficient of the fully plasticised PVC as a function of temperature.

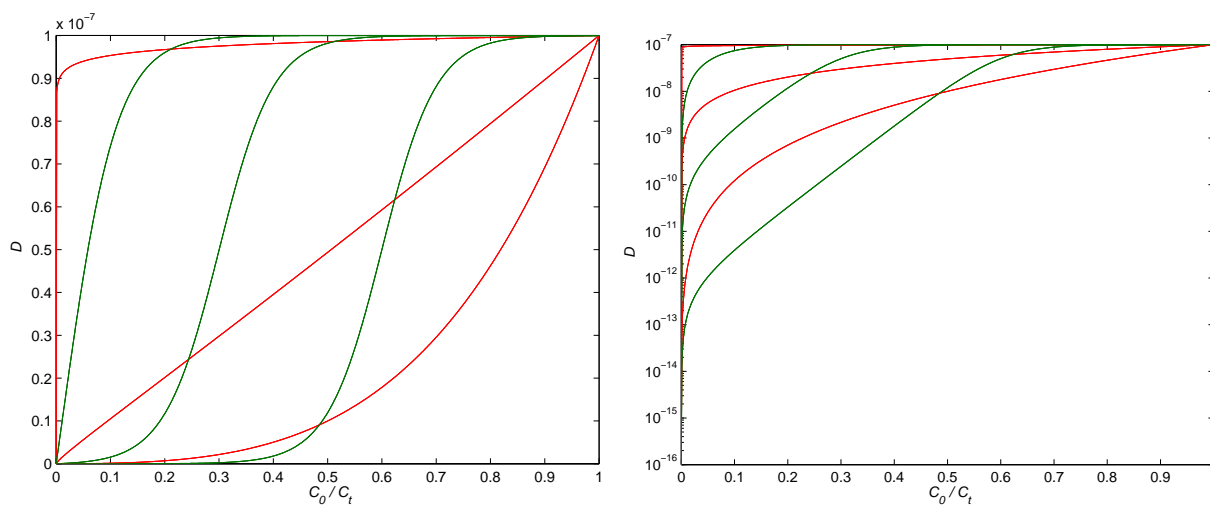


Figure 3.13: Plot of the overall optimal parameters for **model 2** ($w=[0.00\ 0.05,\ 0.17]$, at 20°C , 40°C , 60°C respectively) and for **model 3** ($p=20$; $w=[0.01\ 0.3,\ 0.6]$, at 20°C , 40°C , 60°C respectively). The left figure is with linear scale of the diffusion coefficient and the right is with logarithmic scale. For both models is the plot of the function going towards the lower right corner as the temperature rise. Especially on the logarithmic plot (right) it can be seen that the optimal function for the two models lies fairly close at each temperature; 20°C corresponds to the two plots most up in the top left corner, 40°C corresponds to the next two and 60°C corresponds to the ones furthest down towards the middle of the graph.

The optimum parameters of models 2 and 3 are shown in figure 3.13 and as it can be seen, the optimal functions, when going from D_{empty} to D_{full} , are fairly close to each other for the two models at all three temperatures examined.

Migration

In this work the focus has been so far to accurately predict migration of additives in a polymer and into food (often as migration from food packaging), in order to comply with the systematic migration limits (SML) set by EU[12, 16–20] as described in chapter 2. For simplification and unification of the experimental work and/or calculations that have to be done in order to get a product approved by the legislation, four food simulants have been chosen by the European Commission[12]:

- (A) Distilled water
- (B) 3% Acetic Acid (weight/volume)
- (C) 10% Ethanol (volume/volume)
- (D) Olive oil or Sunflower oil (in some cases Iso-octane)

In the specific case of milk and similar products, it is suggested to use 50% ethanol as the food simulant.

For systems with a low concentration of the additive in the polymer and consisting of only one polymer layer, this migration can be solved analytical by the solution of Fick's second law of diffusion as done by Crank in his book: "Mathematics of diffusion"[41]. Equation 4.1 is the solution by Crank for the simple system of migration from a polymer layer and into a solvent, which also is the solution suggested by Piringer for this system[14].

$$\frac{M_t}{M_\infty} = 1 - \sum_{n=1}^{\infty} \frac{2\alpha(1+\alpha)}{1+\alpha+\alpha^2q_n^2} \exp\left(\frac{-Dtq_n^2}{L^2}\right) \quad (4.1)$$

where M_t is the migration at time t , M_∞ is the migration at infinite time, D the diffusion coefficient, L is the thickness of the polymer and q_n is the positive roots of $[\tan q_n = -\alpha q_n]$. α is a dimensionless quantity taking the solubility of the migrant in the solvent and the volume ratio of the polymer to the solvent into account. $\alpha = \frac{1}{K} \frac{V_s}{V_p}$, where $\frac{V_s}{V_p}$ is the volume ratio of the

solvent over the polymer and K is the partition coefficient of the migrant in the polymer over the solvent, $K = \frac{C_{p,\infty}}{C_{s,\infty}}$.

For highly plasticised PVC, the concentration of the migrant (the plasticiser itself) is so high, that the depletion of the plasticiser from the polymer effects the structural behavior of the polymer. Such system are not readily solved by solutions such as Eq. 4.1. The analytical solution (eq. 4.2), originally developed by Kondyli et al. to systems under strong agitation of the solvent[40], has been used with some success for this kind of systems[15].

$$\begin{aligned} \frac{M_t}{M_\infty} = & \frac{ut}{2L} \operatorname{erf} \left(\frac{ut}{2\sqrt{Dt}} \right) - \frac{ut-L}{2L} \operatorname{erf} \left(\frac{L-ut}{2\sqrt{Dt}} \right) + \frac{1}{2} \\ & + \frac{\sqrt{Dt}}{L\sqrt{\pi}} \left\{ \exp \left[-\frac{(ut)^2}{4Dt} \right] - \exp \left[-\frac{(L-ut)^2}{4Dt} \right] \right\} \end{aligned} \quad (4.2)$$

Migration in multilayer systems (migration from and between several polymer layers and into a solvent) can not be solved by analytical solution such as eq. 4.1 and 4.2. For this kind of systems, solutions can be found only when numerical methods are used like the finite element method (FEM). Within this method the system is split up into multiple, simplified, linked elements that are solved simultaneously numerically. In this work such a solution has been programmed in MATLAB using the algorithms of COMSOL to solve the partial differential equations (PDE). The mesh structure and a concentration profile using this solution for an example system is shown in figure 4.1.

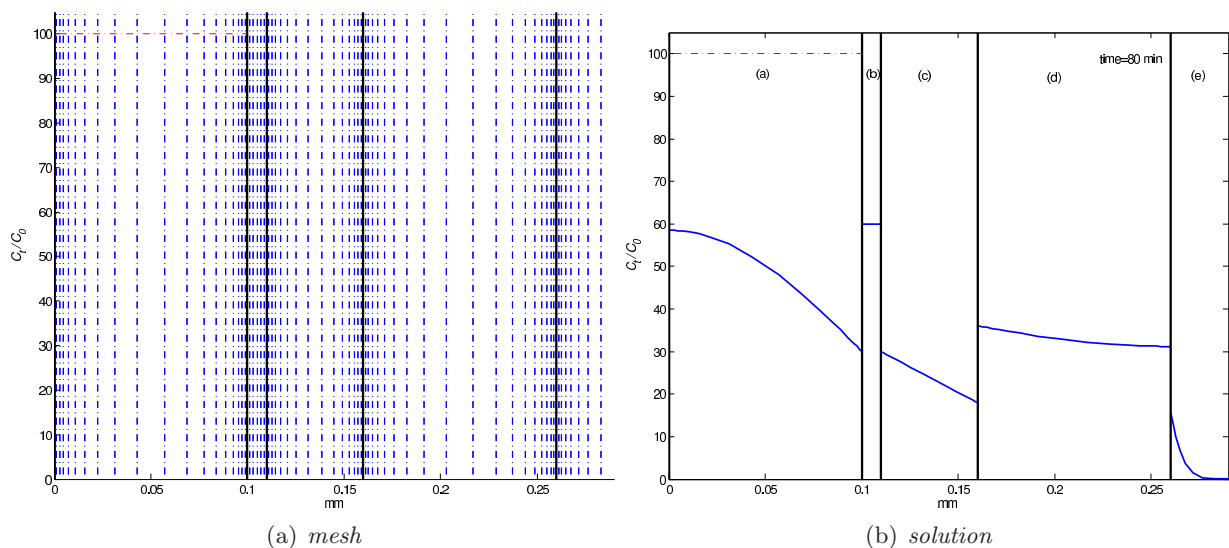


Figure 4.1: (a) The mesh structure set up for the solution of a system of 4 polymer layers (thickness from left to right: 0.1mm; 0.01mm; 0.05mm; 0.1mm) and a solvent on the far right. (b) The concentration profile after 80 min, with diffusion coefficients from left to right of $1 \cdot 10^{-12}$; $1 \cdot 10^{-10}$; $2 \cdot 10^{-12}$; $5 \cdot 10^{-12}$ [cm^2/s], and partitions coefficients of $K_{ab} = K_{cd} = 2$ and $K_{bc} = K_{de} = 0.5$

The commercially available software "AKTS-SML[®]"[42] solves the migration problem in the same way, but lacks the possibility to change the algorithm to calculate the diffusion coefficient as a function of the local concentration, something that was needed in this work. During this PhD, I had the chance to get trained in the use of the "AKTS-SML[®]", and have compared results from the developed MATLAB/COMSOL code to results from the commercial software. In figure 4.2 is shown a solution with "AKTS-SML[®]" for benzophenone migrating in a confined LDPE/LDPE/PP polymer. This solution is compared to experimentally derived concentration profiles (from IR measurements done by AKTS).

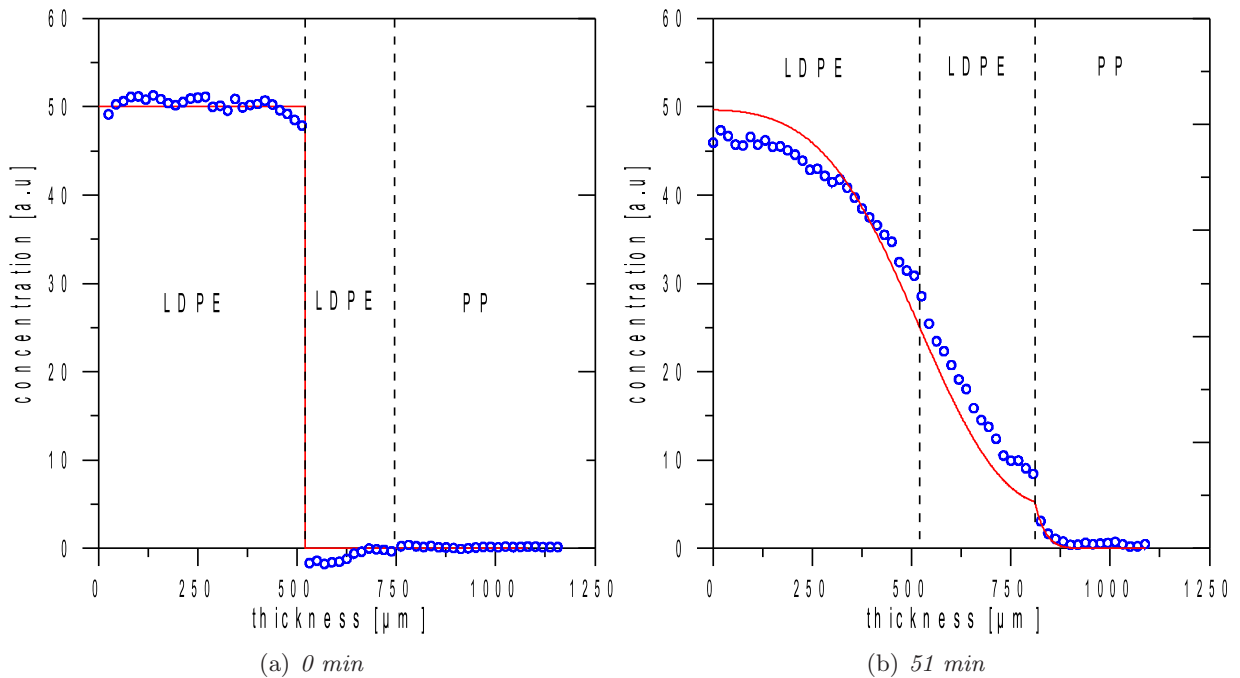


Figure 4.2: Migration of benzophenone in a confined LDPE/LDPE/PP polymer solved with "AKTS-SML[®]". Circles are experimentally derived concentration values from IR measurements done by AKTS.

4.1 Modeling of migration in highly plasticised PVC

The migration of additives in most polymers can be modeled with good results by analytical models like eq. 4.1 for simple systems. For very complex systems a numerical solution may be required of the Partial differential equations (PDEs) of the Ficks second law of diffusion by the use of finite element method (FEM), either by specialised software for migration (i.e. "AKTS-SML[®]"[42] or "FABES-MIGRATEST[®] EXP"[43]) or by more generalized tools like "COM-SOL Multiphysics[®]"[44]. These solutions work only because the migration of the additive has very little or no influence on the system, i.e. the concentration change of the additive in the polymer does not affect the physical or chemical structure of the polymer.

For highly plasticised PVC this is however not the case, when the migrant of interest is either the plasticiser itself or a migrant that has a plasticising effect. For PVC the diffusion coefficient of the migrant can change from around 10^{-7} cm²/s for fully plasticised PVC to around 10^{-16} cm²/s for unplasticised, rigid PVC. This means that in highly plasticised areas the migration will be fast and in areas with little plasticiser the structure will be very crystalline and with slow migration. For PVC to be highly plasticised and flexible it needs to contain a volume percent of the plasticiser between 30-60%. Using analytical solution this problem has been directed in the article: "Modeling of the Migration of Glycerol Monoester Plasticizers in Highly Plasticized Poly(vinyl chloride)". In this article it is described how this problem can be modeled with some success using the analytical solution (eq. 4.2 original derived by Kondyli et al.[40] for migration into solvents under agitation. This article can be seen in appendix A.

As an extension of this work it was investigated if the numerical solution by the FEM method could be used to allow the diffusion coefficient to be dependent on the local plasticiser concentration. This work is shown in the section 3.3 "Concentration dependent diffusion coefficient".

4.1.1 Conclusion

Highly plasticised PVC is a very complex polymer to model the migration, especially when the concentration of the plasticiser changes over time. Using either the specialised analytical solution (eq. 4.2) or the approach of concentration dependent diffusion coefficients with the numerical solution by FEM can give good fit to experimental data. The problem however with both of these solutions is that still some parameters have to be fitted to the experimental data, making both approaches difficult to use if no experimental data exist.

4.2 Modeling of antistatic additive migration

4.2.1 The antistatic additive project

The purpose of the antistatic project was to investigate and obtain an improved understanding of the mechanisms that make different commercial available antistatic polymer additives produced by Danisco effective antistatic agents in mainly polypropylene, but also in polyethylene and other polyolefines. All antistatic agents produced by Danisco are different variants of glycerol monostearate (GMS), and more specifically these products are mainly composed by monoglycerides (but also some di- and triglycerides) from palmitic and stearic acids (see figure 4.3).

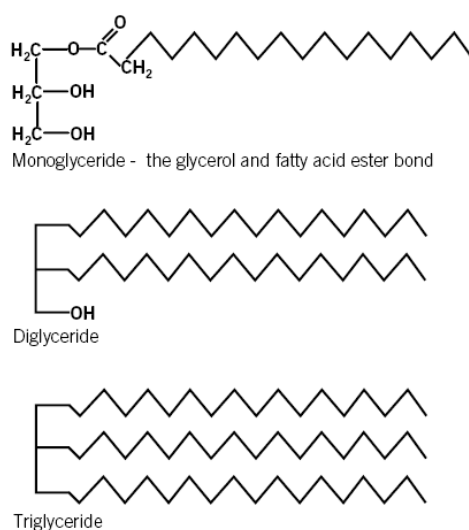


Figure 4.3: The main components of glycerol monostearate (GMS) used as antistatic additive. Mono, di- and triglycerides where the fatty acid profile is most commonly a mixture of palmitic and stearic acids.

It is believed that the GMS molecules migrate to the surface of the polymer and together with water from the air they aggregate resulting to a current conducting layer (see figure 4.4), which prevents building up of an antistatic charge on the polymer. For some reason the GMS-based antistatic additive does not perform equally well in different polymers, even when added in the same amount to the polymers. It is believed that the migration rate of GMS in the polymer is the main reason for this behavior, i.e. too fast or too slow migration of GMS to the surface will counteract the antistatic mechanism.

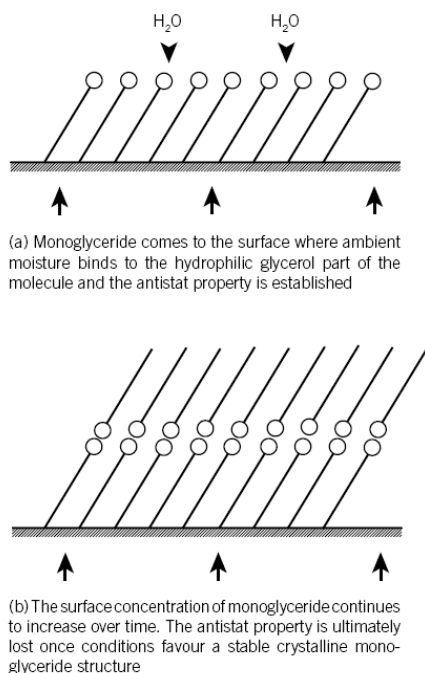


Figure 4.4: The proposed mechanism of aggregation of the glycerol monostearate and water on the surface of the polymer to produce the antistatic effect.

A new research project was therefore launched by Danisco in summer 2009, where Rasmus Lundsgaard contributed with expertise on migration modeling of additives in polymers. New migration experiments were conducted at Danisco, and the purpose of the work presented here was to model these new migration data obtained using the previously developed migration model (see section 4). The modelling results of the migration data available could hopefully lead to a better understanding of the transport of the antistatic additive from the bulk polymer to the surface.

The experimental work at Danisco included 4 different types of experiments run over 60 days on the same systems and at same sampling times. The test systems consisted of either low density polyethylene (LDPE) or polypropylene (PP), where problems were encountered only when the current antistatic additive was used for the PP polymer. The antistatics used were either an already commercially successful antistatic additive (DIMODAN HP), or a newly developed candidate (PGE 308). The PGE 308 is still under development at Danisco, and for this reason can no further details be given regarding the structure of PGE 308.

A short description of the 4 experiments that were conducted at Danisco are presented in table 4.1.

Table 4.1: The 4 simultaneous experiments conducted in the antistatic additive study at Danisco and RISØ-DTU.

Experiment	Description and conclusion									
Static decay time:	<p>Measurement of antistatic performance. The general conclusion from this experiment was:</p> <table border="1"> <thead> <tr> <th></th> <th>DIMODAN HP</th> <th>PGE 308</th> </tr> </thead> <tbody> <tr> <td>LDPE</td> <td>Good</td> <td>Very good</td> </tr> <tr> <td>PP</td> <td>poor to none</td> <td>none</td> </tr> </tbody> </table>		DIMODAN HP	PGE 308	LDPE	Good	Very good	PP	poor to none	none
	DIMODAN HP	PGE 308								
LDPE	Good	Very good								
PP	poor to none	none								
Contact angle measurement:	<p>This experiment was conducted by measuring the contact angle for each sample with only two solutes. The surface tension from these experiments were thereby presented as a polar and a dispersive part. The measured surface tension values from all the experiments did not lead to some safe conclusion,</p>									
XPS:	<p>X-ray photo-electron spectroscopy, which was used to measure the specific oxygen concentration in layers carved from the surface of the polymer. This measurement was also conducted by Rasmus Lundsgaard at RISØ-DTU (a national laboratory under DTU). These measurements were conducted together with master student Julien Danguillaume as a special course[45]. Unfortunately the XPS equipment at RISØ suffered from a lot of breakdowns in the 60 days test period, so oxygen surface concentration values measured were strongly deviating. Results from this experiment are shown in appendix B</p>									
Migration:	<p>Measurement of the amount of additive migrated to the surface at the sampling time-points selected. This was done by dipping the polymer into iso-octane for a predefined time interval (10 sec.), and then measure the amount of additive in the iso-octane. These data have been used for the modeling presented here.</p>									

4.2.2 Modelling

Initially the migration to the surface of all the measured additives in the two polymers as either a ratio of the total additive in the systems (M_t/M_∞) or as final amount (in mmole) were plotted (see figure 4.5 and 4.6.

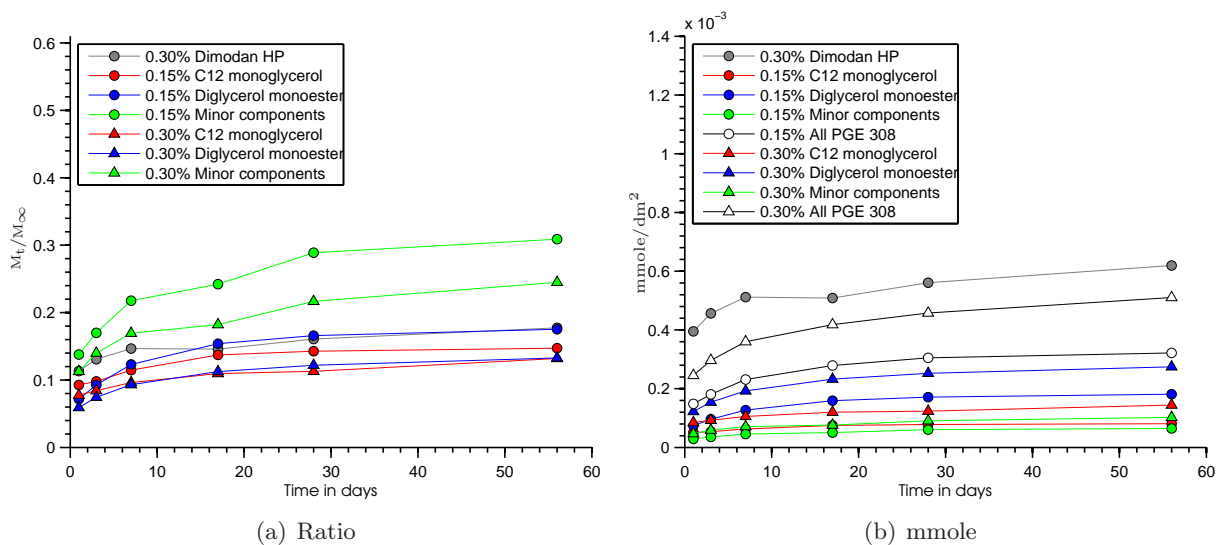


Figure 4.5: The Migration in LDPE over time, plotted as ratio of the total additive in the systems (M_t/M_∞) or as final amount in mmole per area (mmol/dm^2).

From the collective plot of all additives migration to the surface of LDPE as a ratio of the total additive in the polymer (figure 4.5 (a)), the migration seem to go towards the same ratio regardless of total concentration in the system (0.15% or 0.30%). Especially for C_{12} monoglyceride does the migration go towards almost identical final ratios, even though there is a factor two of difference in concentration. This information points towards a partition function between bulk and surface being the controlling part for the final migration to the surface. When plotting the migration as the final amount migrated (figure 4.5 (b)), this information is not clear.

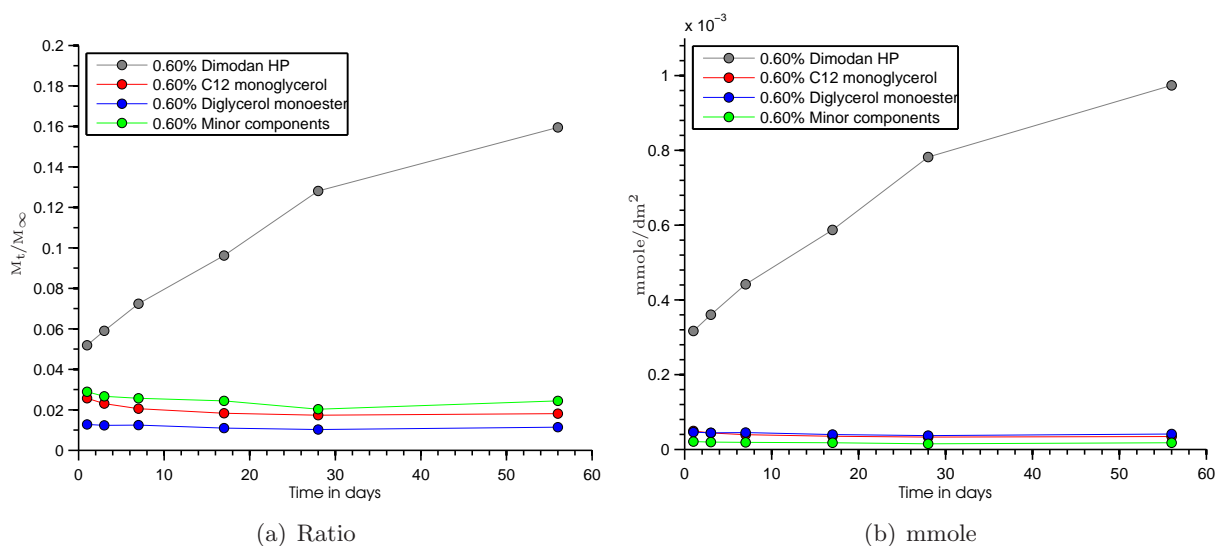


Figure 4.6: The Migration in PP over time, plotted as ratio of the total additive in the systems (M_t/M_∞) or as final amount in mmole per area (mmol/dm^2).

Comparing the migration plots for the two polymers, we can see that the PGE308 components migrate more to the surface in LDPE than in PP (both as ratio and as total amount), whereas

Dimodan HP seems to migrate towards the same ratio in both polymers.

From the migration data from Danisco, an estimate of the diffusion coefficient of the antistatic additive migration to the surface was calculated utilizing equation 3.1 as in the chapter on diffusion coefficients (chapter 3). But as shown in figure 4.7, it seems that there was not enough data points in the first part of the migration where the migration is expected to have close to a linear relationship to the square root of time. Moreover, the measured migration for C₁₂ monoglyceride in PGE 308 in PP seem to have a migration from the surface into the polymer (see figure 4.7 (b)). This was discussed in the project group at Danisco and it was believed to be due to statistical uncertainties in the experimental equipment as the concentrations of the additive are very low.

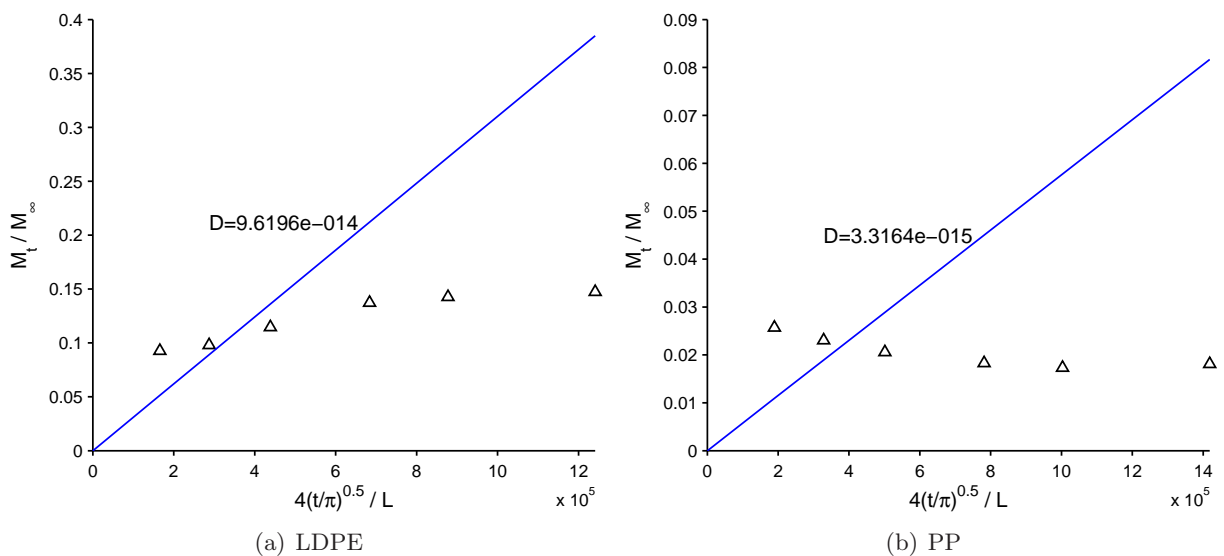


Figure 4.7: Estimation of the diffusion coefficient of C₁₂ monoglyceride in PGE 308 LDPE or PP as a linear function of the square root of time (eq. 3.1).

The calculations of diffusion coefficient for the additives were done both using the first three sampling times (blue points in figure 4.8) and using the first sampling time (red points in figure 4.8). Moreover, for comparison reasons, the semi-empirical model (eq. 3.28) by Piringer with general polymer parameters for PP and LDPE[14] was also used. This is shown in figure 4.8 as the solid line. As it can be seen there is a large difference between the experimentally derived and the fully estimated diffusion coefficients, by approximately 5 orders of magnitude.

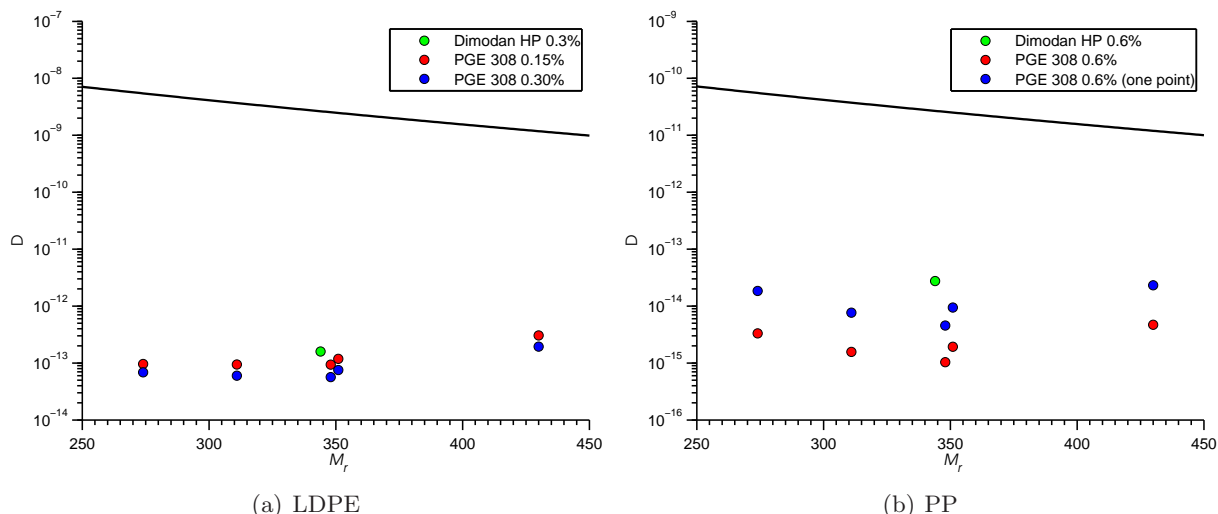


Figure 4.8: The estimated diffusion coefficients as function of the molecular weight of the migrant (M_r) for DIMODAN HP and PGE308 (PGE 308 has several components depending of chain length) in LDPE and PP. The colored data points are calculated from the experimental data as shown in figure 4.7. The full line is the fully estimated diffusion coefficient from parameters suggested by Piringer[14].

In figure 4.9 is plotted the estimated migration of C_{12} monoglyceride from PP or LDPE polymer using both the experimental (blue and green lines) and the estimated diffusion coefficients (red lines). On these plots the migration using the estimated diffusion coefficient seems to be instant, but this is due to the long time scale of the plot. This shows that the migration in both PP and LDPE should have run to equilibrium much faster than the actual migration taking place (experimental data). From the information shown here, the whole theory that the migration inside the polymer is the controlling step of the concentration change on the surface of the polymer was strongly questioned. It was decided at Danisco to test this hypothesis of much faster migration inside the polymer despite the experimental data already in place. If our theory of much faster migration inside the polymer was correct, the same polymer sheet that have just been cleaned off on the surface should within only a couple of days have almost the same concentration again. This was indeed showed, even though strongly questioned by Danisco.

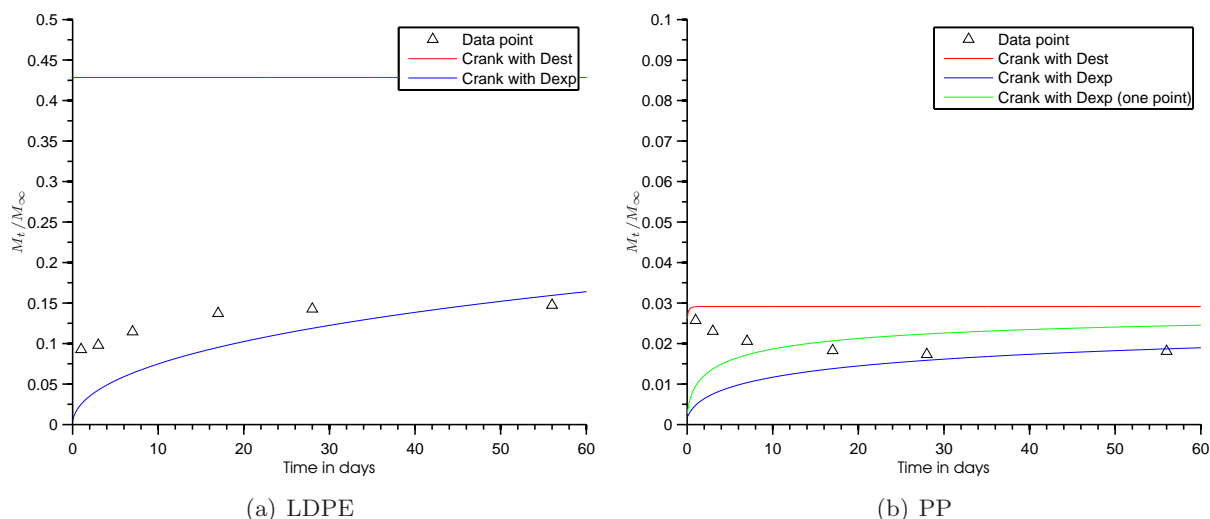


Figure 4.9: The modeled migration of the C_{12} monoglyceride in PGE 3008 to the surface of either LDPE or PP over time. The red line is migration estimated using the diffusion coefficient fully estimated from parameters by Piringner[14], and green and blue lines are the migration with diffusion coefficients estimated from the first data points of the migration.

The new knowledge of the migration of the additive in the bulk polymer being faster than what the experiments showed, lead to some new ideas on what was causing this migration to (and from the) surface of the polymer. Diffusion is even faster at higher temperatures (e.g under the extrusion), and the additive is mixed with the polymer before the final polymer film is extruded. Thus, it is possible that already at the first sampling time, some equilibrium concentrations of the additive in the bulk polymer and on the surface have been reached. This could also explain how in some of the experiments there seems to be a migration back in to the polymer. This is because the "partition coefficient" between surface and bulk is different depending on temperature. To obtain an estimate of this initial concentration of the additive on the surface, it was chosen to use the first 2-3 data points from the migration and extrapolate back linearly as a function of the square root of time as shown by the red line in figure 4.10.

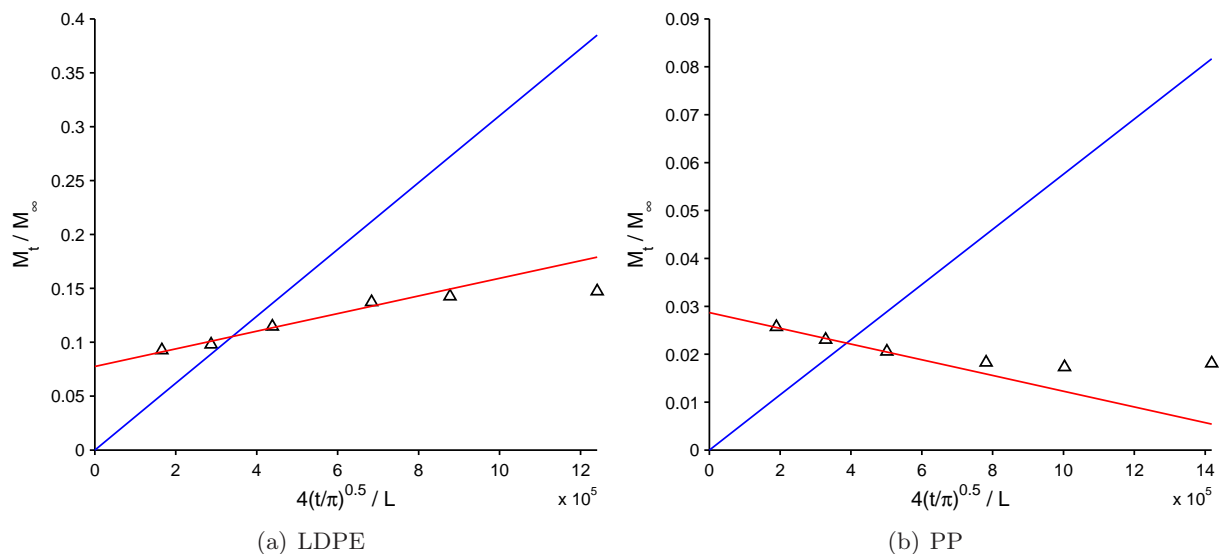


Figure 4.10: Estimation of the initial concentration of C_{12} monoglyceride from PGE 308 in LDPE and PP (red line). The blue line shows the correlation of the data to the square root of time using eq. 3.1.

It was then chosen to model the migration between the bulk polymer and the surface layer by using the estimated diffusion coefficient for the bulk parameter. We model the surface layer as an arbitrary specific layer of 0.05mm and fit the diffusion coefficient and partition coefficient between the two layers against the migration data. The specific size of the surface layer is not of paramount importance as the fitted partition coefficient (ratio of the amount of the migrant in the two layers) is purely dependent of this size. In figure 4.11 is shown how the concentration in LDPE will look in the two layers at start and end using this new approach.

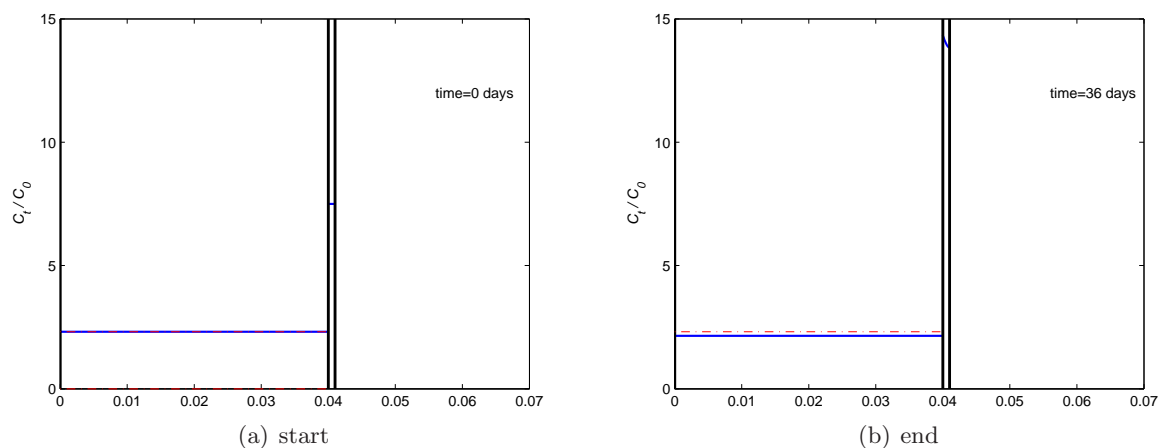


Figure 4.11: Estimated migration of C_{12} monoglyceride in LDPE by the new approach. With the new approach there is already an additive concentration at the surface at the starting point. The dotted red line at the plot of the end concentration illustrates the starting concentration values.

In other words the only fitted parameters in this approach are the diffusion coefficient on the surface layer (as it is believed now that the antistatic additive aggregates on the surface is the

time dependent step of the whole process), and the partition coefficient between the two layers. After a first attempt of fitting on these two parameters to the migration data, it was seen that the diffusion coefficient in the surface layer was almost constant for each polymer. For this reason it was chosen to set this parameter constant for each polymer (LDPE: $D = 1 \cdot 10^{-14} \text{ cm}^2/\text{s}$; PP: $D = 3.2 \cdot 10^{-15} \text{ cm}^2/\text{s}$) and then fit only the partition coefficient. In figure 4.12 is shown the estimated migration of C_{12} monoglyceride from PGE 308 in both LDPE and PP using this new approach. Even though only fitted to one parameter, a very good fit to the experimental data is obtained for all the systems under study. In appendix refApp:anti are presented migration plots of all systems.

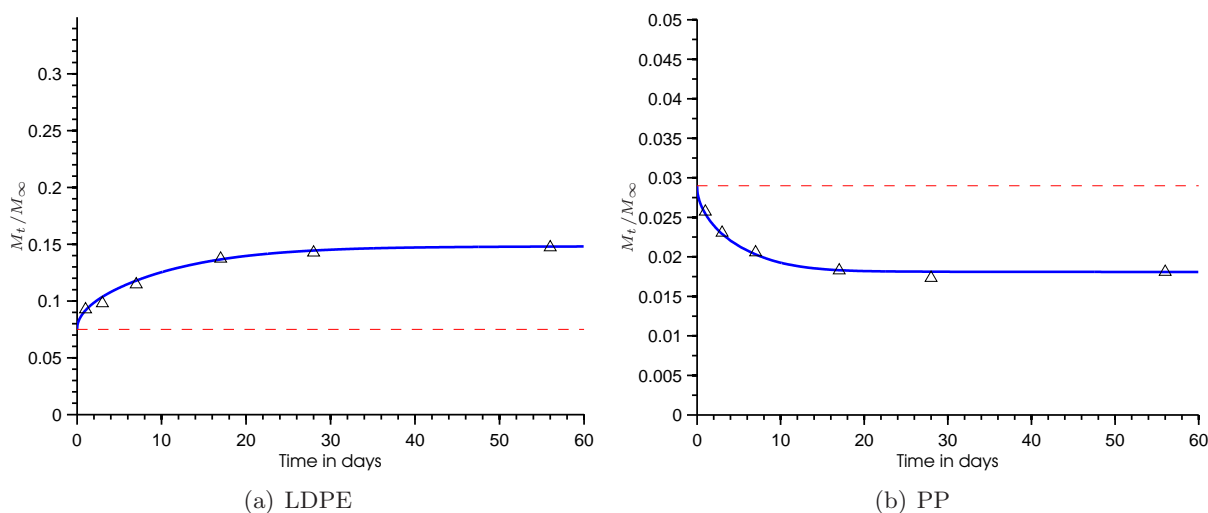


Figure 4.12: Estimated migration of C_{12} monoglyceride in LDPE and PP by the new approach, with a starting concentration in the surface layer and a partition coefficient of the additive between bulk and surface of the polymer. By this new approach the fit to the experimental data is very good.

When looking on the estimated starting concentration values on the surface layer for all the systems there seems to be a correlation among the different systems. In table 4.2 the estimated starting concentration values are listed as M_0/M_∞ , which is the ratio of the migration at the surface at the starting point over the infinite migration ($M_\infty = L \cdot C_{p0}$).

Table 4.2: Estimated starting concentration values of the antistatic additive on the surface layer as M_0/M_∞ , calculated by regressing the three first data points as a function of the square root of time (see figure 4.10). M_r is the molecular weight in g/mol .

additive conc.	M_r	LDPE		PP
		M_0/M_∞		M_0/M_∞
		0.15%	0.30%	0.60%
Dimodan				
C₁₆/C₁₈ monoglycerid	344		0.094	0.042
PGE 308				
C₁₂ monoglycerid	274	0.075	0.065	0.029
Diglycerol monoester	348	0.040	0.039	0.013
Total main	326	0.051	0.047	0.018
Minor components	430	0.088	0.079	0.032
Total all	342	0.056	0.051	0.020

It is now postulated that there is a linear relationship between the concentration of the additive in the polymer and the estimated concentration of the additive at the surface at the starting point. The average factor for the change from 0.15% to 0.30% of the PGE 308 components in LDPE is -0.0058. Using this average concentration factor, all the values of PGE 308 in LDPE can be recalculated as if the additive concentration was 0.60%. These new recalculated surface start concentration values from LDPE can then be used to find an average polymer change factor for the change between LDPE and PP. The average polymer change factor was found to be 0.49. The two average change parameters make it possible to recalculate the surface start concentration values both with change of additive concentration and between LDPE and PP polymers. In table 4.3 the three sets of surface start concentration values are given when recalculated to be from LDPE for an additive concentration of 0.60%. As it can be seen it seems that this initially postulated linear correlation in both concentration change and change in polymer is confirmed.

From these three sets of recalculated surface start concentration values obtained as if there was only one system, a new overall average surface start concentration value set can be derived (see table 4.3).

Table 4.3: Surface start concentrations from the three data sets (see table 4.2, recalculated using the two average change parameters (polymer change parameter: 0.49; additive concentration change parameter: -0.0058/(0.15%)). The three sets are recalculated to be as data from LDPE with a additive concentration of 0.60%.

M_0/M_∞		PP	LDPE	LDPE	Average
		0.60%	0.15%	0.30%	
Dimodan					
C₁₆/C₁₈ monoglycerid		0.086		0.082	0.084
PGE 308					
C₁₂ monoglycerid		0.059	0.058	0.053	0.057
Diglycerol monoester		0.027	0.023	0.027	0.026
Total main		0.037	0.034	0.035	0.035
Minor components		0.065	0.071	0.067	0.068
Total all		0.041	0.039	0.039	0.040

Using this new overall average surface concentration data set and the polymer and concentration

change factors, an estimation for all systems can be accomplished. This is shown in table 4.4. A very good correlation to all the "experimental" data is obtained.

Table 4.4: Estimated surface start concentration for all possible systems in the LDPE polymer. Estimations are done using the new average surface concentration set (see table 4.3) and the two average change parameters. The estimated surface concentrations result in very accurate correlation of the two sets of experimental data derived surface concentrations.

M_0/M_∞		0.15%		0.30%		0.45%		0.60%	
		Est	Exp	Est	Exp	Est	Est	Exp	
LDPE									
Dimodan									
PGE 308	C₁₆/C₁₈ monoglycerid	0.101		0.096	0.094	0.090	0.084		
	C₁₂ monoglycerid	0.074	0.075	0.068	0.065	0.063	0.057		
	Diglycerol monoester	0.043	0.040	0.037	0.039	0.031	0.026		
	Total main	0.053	0.051	0.047	0.047	0.041	0.035		
	Minor components	0.085	0.088	0.079	0.079	0.074	0.068		
	Total all	0.057	0.056	0.051	0.051	0.045	0.040		
PP									
Dimodan									
PGE 308	C₁₆/C₁₈ monoglycerid	0.059		0.053		0.047	0.041	0.042	
	C₁₂ monoglycerid	0.045		0.039		0.034	0.028	0.029	
	Diglycerol monoester	0.030		0.024		0.018	0.013	0.013	
	Total main	0.035		0.029		0.023	0.017	0.018	
	Minor components	0.051		0.045		0.039	0.033	0.032	
	Total all	0.037		0.031		0.025	0.019	0.020	

The same methodology was followed using the obtained partition coefficients, but the correlation did not prove to be satisfactory. In table 4.5 the fitted partition coefficients are listed for all the systems.

Table 4.5: Fitted partition coefficients (K_p) for all tested additives between bulk and surface layers (0.05mm) in both LDPE and PP. No direct correlation was found between the three data sets of fitted partition coefficients.

additive conc.	M_r	LDPE		PP
		K_p		K_p
		0.15%	0.30%	0.60%
Dimodan				
PGE 308	C₁₆/C₁₈ monoglycerid	344	0.12	0.02
	C₁₂ monoglycerid	274	0.15	1.50
	Diglycerol monoester	348	0.12	2.50
	Total main	326	0.13	2.15
	Minor components	430	0.06	1.20
	Total all	342	0.11	1.90

In appendix C is shown the migration plots of all the systems using the fitted partition coefficients listed in table 4.5 and the estimated surface start concentrations from table 4.4.

4.2.3 Conclusion

The main conclusions from this modeling work on antistatic additive migration in LDPE and PP is that the migration in the polymer bulk is not the time limiting step of the migration process of the antistatic agent to the surface. This is a very important conclusion as the opposite has been a strong belief of Danisco for more than 10 years. The next step stemming from this conclusion is to discover the controlling step which defines how fast the additive migrates to the surface. The second main conclusion from this modeling work is that it is possible to obtain a very good fit to the migration data with the proposed model. The new model stimulates that the system has a thin surface layer and specific diffusion coefficients for both bulk polymer and surface layer. The partition coefficient of the additive between the bulk and the surface is temperature dependent. Moreover is the migration in the polymer much faster at higher temperature, which means the migration to the surface layer started to happen already in the extrusion process of the polymer film.

From the model it can be concluded that there is a strong correlation between the systems regarding the additive surface concentration right after the extrusion process. This correlation does not seem to hold for the final surface concentration. This could point towards that over time some sort of structural change of the additive molecules happens on the surface that makes it more or less favorable for them to be there. To understand what happens on the surface of the polymer with the antistatic additive molecules, which turns out to be the controlling part of the migration to the surface, a correlation has to be found between the partition coefficient and some other parameter for the additive (i.e. molar volume or polarity).

Modeling partition coefficients in polymer/solvent systems by molecular dynamics

Accurate partition coefficient data of migrants between a polymer and a solvent are of paramount importance for estimating the migration of the migrant over time, especially for estimating the concentration of the migrant at infinite time in the two solvents (i.e. the polymer and the food simulant).

Most predictive models for partition coefficients in polymer/solvent or polymer/polymer systems are based on thermodynamic models for the estimation of the activity coefficient. A comparison study by Piringer and Baner in 2008[14] for up to 13 organic substances in different polymers and solvent systems showed an average absolute error ratio for the estimated partition coefficient with these activity coefficient models around 5-10 (best case scenario), and sometimes up to 10.000. Many of the thermodynamic models in that study predict a partition coefficient for the polyethylene (PE) / ethanol systems larger than unity for one or more compounds (higher affinity for PE than for ethanol), even though the experimental partition coefficients for this system are below unity (higher affinity for ethanol than for PE). In a recent article by Gillet et al.[46], another approach was proposed based on a generalized Flory-Huggins model together with Metropolis Monte Carlo (MC) calculations for the Flory-Huggins interaction parameters. This approach aims towards keeping the flexibility of the Flory-Huggins model for calculations at the macroscopic scale, while obtaining only the system-specific interaction parameters from the fairly cheap (for polymeric systems) computational MC calculations at the atomistic scale. A more direct approach would include the performance of all calculations at the atomistic scale using Molecular Dynamics (MD) simulations to calculate the free energy of solvation by thermodynamic integration[47]. From this free energy of solvation of the solute into each of the two solvents ($\Delta_{solvA}G$ and $\Delta_{solvB}G$ in eq. 5.1), the partition coefficient of the solute between the two solvents can be calculated[48, 49].

$$\log K_{\text{solvA/solvB}} = \frac{\Delta_{\text{solvB}}G - \Delta_{\text{solvA}}G}{2.303RT} \quad (5.1)$$

In the current work this proposed methodology was firstly used for the calculation of partition coefficients of additives into squalane (to mimic low-density polyethylene (LDPE)) and food simulant A (distilled water) or food simulant C (10% ethanol, 50% ethanol). These specific systems were chosen because good experimental data exist for the partition coefficients in all of them with *cis*-3-hexenol and decane[14]. The choice of these two specific solutes is based on their fairly simple structure and the fact that one is hydrophobic and the other hydrophilic.

The calculations and the methodology used for the systems on squalane and ethanol/water is presented in the article "Partition coefficients of organic molecules in squalane and water/ethanol mixtures by Molecular Dynamics Simulations" submitted to the Journal of Fluid Phase Equilibria (FPE) for review. This article as it is submitted is presented in the section 5.2 "Partition coefficients of organic molecules in squalane and water/ethanol mixtures by Molecular Dynamics Simulations".

5.1 Molecular Dynamics

Molecular Dynamics (MD) is a time-dependent algorithm used in Molecular Simulations where molecules are represented as specific centers in a virtualbox and all the inter atomic interactions are modeled by bonded and non-bonded interaction functions. The time development of the system happens by movement of the centers in the box according to the Newton's laws of motion. Depending on the choice of scale of the force field the centers in this work represent all atoms of the molecule (All Atoms force field, like OPLS-AA[7] and CHARMM27[5, 50]). The molecules can also be represented with most hydrogen atoms implicit together with the nearest center, called United Atom force fields (UA). This means for instance that CH₃ or CH₂ are calculated as one center, in this work the TraPPE force field).

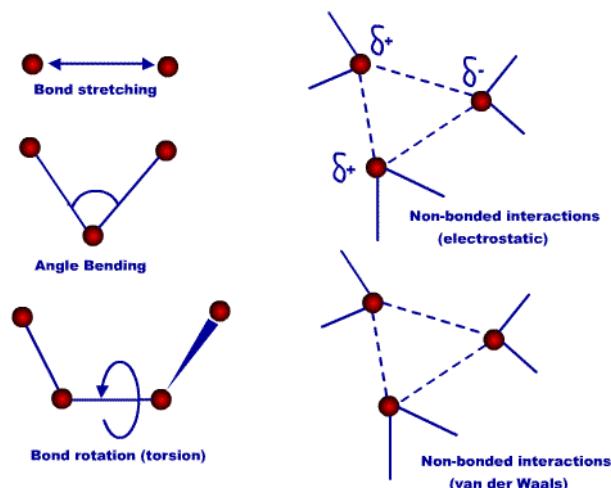


Figure 5.1: Bonded and nonbonded interactions in molecular dynamics[51].

The molecular dynamics calculations in this work are performed using the open-source code GROMACS (version 4)[6]. In GROMACS the non-bonded and bonded interactions (see figure 5.1) are modeled by the following equations:

Lennard-Jones interactions are calculated between all non-bonded centres and bonded centres more than 2 bonds away. Most force fields use a special scaling factor (S) for the interaction specifically between atoms with three bonds distance (1-4 interaction). For TraPPE $S_{LJ}=0$, for OPLS-AA $S_{LJ}=0.5$ and for the CHARMM27 force field the 1-4 LJ interactions are predefined in the force field.

$$E_{LJ}(r_{ij}) = 4\epsilon_{ij} \left(\left(\frac{\sigma_{ij}}{r_{ij}} \right)^{12} - \left(\frac{\sigma_{ij}}{r_{ij}} \right)^6 \right) S_{LJ} \quad (5.2)$$

where r_{ij} is the distance between center i and j , ϵ_{ij} is the depth of the LJ potential well and σ_{ij} is the finite distance of the LJ potential.

Coulomb interactions are calculated in the same way, also often with a special scaling factor (S_C) used for the 1-4 interactions. For TraPPE $S_C=0.5$, for OPLS-AA $S_C=0.5$ and for CHARMM27 $S_C=1$.

$$E_C(r_{ij}) = \frac{q_i q_j}{4\pi\epsilon_0\epsilon_r r_{ij}} S_C \quad (5.3)$$

where q is the atomic charge and ϵ_0 is the dielectric constant in vacuum and ϵ_r is the dielectric constant of the medium.

Bond stretching between bonded molecules are modelled by a simple harmonic potential:

$$E_b(r_{ij}) = \frac{1}{2} k_{ij}^b (r_{ij} - b_{ij})^2 \quad (5.4)$$

where k_{ij}^b is the bond force constant and b_{ij} is the optimal bond length.

Angle bending between 1-3 bonded molecules are also modelled by a harmonic potential:

$$E_a(\theta_{ijk}) = \frac{1}{2}k_{ijk}^\theta (\theta_{ijk} - \theta_{ijk}^0)^2 \quad (5.5)$$

where k_{ijk}^θ is the angle force constant, θ_{ijk} is the angle between center i, j and k and θ_{ijk}^0 is the optimal angle.

Torsional angle bending (1-4 angle) is modelled by a Ryckaert-Bellemans (RB) function:

$$E_{rb}(\phi_{ijkl}) = \sum_{n=0}^5 C_n (\cos(\phi_{ijkl}))^n \quad (5.6)$$

where ϕ_{ijkl} is the 1-4 torsional angle (there are different definitions for when the torsional angle is 0, it can be either at the trans or the cis position. GROMACS follows the 'polymer convention' of $\phi_{trans} = 0$), C_n are the Ryckaert-Bellemans parameters specific for each set of center $ijkl$.

5.2 Partition coefficients of organic molecules in squalane and water/ethanol mixtures by Molecular Dynamics Simulations

Rasmus Lundsgaard¹, Georgios M. Kontogeorgis¹ & Ioannis G. Economou²

(1) Center for Energy Resources Engineering (CERE), Department of Chemical and Biochemical Engineering, Technical University of Denmark, Kgs. Lyngby DK-2800, Denmark;

(2) The Petroleum Institute, Department of Chemical Engineering, Abu Dhabi, PO Box 2533, United Arab Emirates

(Submitted to Journal of Fluid Phase Equilibria, September 2010)

5.2.1 Abstract

Accurate partition coefficient data of migrants between a polymer and a solvent are of paramount importance for estimating the migration of the migrant over time, including the concentration of the migrant at infinite time in the two solvents. In this article it is shown how this partition coefficient can be estimated for both a small hydrophilic and a hydrophobic organic molecules between squalane (used here to mimic low density poly ethylene) and water/ethanol solutes using thermodynamic integration to calculate the free energy of solvation. Molecular dynamics simulations are performed, using the GROMACS software, by slowly decoupling of firstly the electrostatic and then the Lennard-Jones interactions between molecules in the simulation box. These calculations depend very much on the choice of force field. Two force fields have been tested in this work, the TraPPE-UA (united-atom) and the OPLS-AA (all-atom). The computational cheaper TraPPE-UA force field showed to be more accurate over the whole range of systems compared to the OPLS-AA force field. Moreover, some of the calculations were done with five different water models to investigate the influence of the specific water model on the calculations. It was found that the combination of the TraPPE-UA force field and the TIP4p water model gave the best results. Based on the methodology proposed in this article, it is possible to obtain good partition coefficients only knowing the chemical structure of the molecules in the system.

5.2.2 Introduction

In the later years it has been approved by EU to estimate migration of additives from a monolayer polymer into a solvent utilizing a generally recognized migration model[16] or even from multilayer polymer systems into a solvent utilizing finite element method (FEM). These models are only as good as the parameters used, i.e. diffusion coefficients and partition coefficients. The model proposed by Piringer[14] made for safe over estimation of diffusion coefficients has been approved by EU, when no or only very little data exist. By the term “safe over estimation” is meant an estimation model that is the worst case scenario estimation for at least 95% of the data. On the other hand, for partition coefficients, there is currently no approved consistent model. For simplification and unification of the experimental work and/or calculations that has to be done in order to get a product approved by the legislation, four food simulants have been

chosen by the European Commission[52]:

- A Distilled water
- B 3% Acetic Acid (weight/volume)
- C 10% Ethanol (volume/volume)
- D Olive oil or Sunflower oil (in some cases Iso-octane)

In the specific case of milk and similar products, it is suggested to use 50% ethanol as the food simulant.

Most models for prediction of partition coefficients in polymer/solvent or polymer/polymer systems are based on thermodynamic models for the estimation of the activity coefficient. A comparison study by Piringer and Baner in 2008[14] for up to 13 organic substances in different polymers and solvent systems showed an average absolute ratio for the estimated partition coefficient with these activity coefficient models for the best around 5-10, and some up to 10000. Many of the thermodynamic models predict a partition coefficient for the polyethylene (PE) / ethanol systems larger than unity for one or more compounds (higher affinity for PE than for ethanol), even though that the experimental partition coefficients for this system are below unity (higher affinity for ethanol than for PE).

In a recent article by Gillet et al.[46], another approach was proposed based on a generalized Flory-Huggins model together with Metropolis Monte Carlo (MC) calculations for the Flory-Huggins interaction parameters. This approach is aimed towards keeping the flexibility of the Flory-Huggins model for calculations at the macroscopic scale, while obtaining only the system specific interaction parameters from the fairly cheap (for polymeric systems) computational MC calculations at the atomistic scale.

A more direct approach is doing all calculations at the atomistic scale using Molecular Dynamics (MD) simulations to calculate the free energy of solvation by thermodynamic integration[47]. From this free energy of solvation of the solute into each of the two solvents, the partition coefficient of the solute between the two solvents can be calculated as shown by Best et al.[48]. In their article, this proposed methodology was used for calculation of partition coefficients of additives into squalane (to mimic low-density polyethylene (LDPE)) and food simulant A (distilled water) or food simulant C (10% ethanol, 50% ethanol).

The purpose of this work is to investigate the proposed methodology to obtain good partition coefficients from only the knowledge of the chemical structure of the molecules involved. The article is organized as follows: Part 5.2.3 refers to the theory behind the calculation of the free energy of solvation and how to get the partition coefficient from it; in Part 5.2.4, the force fields for the various molecules are presented and their implementation in the GROMACS software;

Part 5.2.5 refers to Computational details, Part 5.2.6 is devoted to Results and discussion and in Part 5.2.7 Conclusions are drawn.

5.2.3 Partition coefficients from thermodynamic integration

It has been shown by Essex et al.[49] that from the free energy of solvation in solvent A and B ($\Delta_{solvA}G$ and $\Delta_{solvB}G$ in equation 1) it is possible to estimate the partition coefficient between the two solvents:

$$\log K_{solvA/solvB} = \frac{\Delta_{solvB}G - \Delta_{solvA}G}{2.303RT} \quad (5.7)$$

Calculating the free energy of solvation by thermodynamic integration from molecular dynamics is, however, not completely straight forward, as slowly stepwise elimination of all the solvent molecules is not possible. Instead, the thermodynamic cycle (figure 5.2) can be used to calculate this change, by calculating the other steps.

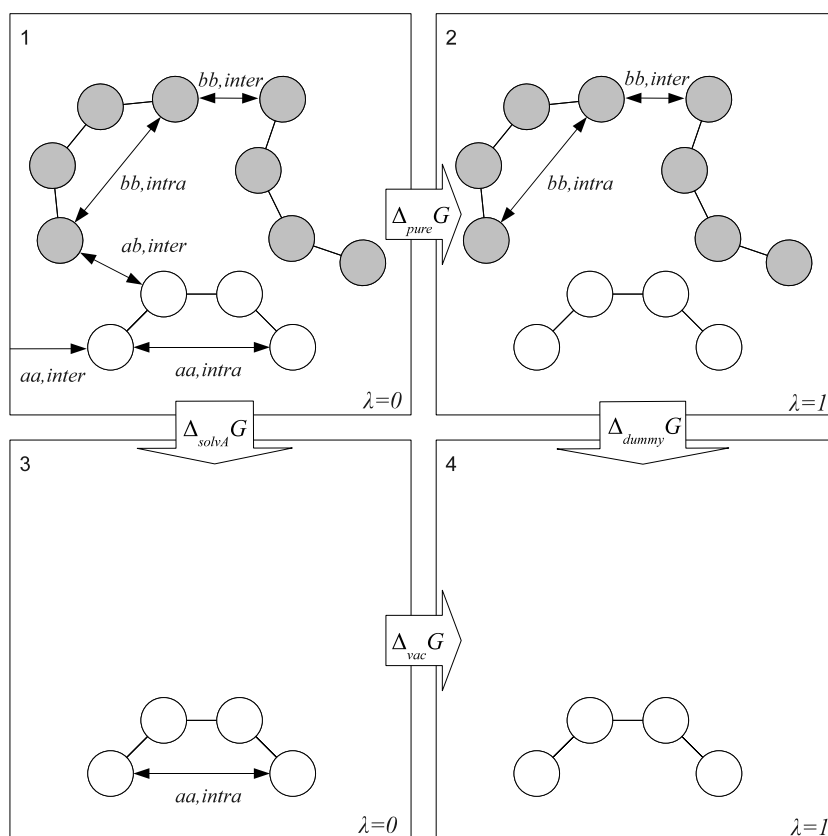


Figure 5.2: Thermodynamic cycle where $\Delta_{pure}G$ is the free energy associated with the change from a solute molecule with full Lennard-Jones (LJ) and Coulombic interactions (both inter, and intra molecular) into no interactions (a dummy molecule), $\Delta_{vac}G$ is the free energy associated with the same process in vacuum (only intra molecular interactions), and finally $\Delta_{dummy}G$ can be seen as the hypothetical free energy of solvation dummy molecules.

Calculations can be done knowing:

- 1 Decoupling of all interactions from solute in solvent gives $\Delta_{pure}G$
- 2 Decoupling of all interactions from solute in vacuum gives $\Delta_{vac}G$
- 3 The change in free energy from a dummy molecule in solvent into vacuum is zero

A dummy molecule is a molecule that has no Lennard-Jones (LJ) and Coulombic interactions (either intra- and intermolecular), but there is still the intramolecular bonded interaction. The intramolecular bonded interactions are, however, the same both in solute and vacuum, hence $\Delta_{dummy}G$ is equal to zero and the equation for the thermodynamic cycle can be written as:

$$\Delta_{solu}G = \Delta_{vac}G - \Delta_{pure}G - \Delta_{dummy}G = \Delta_{vac}G - \Delta_{pure}G \quad (5.8)$$

As inter- and intramolecular LJ and Coulombic interactions in standard simulation algorithms are indistinguishable from each other when doing the slowly decoupling of interactions from the solute (going from box 1 to 2 in figure 5.2), the separate calculation in vacuum is necessary to compensate for changes in solute-solute intramolecular interactions that take place for the solute in the solvent (box 3 to 4 in figure 5.2). By separating the energy into individual components this becomes a bit clearer. The initial state of the $\Delta_{pure}G$ calculation (box 1 in figure 5.2) can in this way be written as:

$$G_{pure}^{\lambda=0} = G_{aa}^B + G_{aa}^{intra} + G_{bb}^B + G_{bb}^{intra} + G_{bb}^{inter} + G_{ab}^{inter} \quad (5.9)$$

Where index a denotes the solute molecule and index b denotes the solvent molecule. G^B represents the free energy from intramolecular bonded interactions (bond stretching, bond angle bending and dihedral torsion). λ is a decoupling parameter used for the slowly decoupling of all LJ and Coulombic interactions of the solute molecule, when $\lambda = 0$ there is no decoupling – ie full LJ and Coulombic interactions. As there only is one solute molecule in the box the intermolecular distance between two solute molecule centers will always be greater than half the box length. For this reason the term can be neglected.

In the final state for the $\Delta_{pure}G$ calculation, the LJ and Coulombic interactions between the solute and the solvent are turned off ($\lambda = 1$), by changing their LJ parameters and point charges to zero. This will however also turn off the intramolecular LJ and Coulombic interactions of the solute, as these are indistinguishable (box 2 in figure 5.2).

$$G_{pure}^{\lambda=1} = G_{aa}^B + G_{bb}^B + G_{bb}^{intra} + G_{bb}^{inter} \quad (5.10)$$

By combining equations 5.9 and 5.10, $\Delta_{pure}G$ can be calculated as:

$$G_{pure} = G_{pure}^{\lambda=1} - G_{pure}^{\lambda=0} = -G_{aa}^{intra} - G_{ab}^{inter} \quad (5.11)$$

For $\Delta_{vac}G$ it is a bit simpler:

$$G_{vac}^{\lambda=0} = G_{aa}^B + G_{aa}^{intra} \quad (5.12)$$

$$G_{vac}^{\lambda=1} = G_{aa}^B \quad (5.13)$$

$$G_{vac} = G_{vac}^{\lambda=1} - G_{vac}^{\lambda=0} = -G_{aa}^{intra} \quad (5.14)$$

Finally, by substituting equations 5.11 and 5.14 into 5.8:

$$\Delta_{solv}G = \Delta_{vac}G - \Delta_{pure}G = G_{ab}^{inter} \quad (5.15)$$

Thus, it is clear that in order to obtain a correct free energy of solvation, independent simulations both in vacuum and in solvent have to be done. For each case, the free energy can be estimated using different methods, such as free energy perturbation, thermodynamic integration or the slow-growth method[53]. For relatively large solutes, thermodynamic perturbation is impractical due to the difficulty in successfully inserting an entire solute molecule into an equilibrated solvent box. Slow-growth methods suffer from hysteresis problems and may introduce uncontrolled systematic errors in the calculations[54]. So for this reason thermodynamic integration has been chosen as the way of estimating the free energy.

The initial state and the final state has two different Hamiltonian functions ($\mathcal{H}_0(x, p_x)$ and $\mathcal{H}_1(x, p_x)$), where x and p are the positions and the momenta of all the atoms respectively. By parameterizing the Hamiltonian ($\mathcal{H}_\lambda(x, p_x)$) with the coupling parameter λ such that when $\lambda = 0$, $\mathcal{H}_\lambda = \mathcal{H}_0$ and when $\lambda = 1$, $\mathcal{H}_\lambda = \mathcal{H}_1$, then the free energy becomes also a function of λ :

$$\begin{aligned} \frac{dA}{d\lambda} &= \left\langle \frac{\partial \mathcal{H}_\lambda(x, p_x)}{\partial \lambda} \right\rangle_\lambda \Rightarrow \\ \Delta A &= \int_0^1 \left\langle \frac{\partial \mathcal{H}_\lambda(x, p_x)}{\partial \lambda} \right\rangle_\lambda d\lambda = \Delta G \end{aligned} \quad (5.16)$$

In this approach it is assumed that \mathcal{H}_λ interpolates smoothly between the two Hamiltonian functions. The calculations are done in practice by considering a set of independent and discrete λ values between 0 and 1. For each λ value, the derivatives of the free energy with respect to

λ are evaluated and averaged. Integrating along the smoothed interpolated function between the two states gives the final free energy difference (eq. 5.17). This means that the overall free energy of solvation can be calculated by:

$$\Delta_{solv}G = \int_0^1 \left\langle \frac{\partial \mathcal{H}_\lambda(x, p_x)}{\partial \lambda} \right\rangle_\lambda^{vac} d\lambda - \int_0^1 \left\langle \frac{\partial \mathcal{H}_\lambda(x, p_x)}{\partial \lambda} \right\rangle_\lambda^{pure} d\lambda \quad (5.17)$$

Splitting this approach up into two steps, firstly decoupling of the Coulombic interactions and then decoupling of the Lennard-Jones interactions will give a more accurate result and a more well-behaved function between the two states, as shown by Shirts et al.[55].

5.2.4 Force fields

Initially, three different force fields were chosen for this work, the ‘‘Transferable Potentials for Phase Equilibria’’ united-atom force field (TraPPE-UA)[8], the ‘‘Groningen Molecular Simulation’’ force field (GROMOS, united atom)[56] and the ‘‘Optimized Potentials for Liquid Simulations’’ force field (OPLS-AA, all atom)[7]. For the GROMOS force field the latest parameter set 53A6 was chosen, as this parameter set specifically is adjusted to reproduce the free enthalpies of hydration in Simple Point Charge (SPC) water[57]. The problem with this force field showed to be the inconsistency in choice of the atomic charges in organic molecules, because this force field is parameterized towards biomolecular systems, which means that the atomic charges should be decided based on analogy to the functional groups in amino acids. As the software PRODRG[58] already was used to make coordinate files of the molecules, the ability of the software to estimate the topology information for GROMOS force fields was also tested. The PRODRG software can estimate atomic charges in the molecule as either reduced or full charges, both were tested. No consistent way of setting these atomic charges was found for the first simple organic molecules used in this work that could give good consistent free enthalpies of hydration. For this reason this force field was not further considered.

In Table 5.1 all the recalculated non-bonded parameters of the TraPPE-UA and the OPLS-AA force fields are shown in the form that they have been used in the GROMACS software, i.e. σ in nm and ϵ in kJ/mol, where ϵ in the original literature of the force fields[7, 8, 59–61] are given as either kcal/mol or K. All the bonded interactions (bond length, bond angles and dihedral angles) are also recalculated from the parameters as in the original articles to parameters used in the functions for bonding energies in Gromacs. It should be noted that there is a small difference in the calculations of the LJ and Coulomb 1-4 interactions (LJ and Coulombic intramolecular interactions between atoms separated by exactly 3 bonds) with the two force fields. For the TraPPE-UA force field the Coloumbic 1-4 interaction are scaled by a factor of 0.5, and the 1-4 LJ interactions do not exist (scaled by a factor of 0). For the OPLS-AA force field both the Coloumbic and LJ 1-4 interaction are scaled by a factor of 0.5.

Table 5.1: Non bonded parameters for TraPPE-UA and OPLS-AA force fields as implemented in the GROMACS software in this work.

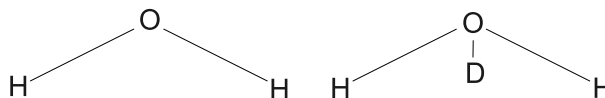
Force field	Atom/group	q_i [e]	σ_{ii} [nm]	ϵ_{ii} [kJ/mol]
TraPPE-UA				
[8]	CH ₃ , (RCH ₃)	0.000	0.375	0.8148
[8]	CH ₂ , (R ₂ CH ₂)	0.000	0.395	0.3825
[59]	CH, (R ₃ CH)	0.000	0.468	0.0831
[60]	CH=, (RCH=R)	0.000	0.373	0.3908
[61]	CH ₂ , (RCH ₂ OH)	0.265	0.395	0.3825
[61]	O, (ROH)	-0.700	0.302	0.7732
[61]	H, (ROH)	0.435	0.000	0.0000
OPLS-AA				
[7]	C, (RCH ₃)	-0.180	0.350	0.276144
[7]	C, (RCH ₂ R)	-0.120	0.350	0.276144
[7]	H, (CH _x)	0.060	0.250	0.125520
[7]	C, (RCH=)	-0.115	0.355	0.317984
[7]	H, (HC=)	0.115	0.242	0.125520
[7]	C, (RCH ₂ OH)	0.145	0.350	0.276144
[7]	O, (ROH)	-0.683	0.312	0.711280
[7]	H, (ROH)	0.418	0.000	0.000000

The LJ interactions between unlike atoms are calculated through the combining rule of the LJ interaction parameters between like atoms (ϵ_{ii} and σ_{ii}). For the OPLS-AA force field, a geometric mean rule is used for both the σ and ϵ :

$$\sigma_{ij} = \sqrt{\sigma_{ii}\sigma_{jj}}, \quad \epsilon_{ij} = \sqrt{\epsilon_{ii}\epsilon_{jj}} \quad (5.18)$$

For the TraPPE-UA force field, on the other hand, the more common Lorentz-Berthelot combining rule is used (equation 5.19). This led to the problem of how to calculate LJ interactions when doing simulations with a combination of the two force fields in the same box. It was chosen for simplification to use the Lorentz-Berthelot combining rule between all unlike atoms in the box, irrespective of which force field was used for the specific atoms.

$$\sigma_{ij} = \frac{1}{2}(\sigma_{ii} + \sigma_{jj}), \quad \epsilon_{ij} = \sqrt{\epsilon_{ii}\epsilon_{jj}} \quad (5.19)$$

**Figure 5.3:** 3 site and 4 site water models. In 4 site models, a dummy atom (D) exhibits Coulombic interactions and oxygen atom exhibits Lennard-Jones interactions only.

Initially, in this work the SPC/E water model[57] was chosen. This is a three site water model and for this reason it is fairly cheap computationally. The partition coefficients calculated between squalane and ethanol-water systems were in general over predicted, as was seen for the system squalane/pure water. For this reason, additional calculations were made with the SPC, SPC/E, TIP4p[62], TIP4pEw[63] and TIP4p2005[64] water models. The TIP4p type water models are four site models with a dummy atom that exhibits only Coloumbic interactions (the oxygen atom has no Coloumbic interactions, see figure 5.3), whereas the SPC and SPC/E both are three site models. The parameters of all 5 water models are shown in Table 5.2 with parameter values as implemented in GROMACS.

Table 5.2: The different parameters for the water models used in this work. All parameters are recalculated as they are implemented in the GROMACS software and not in the way they are listed in the original literature.

		SPC [57]	SPC/E [57]	TIP4p [62]	TIP4pEw [63]	TIP4p2005 [64]
σ_{ii}	[nm]	0.3116	0.3116	0.3154	0.316435	0.31589
ϵ_{ii}	[kJ/mol]	0.6485	0.6485	0.6487	0.6810	0.7749
q_O / q_O	[e]	-0.8200	-0.8476	-1.0400	-1.04844	-1.1128
q_H	[e]	0.4100	0.4238	0.5200	0.52422	0.5564
r_{OH}	[nm]	0.1	0.1	0.09572	0.09572	0.09572
r_{HH}	[nm]	0.16330	0.16330	0.15139	0.15139	0.15139
α_D				0.1280	0.10668	0.13194

$$r_D = r_O + \alpha_D(r_{H1} - r_O) + \alpha_D(r_{H2} - r_O) \quad (5.20)$$

The position of the dummy atom (r_D) can be calculated as a function of the positions of the hydrogens (r_{H1} and r_{H2}) and the oxygen (r_O) atoms as shown in equation 5.20. The α_D number is a ratio of the oxygen-dummy distance ($|OD|$) over half the distance from the oxygen to the baseline between the two hydrogen atoms.

$$\alpha_D = \frac{|OD|}{2 \cos |\angle DOH| \cdot |OH|} \quad (5.21)$$

5.2.5 Computational details

All the calculations have been done using the Gromacs 4.0.5 software[6] on either an Ubuntu Linux workstation (Intel Quad-core 3.00GHz) or on an Apple OSX workstation (Intel Xeon Quad-core 2.80 Ghz). As Gromacs is developed towards MD simulations of biomolecules, the binaries are by default compiled with single precision. In this work all calculations have been done with binaries compiled with double precision. The MD calculations were done using the approach of Mobley et al.[65] with the Langevin (stochastic) dynamics integrator to also control

the temperature[66]. This was done with a frictional constant of 1 ps^{-1} , a reference temperature of 298K and a overall step size of 2fs. A cut-off radii of 1 nm for the short-range neighbor list was used, while electrostatic interactions were calculated using Reaction-Field[67] method with a 1 nm cut-off radii and LJ interactions with a switched cut-off 0.8 - 0.9 nm. In the NPT runs the Berendsen barostat[68] with a time constant of 0.5 ps and an isothermal compressibility of $4.5 \cdot 10^{-5} \text{ bar}^{-1}$ was used to enforce a proper pressure coupling. The box size was scaled at every time step, and the reference pressure was set to 1 bar. The soft-core expression[69] has shown to eliminate singularities and numerical instabilities in free energy calculation, especially at the end points of the transformation between states (λ close to 0 or 1)[53]. For this reason the soft-core expression was used for the secondary step (the turn off of LJ interactions). The soft-core parameter was set to 0.5, the power for λ in the soft-core function was 1 and the soft-core σ value was 0.3 nm.

For each simulation cycle the procedure was as follows:

- 1 Energy minimization using two minimization algorithms
 - a L-BFGS algorithm of Nocedal (5000 steps)
 - b Steepest descent minimization (500 steps)
- 2 Equilibration run with constant volume (10 ps, NVT)
- 3 Equilibration run with constant pressure using the Berendsen barostat (100 ps, NPT)
- 4 Production run the (5000 ps, NVT)

This cycle on this type of hardware takes approximately 50 min. which means that calculation of a partition coefficient with the methodology proposed in this article takes approximately $20 \times 50 \text{ min} = 17 \text{ hours}$. When this project started only Gromacs version 3.3 was available, but with the update to version 4.0.x, an increase in speed of up to 20% was seen. Moreover, the choice of parallelization software had an influence on the speed when running on more than one core (in this work the "Open MPI" software has been used).

The number of solvent molecules in the boxes where:

Squalane	:	31	
Ethanol/Water			
0% (pure water)	:	0 / 890	
9% (mol./mol.)	:	65 / 667	$\approx 20\%$ (vol./vol.)
20% (mol./mol.)	:	130 / 494	$\approx 40\%$ (vol./vol.)
61% (mol./mol.)	:	260 / 166	$\approx 80\%$ (vol./vol.)
100% (pure ethanol)	:	272 / 0	

5.2.6 Results and discussion

Analysis of the stepwise λ decoupling methodology

As explained earlier, the enthalpy of solvation can be calculated by thermodynamic integration over the stepwise decoupling of solvent-solute interactions. In this work the approach of Shirts et al.[55] has been chosen which essentially means firstly a slowly decoupling of Coloumbic interactions as a function of λ (see figure 5.4).

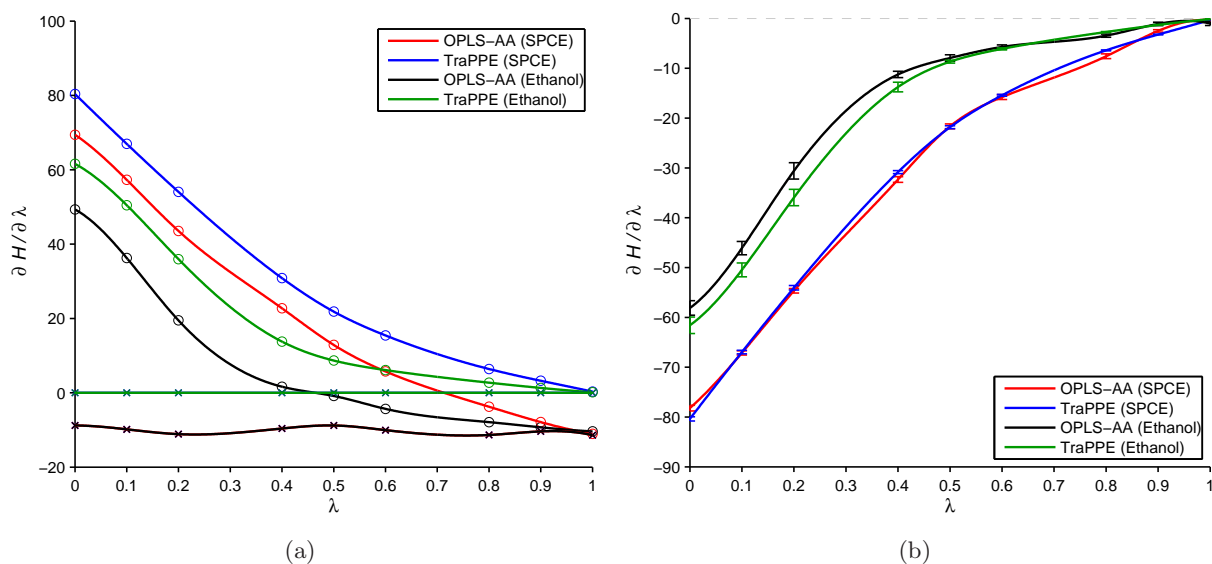


Figure 5.4: Decoupling of Coulombic interactions between cis-3-hexenol and SPC/E water or ethanol ($\lambda = 0$ is full interaction and $\lambda = 1$ is no interaction). Differences are seen between the decoupling functions with the two force fields, due to one being all-atom and the other united-atom (a). Circles are simulations in solvent, and crosses are in vacuum. The decoupling of solute-solvent interactions (difference between vacuum and solvent simulations) shows very similar decoupling function for the two force fields (b).

When $\lambda = 0$, full Coloumbic interactions are exhibited by the solute molecules, while for $\lambda = 1$ Coloumbic interactions are zero. As the decoupling of the Coloumbic interactions has shown to be a very smooth function and the calculations of the electrostatics is the most time consuming part of MD simulations, it was chosen to perform calculations for the following λ values $\{0.0; 0.1; 0.2; 0.4; 0.5; 0.6; 0.8; 0.9; 1.0\}$. In figure 5.4, the decoupling of Coloumbic interactions are shown for cis-3-hexenol in either SPC/E water or ethanol with both OPLS-AA and the TraPPE-UA force fields. In Figure 5.4 (a), are shown the decoupling in both the solvent and in vacuum. As described earlier (equation 5.15), the difference between these two simulations is exactly the decoupling of intermolecular Coloumbic interactions between solvent and solute, which can be seen in Figure 5.4 (b).

The decoupling of LJ interactions is made after the decoupling of the Coloumbic interactions, which means that the solute molecule in this step has no atomic charges. This means that the calculations are computational less expensive and for this reason the calculations were done for

this step at a more dense λ mesh, that is for $[\lambda=\{0.0; 0.1; 0.2; 0.3; 0.4; 0.5; 0.6; 0.7; 0.75; 0.8; 0.85; 0.9; 0.95; 1.0\}]$. Even though the simulation at each λ value is completely independent of each other, the plot of all the simulations reveals a fairly smooth function of the decoupling of LJ interactions of the solute, as can be seen in figure 5.5.

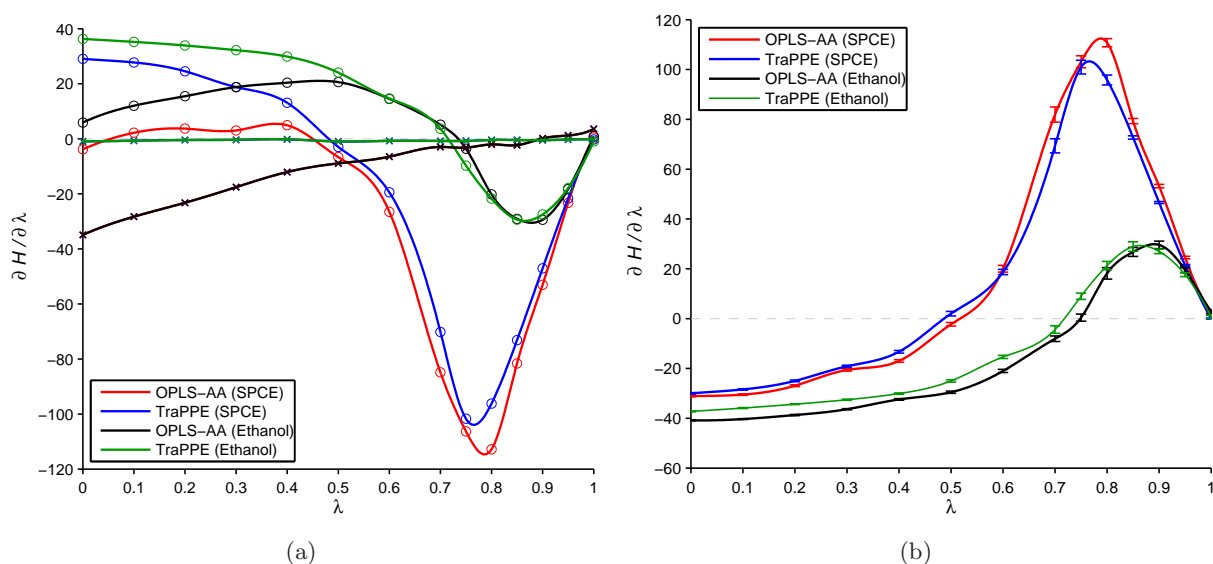


Figure 5.5: Decoupling of Lennard-Jones interactions between cis-3-hexenol and SPC/E water or ethanol ($\lambda = 0$ is full interaction and $\lambda = 1$ is no interaction). (a) refers to the decoupling function in either vacuum (crosses) or solvent (circles), whereas (b) refers to solute-solvent interaction decoupling by the two force fields.

In figure 5.5 (a) the decoupling of LJ interactions of cis-3-hexenol in SPC/E water (line with o) and in vacuum (line with x) is shown. Even though the functions for the decoupling of all LJ interactions of cis-3-hexenol for the two force fields looks very different, the collective function for the decoupling of only the LJ interactions between cis-3-hexenol and the solvent is fairly similar for the two force fields (figure 5.5 (b)). This plot of the decoupling of only LJ interactions between solute and solvent (not intra molecular LJ interactions) is obtained by subtracting the vacuum simulation from the SPC/E simulation (see equation 5.15).

Partition coefficients in squalane and ethanol/water

Table 5.3: Calculated free energies of solvation of cis-3-hexenol or decane using OPLS-AA and TraPPE-UA force fields together with SPC/E or TIP4p water models. Large differences are seen between the two force fields for calculated energies with long chain hydrocarbons (i.e simulation with squalane and decane).

Solute	Solvent (Vol. / Vol.)	OPLS-AA [kJ/mol]				TraPPE-UA [kJ/mol]			
		SPC/E		TIP4p		SPC/E		TIP4p	
Cis-3-hexenol	Squalane	-20.9	±1.2			-15.6	±1.1		
Cis-3-hexenol	Water	-14.3	±1.1	-17.2	±0.6	-15.3	±0.9	-18.7	±0.8
Cis-3-hexenol	20% Ethanol	-18.9	±2.2	-24.0	±1.4	-20.7	±2.9	-21.0	±1.1
Cis-3-hexenol	40% Ethanol	-29.9	±2.0	-29.1	±1.3	-27.0	±1.9	-26.2	±1.4
Cis-3-hexenol	80% Ethanol	-32.6	±1.5	-32.5	±1.1	-30.8	±1.1	-30.3	±0.9
Cis-3-hexenol	Ethanol	-33.5	±1.1			-32.0	±1.0		
Decane	Squalane	-34.1	±1.4			-20.6	±1.6		
Decane	20% Ethanol	2.6	±2.2	-1.4	±1.9	6.3	±2.0	5.7	±1.4
Decane	40% Ethanol	-13.6	±2.1	-13.6	±2.8	-8.7	±2.1	-5.8	±1.1
Decane	80% Ethanol	-22.5	±1.3	-22.7	±1.2	-14.2	±1.1	-15.2	±1.1
Decane	Ethanol	-27.9	±1.1			-18.7	±0.9		

The estimated free energy of solvation ($\Delta_{solv}G$) of cis-3-hexenol or decane into several solvents is listed in table 5.3. The choice of these two solutes is based on the availability of experimental partition coefficients, and that these two solutes represent each a hydrophilic or a hydrophobic solute. It has not been possible to find any experimental free energy of solvation for these two solutes into any of the solvents. However, Cabani et. al.[70] report the experimental free energy of hydration to be increasing with chain length up to n-octane, which has a value of 12.10kJ/mol, so a good estimate from decane would be approximately 13kJ/mol. For 1-hexanol a value of -18.26kJ/mol (the double bond will probably lower this value a bit) is reported, but both values seem to be in the same order as those calculated in this work for cis-3-hexenol and decane. Large differences are seen between the two force fields for the calculated energies of long chain hydrocarbons (i.e. simulation with squalane and decane). As only experimental free energy of solvation into water has been found in the literature it is difficult to conclude from only the free energy calculations which force fields is the best for the hydrocarbon simulations, but for decane in 20% ethanol the value with the TraPPE-UA force field is the closest compared to the value reported by Cabani et. al.[70] into pure water.

Table 5.4: Logarithmic Partition coefficients ($\log K_p$) of cis-3-hexenol and decane between squalane and ethanol/water solvents. For decane in pure ethanol three experimental values was found in the literature, showing a big uncertainty with $\log K_p$ values from -0.26 to 0.54. (a)=[71], (b)=[72], (c)=[73] and (d)=[46].

Solute		Ethanol in water (vol. / vol.)									
		0%		20%		40%		80%		100%	
Cis-3-hexenol	Experimental	-0.48^(a)		-1.11^(b)		-1.60^(a)		-2.47^(b)		-2.52^(a)	
Cis-3-hexenol	OPLS-AA SPC/E	1.15	± 0.27	0.35	± 0.43	-1.57	± 0.41	-2.0	± 0.33	-2.21	± 0.27
Cis-3-hexenol	OPLS-AA TIP4p	0.66	± 0.23	-0.54	± 0.31	-1.43	± 0.30	-2.03	± 0.28	-2.21	± 0.27
Cis-3-hexenol	TraPPE-UA SPC/E	0.06	± 0.25	-0.90	± 0.54	-1.99	± 0.38	-2.66	± 0.27	-2.88	± 0.25
Cis-3-hexenol	TraPPE-UA TIP4p	-0.55	± 0.24	-0.94	± 0.26	-1.85	± 0.30	-2.57	± 0.25	-2.88	± 0.25
Decane	Experimental			4.30^(a)		3.62^(a)		0.54^(a) 1.00^(c)		-0.26^(a) 0.54^(c) 0.06^(d)	
Decane	OPLS-AA SPC/E			6.43	± 0.46	3.58	± 0.44	2.02	± 0.34	1.08	± 0.31
Decane	OPLS-AA TIP4p			5.73	± 0.42	3.59	± 0.55	1.99	± 0.33	1.08	± 0.31
Decane	TraPPE-UA SPC/E			4.72	± 0.45	2.20	± 0.46	1.12	± 0.34	0.34	± 0.32
Decane	TraPPE-UA TIP4p			4.56	± 0.37	2.61	± 0.33	0.96	± 0.34	0.34	± 0.32

From the calculated free energies of solvation for cis-3-hexenol and decane, the partition coefficients of these two solutes can be calculated by equation 1 (see Table 5.4). Experimental data of this kind are rare, so the data quality can be hard to know. But for decane in pure ethanol three experimental values were found in the literature, ranging from a log K_p value of -0.26 (higher affinity to ethanol) to a log K_p value of 0.54 (higher affinity to LDPE). This makes it hard to conclude on the actual quality of the proposed methodology for estimating partition coefficients. The choice of squalane was to mimic a long chain hydrocarbon solute with a density close to low-density polyethylene (LDPE). Simulation of pure squalane ($C_{30}H_{62}$) gave a density of $809 \text{ kg}/m^3$ at 298K and 1 atm (LDPE has a density around $839 \text{ kg}/m^3$). Simulation was also done up to a chain size of C_{80} (giving a density of $843 \text{ kg}/m^3$) but no substantial difference in the free energy of solvation was seen when increasing the chain size from C_{30} to C_{80} . For this reason it was chosen to use the computational cheaper squalane molecules to mimic the LDPE solute.

As seen in the calculated partition coefficients for the systems with squalane and ethanol/water, it appears that the SPC/E water model over predicts the values. For this reason an investigation was done of the SPC and TIP4p type water models for this type of calculations to see if any improvement could be achieved by changing the water model.

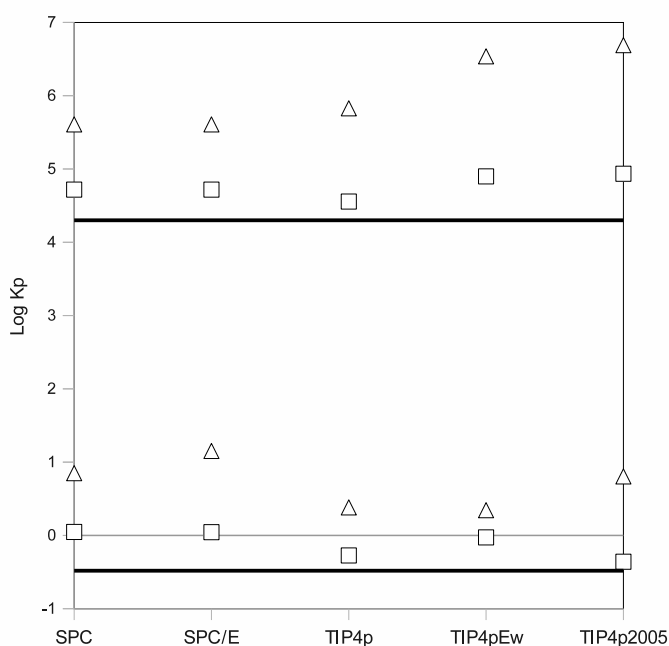


Figure 5.6: The calculated partition coefficients of cis-3-hexenol and decane in squalane and water, calculated with 5 water models. Black line is experimental data (for LDPE), square points are calculations with OPLS-AA force field and triangle points are with TraPPE-UA force field.

In figure 5.6, the calculated partition coefficient of cis-3-hexenol and decane between squalane and pure water, using SPC, SPC/E, TIP4p, TIP4pEw and TIP4p2005 water models is plotted. As it can be seen, the OPLS-AA force field has a general tendency to over predict the

partition coefficients compared to the TraPPE-UA force field. For the hydrophilic cis-3-hexenol simulations, only the TraPPE-UA simulations with the TIP4p and the TIP4p2005 water models are able to predict a negative logarithmic partition coefficient (higher affinity of cis-3-hexenol towards water than squalane). For the decane simulations the partition coefficient with the TIP4p water model is a bit closer to the experimental partition coefficient. For this reason it was chosen to make the same calculations once again with the TIP4p model instead of the previous calculations with the SPC/E model. All calculated partition coefficients with both water models are shown in table 5.4.

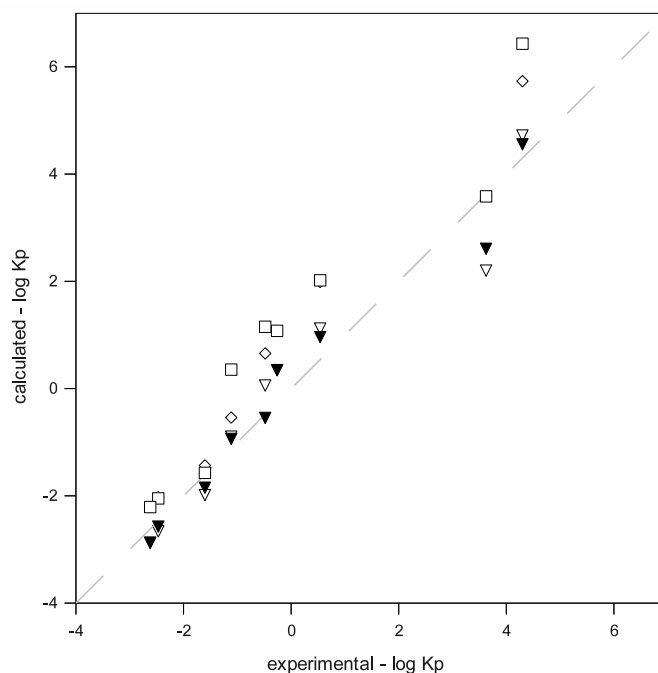


Figure 5.7: The logarithmic calculated partition coefficients versus the logarithmic experimental partition coefficients. The combination of TraPPE-UA force field with the TIP4p water model (green points) seems to give good prediction over the whole range. Squares = OPLS-AA and SPC/E; Diamonds = OPLS-AA and TIP4p; White triangles = TraPPE-UA and SPC/E; Black triangles = TraPPE-UA and TIP4p.

In figure 5.7, which is a plot of all experimental and calculated data listed in table 5.4, it can be seen that over the whole range of chosen systems the combination of the TraPPE-UA force field together with the TIP4p water model gives the best results.

5.2.7 Conclusions

Using the proposed methodology of calculations of free energy of solvation of a small organic molecule into different solutes from MD simulations, it was possible to obtain good estimates of the partition coefficient for the organic molecule between two solutes. By splitting the decoupling of the interactions up into two steps (first electrostatics, then Lennard-Jones) and having all simulations completely independent of each other, it gives a possibility to save some calculation time as fewer calculations are done when only few changes are seen for the decoupling function.

As calculations of the electrostatics are by far the most time consuming and the decoupling function of only the electrostatics showed to be a very smooth function, a lot of simulation time can be saved by a careful choice of needed simulations of the electrostatic decoupling. In this work most of the electrostatic decoupling calculations are done at only 9 separate λ decoupling parameter values (see part 5.2.3). The decoupling of Lennard-Jones interaction (in a box with no charges, hence no electrostatic calculations) is somewhat cheaper, but as the function is not as smooth as for the electrostatic decoupling, more independent simulations have to be used. In this work, 14 independent simulations have been used to find the Lennard-Jones decoupling function, but each decoupling function had to be manually inspected to assure that a smooth function for the decoupling is found.

Squalane was used to mimic LDPE in order to make calculations simpler and cheaper. The density of squalane from MD simulations was a little lower than the density of LDPE, but extension of the carbon chain length of squalane up to 80 carbon atoms could not be concluded to show a significant change in the calculated free energy of solvation as the difference was within the statistic uncertainty of the calculations.

It was expected that the OPLS-AA all atom force field with explicit hydrogen parameters would do better than the united atom TraPPE-UA force field. But the TraPPE-UA force field showed to be both computational cheaper and also more accurate compared to experimental data seen in all calculations. So from this work there is no doubt that TraPPE-UA is the best force field for this type of simulations. From the tested water models it was also seen that for the hydrophilic molecules the choice of water model has some importance and that the TIP4p and TIP4p/2005 models performed a bit better than the other models. For the hydrophobic molecules the difference between water models was very little. The TIP4p type water models have one more center (the dummy atom carrying the charge of the oxygen) than the SPC type models, which makes the TIP4p type water models computational more expensive. This means that even though the TIP4p model performs a little better overall, the SPC/E model can still be the best model of choice depending on system and computational power available.

This work has only focused on calculations towards water/ethanol solvent systems (simulant A and C by EU legislation). Further work has been done with calculation by this methodology into food simulant B (3% acetic acid), which will be presented in a forthcoming publication.

5.2.8 Acknowledgement

The authors acknowledge Danisco A/S, the graduate school in Chemical Engineering at DTU (MP₂T) and The Technical University of Denmark (DTU) for making this project possible.

5.3 Modeling Acetic Acid by Molecular Dynamics

After successful application of the proposed methodology to systems with food simulant A (distilled water) and food simulant C (10% ethanol, 50% ethanol) as shown in the article submitted to Journal of Fluid Phase Equilibria (FPE) (section 5.2), it was decided to test its applicability to systems containing food simulant B (3% Acetic Acid). Despite the large collection of experimental partition coefficient values given by Baner and Piringer in their book "Plastic packaging - Interactions with food and pharmaceuticals"[14], no data exist for systems with food simulant B. Tehrany et al.[74, 75] recently published some experimental data of partition coefficients for systems containing all four food simulants and polyamide (PA) or polyethylene terephthalate (PET). In the current study PE and specifically LDPE was chosen as the polymer to keep the system as simple as possible. It was also decided not to try to model binary systems of polymer (PA or PET) and acetic acid because of lack of existing data. Instead it was chosen to make an investigation of how well the acetic acid system is modeled with the two force fields already used in (see section 5 and the article presented in the section 5.2 "Partition coefficients of organic molecules in squalane and water/ethanol mixtures by Molecular Dynamics Simulations", TraPPE and OPLS-AA).

In the article by Chocholousova et. al.[76] a similar investigation has been done using the CHARMM27[5] force field. In this article the acetic acid dimer structure in the gas phase was studied and COSMO calculations were performed to find the sp^2 carbon distances of the lowest energy state acetic acid dimers (see figure 5.8). It was then suggested that when these specific distances occur in molecular dynamics calculations of both the gas and liquid phases it can be then safely concluded that this specific structure is present. The authors also concluded that the use of the sp^2 - sp^2 carbon distances is a simplification and that the use of experimentally measured values of the distance and angle of the OH - H hydrogen bonds would be a scientifically sounder choice .

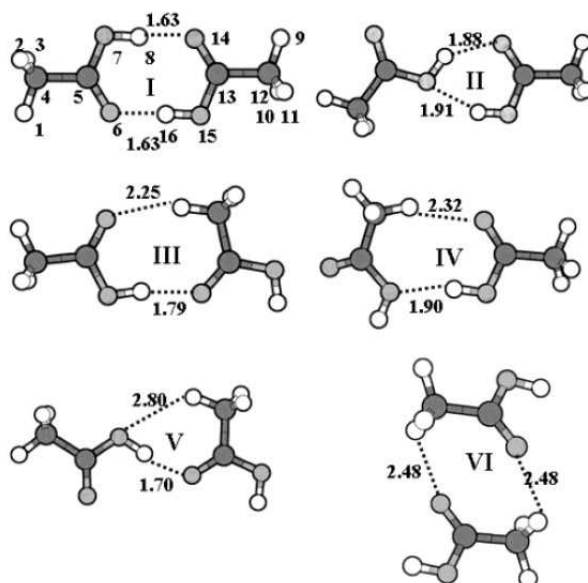


Figure 5.8: Lowest energy state dimers of acetic acid in the gas phase calculated using COSMO software by Chocholousova et. al.[76]

In this current acetic acid study, it was chosen to use the CHARMM27[5, 50] force field as Chocholousova et al. did in order to compare the two sets of results[76]. Below are the three force fields compared:

- TraPPE Force field[8, 77]
 - United-atom; parameterized with VLE data; Standard Lorentz-Berthelot combining rule; no LJ 1-4 intramolecular interactions ($S_{LJ} = 0$) and Coloumbic 1-4 interactions are scaled by 0.5 ($S_C = 0.5$); Originally with fixed bond lengths, but in this work modeled with harmonic potential from the CHARMM27 force field (due to segmentation faults).
- OPLS-AA Force field[7]
 - All-atom; parameterized for protein simulations; Geometric mean combining rule; LJ and Coloumbic 1-4 intramolecular interactions are scaled by 0.5 ($S_{LJ} = 0.5$ and $S_C = 0.5$).
- CHARMM27 Force field[5, 50]
 - All-atom; parameterized for protein simulations; Standard Lorentz-Berthelot combining rule; LJ 1-4 intramolecular interactions are predefined in the force field and full Coloumbic 1-4 intramolecular interactions ($S_C = 1$); Angle bending has an extra 1-3 distance term.

After having used all three force fields abovementioned, some key differences among them have been identified. For the OPLS-AA it has been chosen to use the geometric mean combining

rule (eq. 5.22) between uneven centers for LJ interactions, as opposed to the most widely used Lorentz-Berthelot combining rule (eq. 5.23) that is being used by both TraPPE and CHARMM27 force fields.

$$\sigma_{ij} = \sqrt{\sigma_{ii}\sigma_{jj}}, \quad \epsilon_{ij} = \sqrt{\epsilon_{ii}\epsilon_{jj}} \quad (5.22)$$

$$\sigma_{ij} = \frac{1}{2}(\sigma_{ii} + \sigma_{jj}), \quad \epsilon_{ij} = \sqrt{\epsilon_{ii}\epsilon_{jj}} \quad (5.23)$$

Moreover is it important to observe how the scaling of the specific 1-4 LJ and Coloumbic interactions are implemented by the different force fields. All the calculations with acetic acid were performed with partial-mesh ewald[78] for long range electrostatic interactions and the TIP4p/2005 water model[64]. In the recent article by Motin et al.[79] highly accurate experimental densities for the acetic acid and water system have been measured. In table 5.3 are shown the calculated densities of these systems with the three force fields and are compared against these experimental data.

Table 5.5: The calculated densities (in kg/m^3) of acetic acid/water systems with TraPPE, OPLS-AA and CHARMM27 force fields at 303.15K. Both OPLS-AA and CHARMM27 seem to give a bit better results than TraPPE, but only CHARMM27 is able to capture the local maximum in the density. X_2 is the mole fraction of acetic acid, and the two columns [H₂O] and [Ace] contain the number of water and acetic acid molecules in the simulation box.

X_2	H ₂ O	Ace	Exp	TraPPE	OPLS-AA	CHARMM27
0.0000	500	0	995.7	995.9	995.9	995.9
0.0950	453	47	1027.5	1011.3	1010.9	1011.0
0.2385	381	119	1049.7	1013.1	1043.9	1034.5
0.4823	259	241	1059.8	1014.7	1046.8	1029.5
1.0000	0	500	1039.1	1015.5	1066.5	1019.8

The TIP4p/2005[64] water model shows very good ability to estimate the density of water, whereas none of the three force fields seems to be able to estimate the density of pure acetic acid as accurately. TraPPE and CHARMM27 force fields both underpredict the pure acetic acid density and the OPLS-AA overpredicts it, by the same percentage on average. When plotting the density values as a function of the concentration of acetic acid (figure 5.9), it is easier to see the local density maxima the experimental data exhibit.

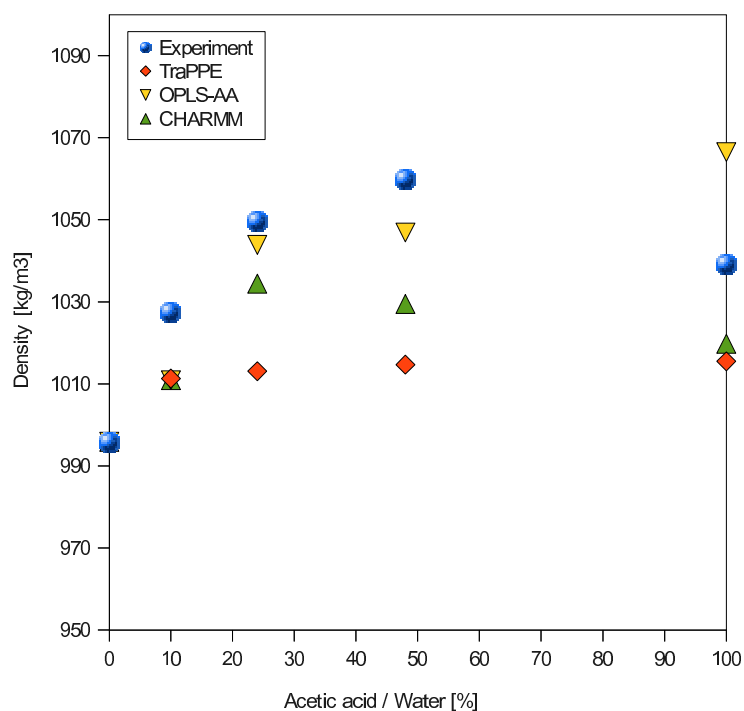


Figure 5.9: Predicted and experimental densities of acetic acid/water systems at 303.15K. Only the CHARMM27 force field is able to predict the local density maxima of the system.

To test if the three force fields were implemented correctly for the acetic acid in the GROMACS software, the radial distribution function was plotted from the hydroxyl hydrogen to both the hydroxyl oxygen and the carboxyl oxygen. The radial distribution function gives the average distribution of center type A (carboxyl oxygens) around center type B (hydroxyl hydrogen) as a function of the distance from B. In figure 5.10 is shown this plot for pure acetic acid with the three force fields. This plot only gives a "1D" representation of the distribution of the two centers of interest, and as such only the average distance information between the two centers and not the specific spatial location is obtained. This means that it is very difficult to conclude whether the peaks in the plot should be attributed to a dimer-like structure or a chain-like structure.

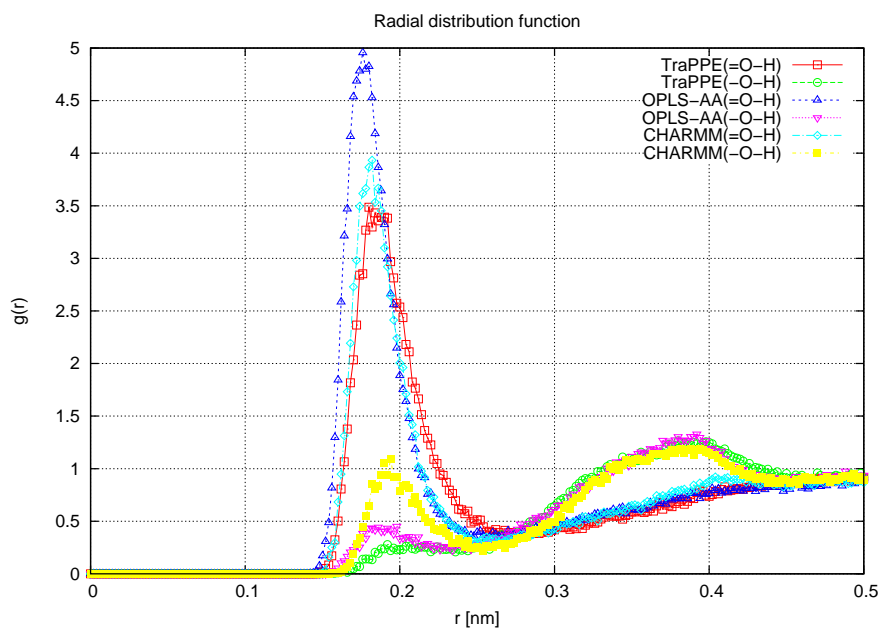


Figure 5.10: Radial distribution function of acetic acid for the three force fields between hydroxyl hydrogen and carboxyl oxygen (=O-H) or hydroxyl oxygen (-O-H).

When comparing the calculated radial distribution functions with those presented in the article by Kamath[77] with a comparison of the newly developed force field for carboxylic acids (the one here denoted as TraPPE) against OPLS-AA and CHARMM27 force fields, it is seen that the same peaks at the same distances are obtained (compare figures 5.10 and 5.11).

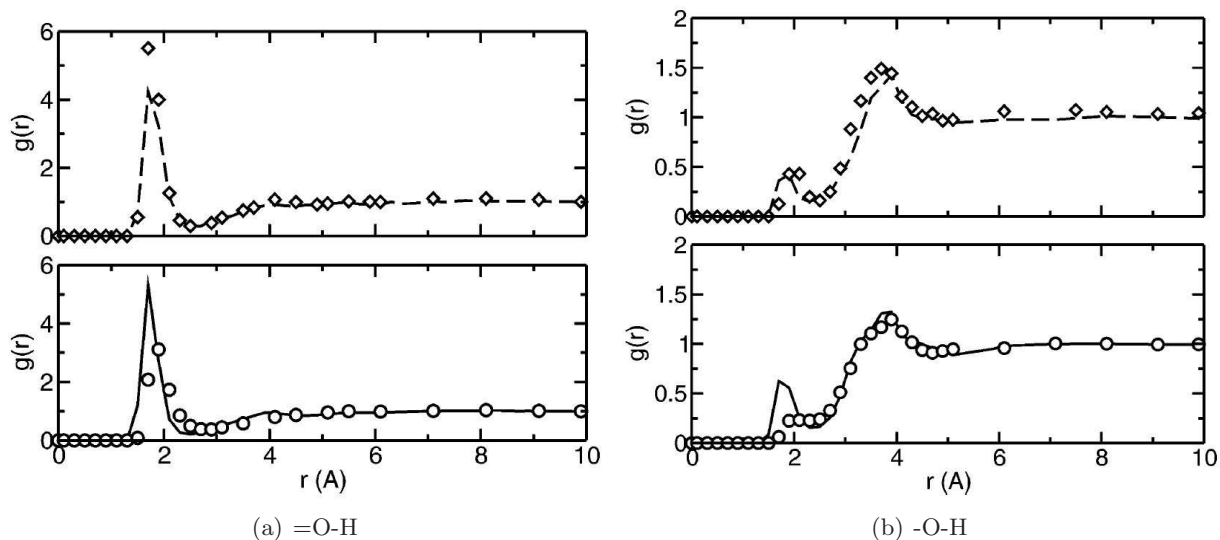


Figure 5.11: Radial distribution function plots of acetic acid from the original article by Kamath[77] between hydroxyl hydrogen and carboxyl oxygen (=O-H) or hydroxyl oxygen (-O-H). Top plots: CHARMM27 (diamonds), OPLS-AA (dashed line); bottom plots: TraPPE (circles), OPLS-UA (solid line).

To obtain structural information on how the acetic acid hydrogen bonds, its spatial distribution function was plotted. The spatial distribution function shows the density of a single type of

center around at least three centers used as a fix point in the 3-dimensional space. This was firstly done for TIP4p/2005 water to see if the calculation was done correctly (see figure 5.12 (b)), by comparing similar plots for TIP4p water as shown by Kusalik[80].

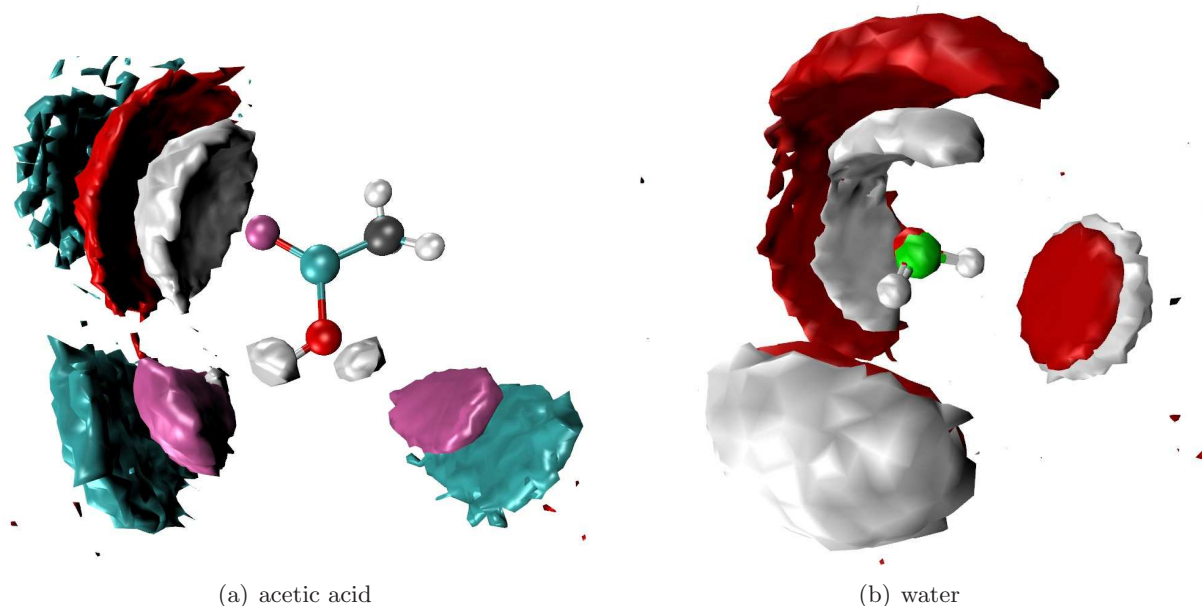


Figure 5.12: Spatial distribution functions (sdf) calculated for TIP4p/2005 water and acetic acid (here with the OPLS-AA force field, hence the explicit hydrogens on the CH_3 center (grey)). The sdf for acetic acid shows that the carboxylic carbon (light blue) most often is in two areas (in front of the two preferred C-C-O-H torsional angles) instead of in only one area, as would be expected for a dimer. Moreover seems the hydroxyl group to approach the carboxyl oxygen from most angles within the hydrogen bond angle (O-H-O of 30 degrees).

The three calculated spatial distribution functions (one for each force field), are almost indistinguishable from each other. In figure 5.12 (a) are the density clouds around the central acetic acid molecule coloured as the atoms in the central molecule. The light blue sp_2 carboxylic carbon density cloud is in all three force fields not located in the central point (between the hydrogen bond donor and acceptor), as it would be expected for a dimer, but instead it is split up into two different areas. These points towards the hydrogen bonding of the liquid acetic acid are more a chain like structure than only a monomer/dimer structure.

To investigate this postulate on the hydrogen bond structuring of acetic acid, a code had to be developed to count the number of acetic acid molecules which agglomerate into hydrogen bond clustering structures. From the GROMACS code a 2 dimensional connectivity matrix can be made of the occurrence of hydrogen bonds in the box in all times steps, so that successive time steps are in one dimension and all occurring hydrogen bonds in all time steps are in the other. The matrix then consists of 1 or 0 depending on whether the specific hydrogen bond occurs at the specific time step or not. In molecular dynamics, the formation of a hydrogen bond depends on the angle and distance between the carboxyl group and the hydroxyl group. In the calculations presented here this definition was set as the default in the GROMACS code, which

means a H-O-H angle of less than 30 degrees and a distance between hydrogen and carboxyl oxygen of less than 0.35nm.

The GROMACS scientific community is very big and strong, and was contacted to find help to write this new code (<http://www.mail-archive.com/gmx-users@gromacs.org/msg26167.html>). Through this community a contact was established to Søren Enemark, a researcher at Department of Chemical and Biomolecular Engineering at the National University of Singapore (private communications, November 2009 - January 2010). His group had developed a code capable of counting hydrogen bond clustering for glycine molecules specifically, but with some change in the code it could also be used the acetic acid. The group from Singapore had developed the code in a somewhat different way (not using the hydrogen bond connection matrix) that was already started in this project, but nevertheless the existence of that code made it possible to check the newly developed code against an already tested one. The results turned out to be the same, and the new code developed for this project in MATLAB was more than 50 times faster than the code from Singapore. The complete code can be found in appendix D.

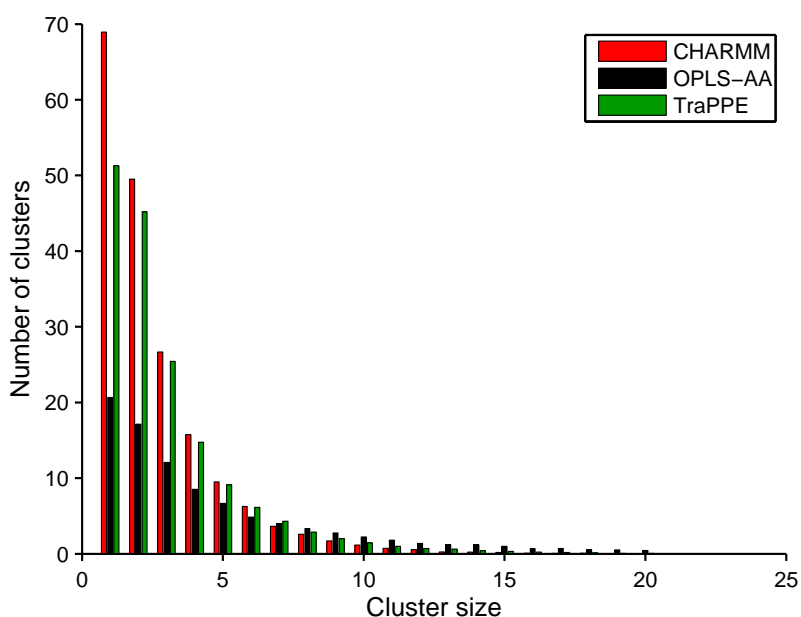


Figure 5.13: Histogram of number of clusters as a function of cluster size in a box of 500 acetic acid molecules averaged over time.

The cluster counting algorithm goes through all proton acceptor and donor centers in each time step and makes a list of the clusters formed during the time step. Two molecules are considered members of the same cluster if there exists a hydrogen bond between them. This means that dimers that consist of two molecules connected by two hydrogen bonds are a subgroup of the clusters of 2 molecules. In figure 5.13 is plotted the histogram of the number of clusters as function of the cluster sizes averaged over all time steps for a box of 500 molecules at 298K. Such a histogram however does not necessarily give a good representation of cluster size distribution, as a big cluster in this histogram counts just as much as a cluster consisting of a single molecule.

By multiplying each cluster average occupancy with the number of molecules in the cluster and then dividing it by the total number of molecules in the box, a ratio of each cluster size occupancy over all molecules is obtained. The relevant histogram is shown in figure 5.14 (a).

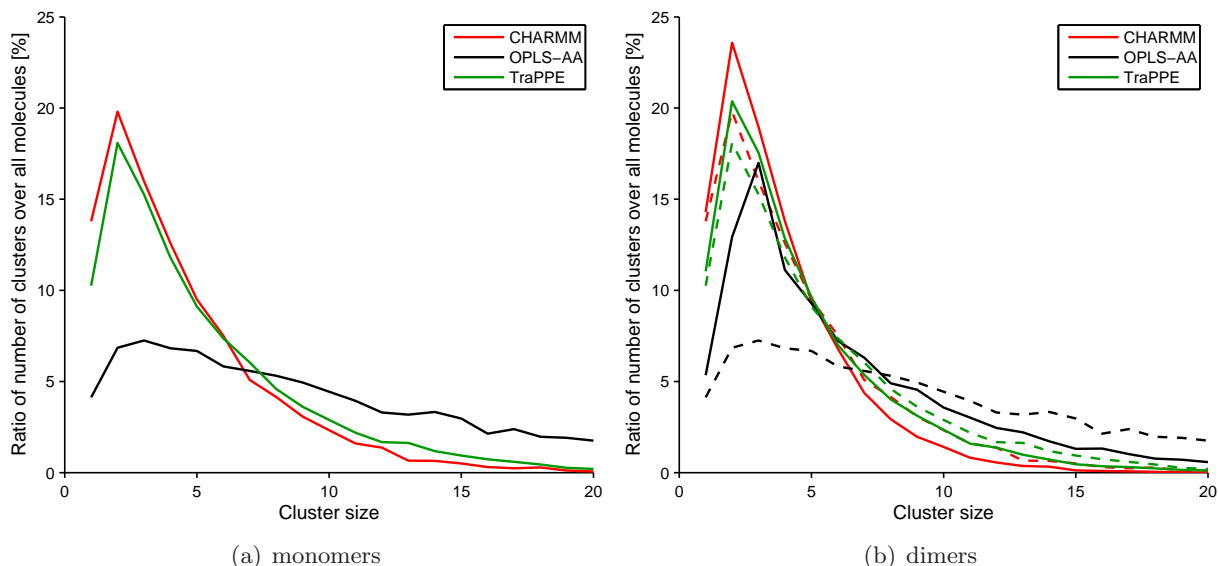


Figure 5.14: Cluster size distribution of liquid acetic acid at 298K. (a) is the distribution when the simulation is started with 500 single acetic acid molecules, and (b) is the distribution with a box of 250 dimers at the starting point (the monomer results as dotted line).

From the histogram of the cluster size distribution (figure 5.14 (a)), it can be seen that with the OPLS-AA force field there is a tendency towards bigger acetic acid cluster sizes. It was expected that the dimer by large would be the most common cluster, so for this reason it was tried to let the simulation start with a box of 250 monomers instead of 500 single molecules. With this approach it was seen that the OPLS-AA force field gave a much closer distribution compared to the distributions obtained when using the two other force fields (figure 5.14 (b)).

Table 5.6: The calculated average occurrence of hydrogen bonds from liquid acetic acid molecules over time (as percentage of all molecules in the box) at 298K. For all three force fields more than 80% of the molecules have 1 or 2 hydrogen bonds. In the table is also listed the average occurrence of a dimer (two acetic acid molecules connected by two hydrogen bonds as both hydrogen bond donor and acceptor). The term “pure dimer” is used for dimers that have no hydrogen bonds other than the dimer hydrogen bond.

	Number of hydrogen bonds from molecule										dimer	pure dimer
	0	1	2	3	4							
TraPPE	7 ±1.2	35 ±2.0	48 ±2.1	9 ±1.3	0.5 ±0.31	10 ±2.0	6 ±1.7					
OPLS-AA	1.7 ±0.63	21 ±2.0	66 ±2.4	10 ±1.1	0.9 ±0.40	1.6 ±0.86	1.2 ±0.71					
CHARMM27	3.5 ±0.77	30 ±1.9	51 ±2.5	15 ±1.3	1.0 ±0.52	4 ±1.8	3 ±1.3					

From the lists generated with the algorithm it is easy to generate different types of statistical data regarding hydrogen bonding of acetic acid. In table 5.6 the occurrence of molecules with 0 to 4 hydrogen bonds is listed, and also the occurrence of the dimer (i.e. two hydrogen bonds at

the same time between a hydroxyl hydrogen and the carboxyl oxygen between two acetic acid molecules). The term “pure dimer” is used for dimers that have no hydrogen bonds other than the dimer hydrogen bonds. As it can be seen the TraPPE force field is best in producing dimers (up to 10%), where CHARMM27 only produces approximately 4% dimers and the OPLS-AA even less. The occurrence of clusters with two molecules was around 20% (see figure 5.14), which shows that only half at best are seen as real dimers. The calculations from Chocholousova et al.[76] (by measuring sp_2 carbon distances) gave a dimer occurrence in liquid acetic acid of 25.3%, which is in the same order of what was calculated in this work for clusters of two molecules. It was decided to calculate the enthalpy of vaporization in order to test the force fields ability to predict an energetic term. The enthalpy of vaporization was calculated as the energy difference between the liquid and the gas phase plus RT (eq. 5.24). This was calculated both from the total energy and the potential energy in the box.

$$H_{vap} = E_{gas} - E_{liq} + RT \quad (5.24)$$

Table 5.7: Calculated enthalpies of vaporization for acetic acid at 298K. Results for each force field seem not to be affected by the use of total or the potential energy difference during the calculations

[KJ/mol]	TraPPE		OPLS-AA		CHARMM27	
	E_{pot}	E_{tot}	E_{pot}	E_{tot}	E_{pot}	E_{tot}
E_{gas}	19.43	37.19	-67.58	-43.22	-273.75	-248.29
E_{liq}	-19.08	-1.44	-115.58	-90.53	-312.65	-287.19
H_{vap}	41.04	41.16	51.52	49.44	41.43	41.42

The structural parameters (density and hydrogen bond clustering) did not show big differences between the force fields, but the calculated potential and total energies with the three force fields are very different (table 5.7). The two all-atom force fields (OPLS-AA and CHARMM27) have both substantially higher energy terms than the united atom force field (TraPPE). As the energy differences (H_{vap} in table 5.7) for all three force fields are close to being the same, this higher energy in the box for the all-atom force fields must be due to more intra molecular interactions from the explicit hydrogens. The energy in the gas phase is mostly due to intra molecular interactions, fact which cancels out the same high energy in the liquid phase when calculating the energy difference between the two phases. Actually E_{gas} was also calculated as a single molecule in vacuum (in a box with no boundary conditions), which means a simulation with no intermolecular interactions as only one single molecule is simulated. This vacuum simulation gave the same total and potential energy per mole as when the simulation was done with a NPT ensemble simulation (isothermal-isobaric simulation) with 108 molecules in the box. From the DIPRR database[81] the reference value for the enthalpy of vaporization at 298K should be 23.7[KJ/mol], close to half of what was calculated in the current work. Calculations were extended towards the critical temperature to see how the temperature dependence of the enthalpy of vaporization was predicted by the molecular dynamics simulation compared to the

DIPPR correlation function. Results are plotted in figure 5.15 (a), which shows that all three force fields predict a different temperature dependence than the DIPPR correlation function. In the work by Andereya and Chase[82], a plot of the proposed temperature dependence of enthalpy of vaporization for different carboxylic acids is included (shown in figure 5.15 (b)). Only the smallest carboxylic acid tends to exhibit a local maximum in the plot of enthalpy of vaporization versus temperature, which is thought to be because of the higher ratio of dimerization of the smaller carboxylic acids in the gas phase.

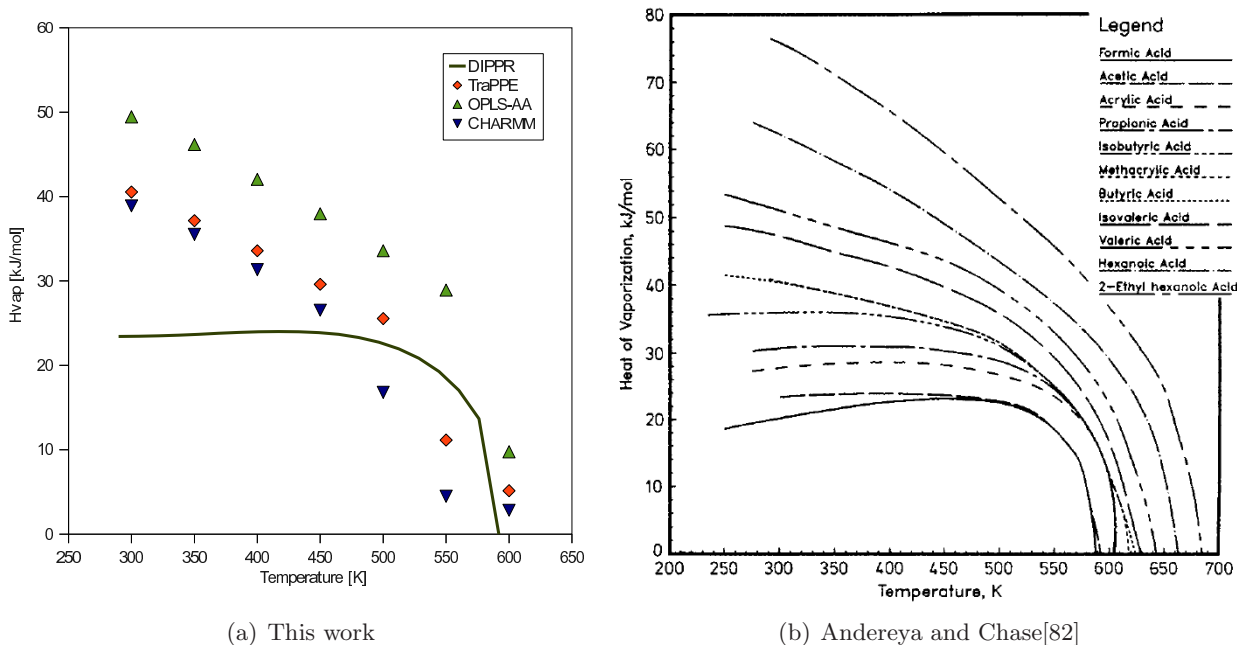


Figure 5.15: (a) The enthalpy of vaporization for acetic acid as function of temperature. All three force fields (points) do not follow the same temperature dependence as the DIPPR correlation function (full line). (b) Proposed dependence to temperature for carboxylic acids by Andereya and Chase[82], where larger carboxylic acids shows the same temperature dependence as the calculated in this work for acetic acid.

From experimental data it is known that acetic acid in the gas phase at 298K should exist almost 100% as dimer. However, when plotting the monomer / dimer ratio in the gas phase (using the developed cluster counting algorithm) especially TraPPE and CHARMM27 force fields show that the simulated gas phase almost purely consists of monomers (see figure 5.16 (a)). All the simulations are started with 54 dimers in a box, but if the dimers break up into two molecules, then these two molecules rarely find themselves close to each other again to form a dimer with any of the force fields. In the article by Chocholousova et al.[76] it is proposed to use higher atomic charges (calculated by COSMO) for the gas phase simulation. Using these higher atomic charges with the CHARMM27 force field, the ratio of monomer/dimer in the gas phase is increased to around 60% (see figure 5.16 (a)). In the article by Chocholousova et al.[76] this ratio is calculated to 80.5%, though calculated by the distance between sp_2 carbons and not from measured hydrogen bonds in the simulation box.

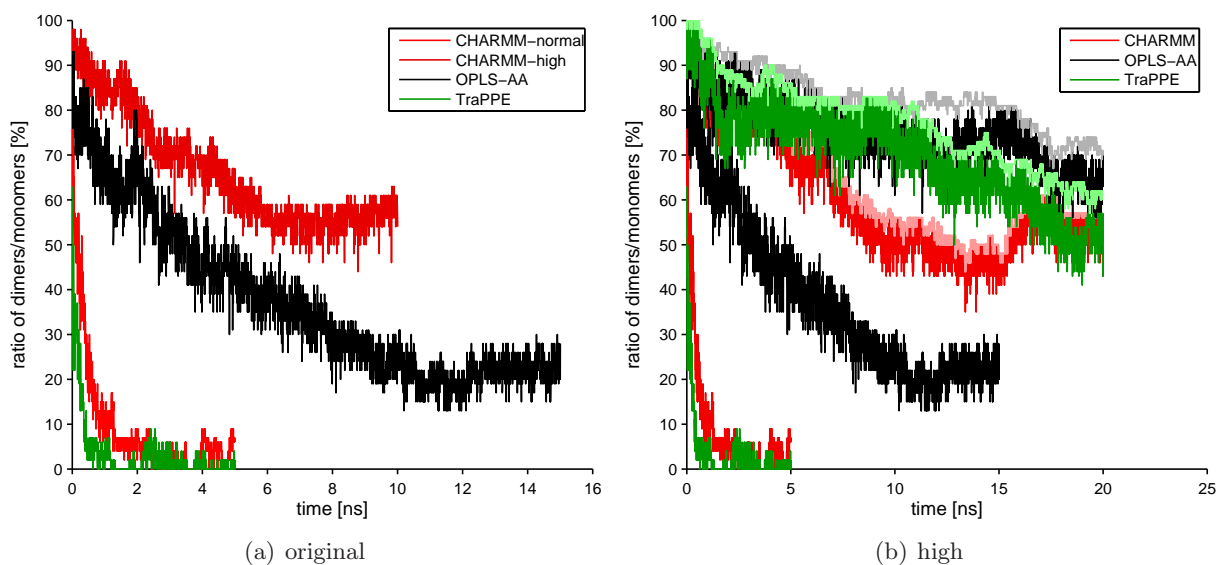


Figure 5.16: Dimer/monomer ratio in the gas phase of acetic acid at 298K calculated with the original atomic charges of the force fields (a), and when using the higher atomic charges from COSMO calculations by Chocholousova et al.[76] (b). The lighter colouring shows the ratio when using "one or more hydrogen bonds" as the definition for a dimer in the gas phase.

These higher atomic charges for the gas phase were then implemented also for the TraPPE and the OPLS-AA force fields (as showed in table 5.8). It should be noted that the bonded parameters in the force fields are fitted together with the LJ and coulombic interaction parameters, meaning that changing the atomic charges alone without refitting the bonded parameters (and probably also the LJ parameters) will lead to an incorrect representation of the molecule. Still simulation of the gas phase using these elevated atomic charges lead to an increase of the monomer/dimer to 60-70% for all three force fields (see figure 5.16 (b)).

Table 5.8: Atomic charges used for acetic acid simulation of the gas phase. The high charges comes from COSMO calculations by Chocholousova et al.[76] for the CHARMM27 force field

[KJ/mol]	TraPPE		OPLS-AA		CHARMM27	
	q_{ori}	q_{high}	q_{ori}	q_{high}	q_{ori}	q_{high}
-H			0.060	0.109	0.090	0.109
C(H_3)	0.120	0.120	-0.180	-0.305	-0.270	-0.305
C(OOH)	0.420	0.726	0.520	0.824	0.750	0.824
=O	-0.450	-0.607	-0.440	-0.607	-0.520	-0.607
-O(H)	-0.460	-0.686	-0.530	-0.686	-0.660	-0.686
H(O-)	0.370	0.447	0.450	0.447	0.430	0.447

Table 5.9: Calculated enthalpy of vaporization using original atomic charges of the force fields, and the higher charges by Chocholousova et al.[76] as shown in table 5.8.

[KJ/mol]	TraPPE		OPLS-AA		CHARMM27	
	q_{ori}	q_{high}	q_{ori}	q_{high}	q_{ori}	q_{high}
H_{vap}	41.16	44.59	49.44	50.35	41.42	45.92

Calculating the energy difference between the liquid and the more accurate represented gas phase did not change the resulting enthalpy of vaporization values (table 5.9). In the article by Jorgensen et al.[7] about the OPLS-AA force field, the stated experimental enthalpy of vaporization is 12.49 Kcal/mol (52.25 KJ/mol) with a reference to the NBS tables by Wagman et al.[83]. The OPLS-AA force field is indeed parametrized using acetic acid as one of the molecules in the parameter fitting set, where enthalpy of vaporization is one of the fitting properties. Looking closer into the experimental data of enthalpy of vaporization for acetic acid in the DIPPR database[81], there are three "outliers" at 298K with a value around 50 KJ/mol. These deviations observed between experimental values of enthalpy of vaporization of acetic acid (only at 298K) were investigated, and an attempt to explain them is provided in the following.

5.3.1 The true enthalpy of vaporization of acetic acid at 298.15K and 1 bar

First of all the DIPPR correlation function is derived after regression of numerous data points[82, 84–86], which all present the same temperature dependency. The three "outliers" at 298K in the DIPPR database[81] all have a note stating "For monomer". This could indicate that the remaining large amount of data were expressed in kJ/(mol monomer/dimer mixture), unfortunately this assumption is far from true.

In the article by Jónasson et al.[87] it is explained that measured data for enthalpy of vaporization is always expressed in kJ/(mol monomer), whereas enthalpy of vaporization estimated by the Clapeyron equation is given in kJ/(mol monomer/dimer mixture). The gas phase dimer fraction as function of the temperature from Jónasson et al.[87] is plotted in figure 5.17. From this figure the expected dimer fraction at 298K should be more than 80%. This could explain the higher estimated enthalpy of vaporization by the three force fields, that is approximately twice as high, if this calculation's result was expressed in kJ/(mol monomer/dimer mixture). But what should be not forgotten is that when performing calculations using molecular dynamics, there is always explicit knowledge of the number of molecules in the box. This means the calculated enthalpy of vaporization always results in energy units per mole of monomer, and not per mole of mixture. Furthermore some of the calculations were done using only one molecule in the gas phase (in vacuum) and the same energy difference between liquid and gas phase came up.

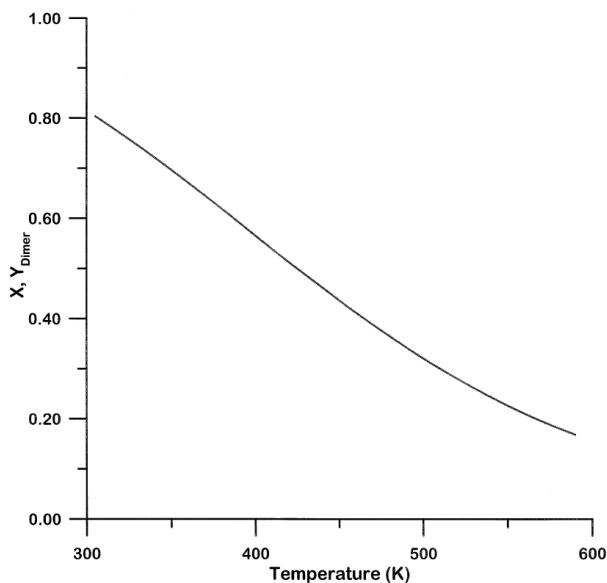


Figure 5.17: Dimer fraction in the gas phase of acetic acid as a function of temperature calculated by Jónasson et al.[87]. At 298K the dimer fraction of the gas phase is above 80%.

The three "outliers" in the DIPPR database are as follows:

- (1) Lebedeva et al.[88] (50.208kJ/mol at 298K, DIPPR ref: 2191) obtained from a Russian conference article, which has not been retrieved so far during this study.
- (2) Chalmers and Watts[89] (52.258kJ/mol at 298K, DIPPR ref: 32) is a calculated value by group contribution, using a reference experimental value of 52.3kJ/mol from Cox and Pilscher[90].
- (3) Cox and Pilscher[90] (52.3kJ/mol at 298K, DIPPR ref: 4433) is a reference book on Thermochemistry, and the enthalpy of vaporization of acetic acid is from the NBS tables by Wagman et al.[83].

By searching in the literature for the origin of data points (2) and (3), it was found out that these two data points actually originate from the NBS tables by Wagman et al.[83] (4). The original value has no further reference or explanation. The NBS tables later became part of the NIST database[91], and on the NIST Chemistry WebBook[91] two values are given for the enthalpy of vaporization of acetic acid at 298K (51.6kJ/mol[92] and 51.6 ± 1.5 kJ/mol[84]).

In the book by Majer and Svovoda[92] the value of 51.6kJ/mol is listed with a reference to Konicek and Wadsö[84]. Therefore the two values in the NIST Chemistry WebBook must be actually from the same reference.

This means that value (2),(3),(4) and the two values contained in the NIST Chemistry WebBook all come from the article by Konicek and Wadsö[84]. In this article the difference between

these two values for the enthalpy of vaporization of acetic acid at 298K is explained. The experimentally obtained enthalpy of vaporization ($\Delta H_v(exp)$) refers to the work of the process $\text{CH}_3\text{COOH}(\text{liq. } 25^\circ\text{C}) \rightarrow \text{CH}_3\text{COOH}(\text{liq. } 25^\circ\text{C, equilibrium mixture at saturation pressure})$. The value of $\Delta H_v(exp)$ at 298K by Konicek and Wadsö[84] is $23.36 \pm 0.10\text{kJ/mol}$. As acetic acid dimerizes in the gas phase, it is proposed by the authors that $\Delta H_v(exp)$ can be split up into two contributions, the "pure" enthalpy of vaporization (ΔH_v°) and the enthalpy of dissociation (ΔH_{diss}). It is stated from an IR study by Claugue and Bernstein[93] that an average enthalpy of dissociation for the six lowest carboxylic acids can be set to a value of 31kJ/mol . Using this value of enthalpy of dissociation and knowing the fraction of dimers in the gas phase (X_D , plotted in figure 5.17) it is possible to calculate the "pure" enthalpy of vaporization (ΔH_v°) of acetic acid (eq. 5.25)

$$\Delta H_v^\circ = \Delta H_v(exp) + X_D \Delta H_{diss} \quad (5.25)$$

The work by Konicek and Wadsö[84] does not give any value for the fraction of dimers in the gas phase. Back Calculating from the given $\Delta H_v^\circ = 51.6$, X_D must be 0.91, which is a bit more than the 80% calculated by Jónasson et al.[87] (see figure 5.17).

From the NBS tables by Wagman et al.[83] the enthalpies of formation ΔH_f° for acetic acid are given for the liquid ($\Delta H_f^\circ(liq) - 484.51\text{kJ/mol}$) and the gas ($\Delta H_f^\circ(gas, M) = -432.25\text{kJ/mol}$) state, but also for acetic acid dimer in the gas state ($\Delta H_f^\circ(gas, D) - 464.21\text{kJ/mol}$). From these values the standard enthalpy of vaporization (ΔH_v°) can be calculated (eq. 5.26):

$$\begin{aligned} \Delta H_v^\circ &= \Delta H_f^\circ(gas, M) - \Delta H_f^\circ(liq) \Rightarrow \\ \Delta H_v^\circ &= -432.25\text{kJ/mol} + 484.51\text{kJ/mol} = 52.26\text{kJ/mol} \end{aligned} \quad (5.26)$$

The value for enthalpy of vaporization by equation 5.26 is equal to what is stated by Jorgensen et al.[7] and by Cox and Pilscher[90]. Using the methodology of Konicek and Wadsö[84] the experimental enthalpy of vaporization can be calculated from the data in the NBS tables (see eq. 5.27)

$$\begin{aligned} \Delta H_v(exp) &= X_D \cdot \Delta H_f^\circ(gas, D) + (1 - X_D) \cdot \Delta H_f^\circ(gas, M) - \Delta H_f^\circ(liq) \Rightarrow \\ \Delta H_v(exp) &= 0.91 \cdot (-464.21)\text{kJ/mol} + (1 - 0.91) \cdot (-432.25)\text{kJ/mol} \\ &+ 484.51\text{kJ/mol} = 23.17\text{kJ/mol} \end{aligned} \quad (5.27)$$

5.4 Conclusion

Using the proposed methodology of calculating the partition coefficient from the free energy of solvation showed to be very successful for the simple systems of LDPE (using squalane) and ethanol/water. Both the hydrophilic and the hydrophobic additive estimated partition coefficients for the LDPE and ethanol/water systems were close to experimental data. Experimental data are scarce and moreover show some scattering when more than one source is available, which makes it hard to define which force field performs better. But from these simple systems, the conclusion must be that overall the most consistent results are the ones derived from the TraPPE force field together with the TIP4p or TIP4p/2005 water model. It is somewhat surprising that the more simple united atom force field (TraPPE) gives more consistent results than the two all atom force fields (OPLS-AA and CHARMM27), but this can be explained by the TraPPE force field is specifically parameterized with phase equilibria data.

The full potential of the methodology for systems containing acetic acid solutions (like food simulant B, 10% acetic acid), has not been tried as no data to compare with were available. Some estimations of structural and energetic properties of acetic acid were calculated using the two force fields of main interest (TraPPE and OPLS-AA) but also the CHARMM27 force field. Only the CHARMM27 force field was able to capture the local density maxima as a function of the concentration change of acetic acid, but none of the force fields stood out as being superior to the others. To fully understand the structural clustering of pure acetic acid, a new cluster counting algorithm was developed. From this algorithm it could be concluded that for all three force fields the hydrogen bond clustering in the liquid phase is not taking place only between monomer and dimer, but also and most importantly chain-like structures are being formed of sizes of up to about 10 molecules with clusters of two being the most predominant.

Regarding the simulation of the gas phase both TraPPE and CHARMM27 force fields showed that the monomer species is the most predominant (less than 2% dimers). For the OPLS-AA force field this ratio was of 20% dimers, but still far from the expected[76]. which is more than 80%. By using new atomic charges calculated by COSMO specifically for the gas phase[76] the ratio of dimers in the gas phase was for all three force fields elevated to around 60-70%.

Calculating the enthalpy of vaporization at 298K gave for all three force fields values almost twice as high as the expected 23.7[KJ/mol] compared to the value given in the DIPPR database[81]. Even the use of the more accurately represented gas phase with the higher atomic charges did not have an effect on the calculated enthalpies of vaporization. Closer look into the data of the DIPPR database and similar calculation with the OPLS-AA force field[7], showed that the calculated enthalpy of vaporization with the OPLS-AA was in agreement with calculations by Jorgensen et al.[7] and that some experimental references for the enthalpy of vaporization of acetic acid at 298K could be found to a value around 50[KJ/mol].

A thorough investigation of the reported value of 50[KJ/mol] for acetic acid at 298K was conducted. This value has been found in 6 different references, where 5 of these references originates

from the work by Konicek and Wadsö[84]. In this work it is explained how the experimental obtained enthalpy of vaporization of acetic acid theoretically can be seen as a an overall energy difference from two contributions, the enthalpy of vaporization of the single acetic acid molecule (monomer) from liquid to gas phase and the enthalpy of dissociation of the dimer in the gas phase. This theoretical enthalpy of vaporization of a single acetic acid molecule is then reported in several references as the enthalpy of vaporization for acetic acid. In my opinion the enthalpy of vaporization is always the energy difference from liquid to gas phase at standard temperature and pressure, disregarding what structural changes that happen in the two phases. The calculated theoretical "pure" enthalpy of vaporization of the acetic acid monomer is from a scientific point of view very interesting and can possibly be used to thermodynamic calculations. The very important point here is that it should be emphasised along with this reported value that it is a theoretical value, and not the experimental or true enthalpy of vaporization.

In the work by Jónasson et al.[87] it is discussed how the enthalpy of vaporization can be calculated as kJ per mole monomer or kJ per mole monomer/dimer fraction. In my opinion this is not true, and the difference seen in calculated energies when changing the monomer/dimer fraction is because of the change in the contribution from the dissociation energy as explained by Konicek and Wadsö[84].

The OPLS-AA force field has been parametrized using a test set of molecules (including acetic acid) towards a range of physical and energetic properties, which includes the enthalpy of vaporization. The used value of vaporization was the "pure" enthalpy of vaporization for the acetic acid monomer, which is correct when simulating that gas phase as a single acetic acid molecule in vacuum. But as the calculations in this work has shown, does this parameter set for acetic acid not capture the correct dimerization in the gas phase, and by this not the correct experimental enthalpy of vaporization. The two other force fields are parametrized towards enthalpy data, but are still not able to predict the correct gas phase composition or enthalpy of vaporization energy.

From this investigation of the simulations of acetic acid with molecular dynamics using the TraPPE, OPLS-AA and CHARMM27 force fields, it must be concluded that the OPLS-AA force field probably is the best of the three force fields. This conclusion is based solely on the OPLS-AA better ability to estimate the theoretical heat of vaporization of the acetic acid monomer, as all three force fields performed equally satisfactory in estimating the density. As neither of the force fields were able to predict the correct representation of the gas phase, it must also be concluded that neither of these three force fields can be used to calculate energetic properties for acetic acid.

Conclusion and Future work

The main purpose of this thesis was to investigate, from a modelling point of view, the migration of GRINDSTED[®] SOFT-N-SAFE (SNS) and other plasticisers from PVC and polyolefin food package materials and into different liquids (specifically the four food simulants set by EU legislation as the ones to be tested in case of migration into foodstuff, i.e. water, 3% acetic acid, 10% ethanol and olive oil) [52]. At first place the migration of GRINDSTED[®] SOFT-N-SAFE, GRINDSTED[®] ACETEM 95 CO (Acetem) and Epoxidised Soybean Oil (ESBO) from Polyvinyl Chloride (PVC) into iso-octane was modeled. The migration problem of small additive molecules from one polymer layer into a solvent in such simple systems can easily be solved since an analytical solution of Fick's second law of diffusion can be obtained. In this case, experimental migration data provided by Danisco were plotted as a function of the square root of time and values for the diffusion coefficients were obtained by linear regression. Using these experimentally obtained diffusion coefficients the migration was modeled using two analytical models, eq. 4.1 by Crank[41] and eq. 4.2 by Kondyli et al.[40], with relatively good accuracy[15]. It turned out that for the specific systems under study where migration of the hydrophobic plasticisers into iso-octane from highly plasticised PVC takes place, the diffusion coefficient should not be considered uniform over the whole polymer layer. The reason behind this observation is that the depletion of the plasticiser from the highly plasticised PVC polymer changes the local structure of the polymer, hence it also changes the local diffusion coefficient in the polymer. It is thought that firstly a fast depletion of plasticiser from a surface layer and into the iso-octane occurs. This depleted layer will then have a much lower diffusion coefficient. The same layer will then act as a barrier for the whole polymer, and by this it will lower the overall migration of the plasticiser contained in the polymer. This means that the obtained diffusion coefficient from experimental migration data will yield an average diffusion coefficient for the whole polymer over the whole time span of available migration data. Diffusion coefficients in PVC can change from 10^{-7} cm²/s for fully plasticised PVC and down to 10^{-16} cm²/s for fully depleted PVC[14]. The obtained diffusion coefficients from the experimental migration data was in the area from 10^{-10} cm²/s to 10^{-9} cm²/s.

Using the model by Vrentas and Vrentas[13] based on the free volume theory, it was tried to fully estimate the diffusion coefficient of SNS in highly plasticised PVC from pure component data alone. This model contains between 7 and 12 parameters depending on how they are defined, and surprisingly they are all physically meaningful. An effort was made to obtain all parameters from either physical pure component data or by group contribution methods, including the interaction parameters (ϕ_1 and ξ). Group contribution methods were examined as they would allow for a pure prediction of the diffusion coefficient without fitting of parameters to the experimental data. The results however showed that the model underpredicts the experimental diffusion coefficient values, which as already mentioned, they should be seen as average diffusion coefficient values of the whole polymer, and they are probably lower compared to the diffusion coefficient of the fully plasticised PVC. Instead of using this elaborated complex model, it was decided to use the much simpler semi-empirical model by Piringer[14], which is suggested for this purpose by the European Commission. The semi-empirical model by Piringer contains only three parameters: an empirical polymer-specific parameter (A_p), the molecular weight of the migrant (M_r) and the temperature (T). Using this simple model, the polymer-specific parameter was obtained by fitting only to the migration data of ESBO (as these data were the only ones showing an Arrhenius type temperature dependence). Using this obtained polymer specific parameter, it was possible to estimate diffusion coefficients for Acetem and SNS at the three different temperatures at which the migration experiment was conducted. The results were very close to the experimental obtained diffusion coefficients at 20°C, but not at higher temperatures. Therefore it was concluded that at the higher temperatures the depletion of the plasticiser from PVC is so fast, that the diffusion coefficients obtained from these migration data are not physically meaningful.

In order to model migration in the polymer with a more realistic diffusion coefficient able to change with local plasticiser concentration, a numerical solution to Fick's second law of diffusion was derived using the finite element mesh method in Matlab[94] and COMSOL[44] environments. Three different models able to describe the plasticiser concentration dependence of the diffusion coefficient were evaluated. None of the three suggested models proved to be substantially better than the others, but all three models seemed to dispose greater predicting capability compared to the static diffusion coefficient (even when using the diffusion coefficient obtained fitted to the migration data). All three diffusion coefficient models have one or two empirical parameters, that showed to be non system-specific.

The numerical model by the finite element method was also used in a new project together with Danisco on development of an improved anti static agent for polyolefins. In this project, in contrary to the overall migration project into foodstuff, the migration to the surface of the polymer is actually the goal. It was possible with a new developed model for the system to correlate estimated migration profiles with very high accuracy to all experimental migration data. This good result leads to the somewhat surprising conclusion that the controlling step in the migration of the additive to the surface was not the migration within the polymer bulk.

Migration is probably due to a temperature dependent partitioning of the additive between the polymer bulk and the surface. A very good correlation between additive concentration and the polymer type to the partition function at starting conditions (right after the extrusion process) was found. The same correlation could not directly be found for the partition function at the final time step, but this function is probably also dependent on some aggregation or restructuring of the additive on the surface. Further work needs to be done for determining a correlation between this partitioning and the chemical structure of the additives, in order to obtain a better understanding of what controls the transport of the additive to the surface of the polymer.

Overall, so far it seemed that there was not an appropriate model for the prediction of partition coefficients of additives between polymers and foodstuff. For this reason it was decided to investigate the possibility of using molecular dynamics for this purpose. Experimentally obtained partition coefficient data for the systems under study are scarce. Thus a methodology developed against experimental data of a system composed of a hydrophilic and a hydrophobic additive between Low Density Polyethylene (LDPE) and different ethanol/water mixtures was done. The calculations included the free energy of solvation of the additive into each of the two solvents. The advantage of this kind of methodologies is that all parameters used (the force fields) are based only on the chemical structure of the molecule (no fitting is needed to pure component data), and that the final partition coefficient is calculated from "measured" solvation data of the additive into the two solvents. This means that the prediction of the free energy of solvation into the two solvents is made on the mesoscopic scale.

The calculated partition coefficients of both the hydrophilic and the hydrophobic additives between LDPE and ethanol/water were correlated with high accuracy against available experimental data. With the increasing computational power of the normal office desktop computers, it is possible today, using this type of calculations, to obtain partition coefficients in less than 20 hours calculation time on an average €1000 computer (quadcore 3GHz). It was decided to test the methodology for acetic acid systems as well, but experimental partition coefficient data were only available for acetic acid systems together with Polyamide (PA) or Polyethylene Terephthalate (PET). As it is well known that acetic acid is a difficult solvent to model, it was chosen to investigate first the predictive capabilities of the force fields for pure acetic acid. It was found that none of the three force fields was able to predict satisfactorily the density of acetic acid / water mixtures. Only the CHARMM27 force field was able to predict the local density maxima of the system. It was expected to see a system consisting mostly of monomer and dimers, was not the the case. For this reason a new hydrogen bond clustering code was developed. With this newly developed code the connectivity size of hydrogen bonded clusters could be counted. Statistics using the cluster counting code showed indeed that the acetic acid molecules in the liquid phase mostly formed chain-like structures, with chains of 2 and 3 molecules in size to be the most predominant ones. Simulation with molecular dynamics does not necessarily give the right representations of the "real" world, but if the simulation fits our knowledge from the mesoscopic and macroscopic scale it can very well give a good indication of what happens at

the microscopic (or atomistic) scale. For example, in the case of liquid acetic acid studied here where it is difficult to distinguish hydrogen bonding in dimers and chain-like structures from spectrophotometric data[95], simulation can very well provide a quantitative estimation.

Furthermore the ability of the force fields to predict the enthalpy of vaporization was tested. All three force fields seemed to overpredict this property to a value about two time higher than that from the DIPPR database[81]. Using the clustering count code on the gas phase simulations it was shown that this phase consisted almost entirely of monomers, where experimental Pressure-Volume data of the gas phase at 298K and 1 bar give a dimer fraction of around 80-90%[87]. This dimer fraction in the gas phase was elevated using higher atomic charges as shown by Chocholousova et al.[76], but the calculated enthalpy of vaporization was still almost twice as high. Further investigation of literature reference data for the enthalpy of vaporization of acetic acid at standard temperature and pressure, showed six data points all having the same value as what the molecular dynamics simulations predicted. Five of the six data points have later been shown to originate from the same work by Konicek and Wadsö from 1970[84]. In the article by Konicek and Wadsö it is explained how the enthalpy of vaporization of acetic acid theoretically can be seen as consisting of two contributions, the "pure" enthalpy of vaporization of the monomer and the enthalpy of dissociation. Konicek and Wadsö then calculated the enthalpy of vaporization of the monomer alone, and it is this value that has been reported in all the later references. This calculated enthalpy of vaporization of the monomer alone maybe of interest from a scientific point of view, but it is very important that this theoretical derived value is not confused with the experimentally obtained enthalpy of vaporization. The OPLS-AA force field is parametrized towards this theoretical "pure" enthalpy of vaporization in a correct way, by only calculating the energy difference for the acetic acid monomer molecule alone between the two phases. However simulations in this work have shown that these parameters do not allow the force field to predict the gas phase dimer fraction accurately enough. It must then be concluded that neither of the three force field parameters for acetic acid can be used for predictions of energetic terms, and that even the structural predictions for the liquid phase (the hydrogen bond clustering) can be questioned until this dimer fraction in the gas phase is correctly predicted by the force field.

Overall it must be concluded that even very complex systems can easily be solved by the numerical solutions of either specialised software for migration (i.e."AKTS-SML[®]"[42] or "FABES-MIGRATEST[®] EXP"[43]) or by more generalized tools like "COMSOL Multiphysics[®]"[44]. But these advanced tools can only predict as good as the information on the systems that is used with them, i.e. the diffusion and partition coefficients. The semi-empirical model by Piringer[14] does not necessarily give the correct diffusion coefficient for the system. The model, however, fulfill the goals for an optimal diffusion coefficient estimation model, because of its simplicity, its ability to safely over predict 95% of all experimental diffusion coefficients and because its approval by the EU for this specific use. The methodology of molecular dynamics to estimate partition coefficients for these systems, gives a consistent and trustworthy estimate of the partition coefficient. This methodologies, however, at this stage are probably too advanced

and tedious to implement directly for the food packaging industry. New software products like Scienomics[96] or Materials Studio[97] attempts to make these advanced molecular simulation calculation methods more easily available to the industry, and may well be on the way to this goal.

Future work

The depletion of plasticiser from highly plasticised PVC was modeled satisfactorily with the diffusion coefficient dependent of the local plasticiser concentration. It should, however, also be investigated how well these systems can be modeled if the diffusion coefficient depends on the local concentration of the iso-octane migration into the polymer, as the depletion of plasticiser from PVC polymer does not mean that PVC will be empty and rigid but probably it will be filled up with solvent (iso-octane).

From the results with the modeling work on migration of the antistatic additive to the surface of Polypropylene (PP) or Low Density Polyethylene (LDPE) it is very important to investigate how the obtained partition coefficient between bulk and surface layer correlate to properties of the additive. This information on what property or properties correlate to partitioning of the additive between surface and bulk of the polymer will give an estimate on what governs this transport to the surface of the polymer.

In order to be able to use the molecular dynamics methodology to predict partition coefficients to all four food simulants, it is important that more experimental data for the acetic acid are produced and that a better force field for acetic acid is developed. To develop such improved parameters it is important to test the force field on its ability to predict also the experimentally proved high dimerisation of acetic acid in the gas phase. The aim of this task should be first of all to obtain optimal parameters specifically for acetic acid, in the same way as models exist for water (SPC[57], SPC/E[57], TIP4p[62], TIP4p2005[64]). When these parameters for acetic acid are established, it can then be investigated how these parameters could be generalised to include more carboxylic acids.

Bibliography

- [1] J. Ferry, *Viscoelastic properties of polymers*. New York, N.Y.: Wiley, 2nd ed., 1970.
- [2] J. S. Vrentas and C. H. Chu, "Concentration-dependence of solvent self-diffusion coefficients," *Journal Of Applied Polymer Science*, vol. 34, pp. 587–592, Aug. 1987.
- [3] J. S. Vrentas and C. M. Vrentas, "Energy effects for solvent self-diffusion in polymer solvent systems," *Macromolecules*, vol. 26, pp. 1277–1281, Mar. 1993.
- [4] S.-U. Hong, "Prediction of polymer/solvent diffusion behavior using free-volume theory," *Industrial & Engineering Chemistry Research*, vol. 34, no. 7, pp. 2536–2544, 1995.
- [5] A. D. MacKerell Jr, D. Bashford, M. Bellott, R. L. Dunbrack Jr, J. D. Evanseck, M. J. Field, S. Fischer, J. Gao, H. Guo, S. Ha, D. Joseph-McCarthy, L. Kuchnir, K. Kuczera, F. T. K. Lau, C. Mattos, S. Michnick, T. Ngo, D. T. Nguyen, B. Prodhom, W. E. Reiher III, B. Roux, M. Schlenkrich, J. C. Smith, R. Stote, J. Straub, M. Watanabe, J. Wiorkiewicz-Kuczera, D. Yin, and M. Karplus, "All-atom empirical potential for molecular modeling and dynamics studies of proteins," *Journal of Physical Chemistry B - Condensed Phase*, vol. 102, no. 18, p. 3586, 1998.
- [6] B. Hess, C. Kutzner, D. van der Spoel, and E. Lindahl, "Gromacs 4: Algorithms for highly efficient, load-balanced, and scalable molecular simulation," *Journal Of Chemical Theory And Computation*, vol. 4, pp. 435–447, Mar. 2008.
- [7] W. L. Jorgensen, D. S. Maxwell, and J. Tirado-Rives, "Development and testing of the OPLS all-atom force field on conformational energetics and properties of organic liquids," *Journal Of The American Chemical Society*, vol. 118, pp. 11225–11236, Nov. 1996.
- [8] M. G. Martin and J. I. Siepmann, "Transferable potentials for phase equilibria. 1. united-atom description of n-alkanes," *Journal Of Physical Chemistry B*, vol. 102, pp. 2569–2577, Apr. 1998.
- [9] A. S. Wilson, *Plasticisers: Principals and Practice*. Maney Materials Science, 1995.
- [10] S. Braucks, "Green paper: Environmental issues of PVC," tech. rep., The Commission of the European Communities, July 2000.

- [11] Danisco, “GRINDSTED® SOFT-N-SAFE - the sustainable plasticiser for PVC,” tech. rep., Danisco, Aug 2006.
- [12] E. Bonino, “Commission recommendation of 1 July 1998 on childcare articles and toys intended to be placed in the mouth by children of less than three years of age, made of soft PVC containing certain phthalates,” *Official Journal of the European Communities*, vol. 485, pp. 35–37, Jul 1998.
- [13] J. S. Vrentas and C. M. Vrentas, “Solvent self-diffusion in rubbery polymer-solvent systems,” *Macromolecules*, vol. 27, no. 17, p. 4684, 1994.
- [14] O.-G. Piringer and A. L. Baner, *Plastic packaging - Interactions with food and pharmaceuticals*. Weinheim Wiley-VCH, 2008.
- [15] R. Lundsgaard, G. M. Kontogeorgis, J. K. Kristiansen, and T. F. Jensen, “Modeling of the migration of glycerol monoester plasticizers in highly plasticized poly(vinyl chloride),” *Journal of Vinyl & Additive Technology*, vol. 15, pp. 147–158, Sept. 2009.
- [16] D. Byrne, “Commission directive 2002/72/EC of 6 August 2002 relating to plastic materials and articles intended to come into contact with foodstuffs,” *Official Journal of the European Union*, vol. 220, pp. 18–58, Aug 2002.
- [17] D. Byrne, “Commission directive 2004/19/EC of 1 March 2004 amending directive 2002/72/EC relating to plastic materials and articles intended to come into contact with foodstuffs,” *Official Journal of the European Union*, vol. 71, pp. 8–21, 2004.
- [18] M. Kyprianou, “Commission directive 2005/79/EC of 18 November 2005 amending directive 2002/72/EC relating to plastic materials and articles intended to come into contact with food,” *Official Journal of the European Union*, vol. 302, pp. 35–45, Sep 2005.
- [19] M. Kyprianou, “Commission directive 2007/19/EC of 30 March 2007 amending directive 2002/72/EC relating to plastic materials and articles intended to come into contact with food and council directive 85/572/EC laying down the list of simulants to be used for testing migration of constituents of plastic materials and articles intended to come into contact with foodstuffs,” *Official Journal of the European Union*, vol. 91, pp. 17–36, 2007.
- [20] A. Vassiliou, “Commission directive 2008/39/EC of 6 March 2008 amending directive 2002/72/EC relating to plastic materials and articles intended to come into contact with food,” *Official Journal of the European Communities*, vol. 63, pp. 6–10, 2008.
- [21] T. F. Jensen, “Migration of plasticizers from PVC to iso-octane.” DANISCO research report.
- [22] T. F. Jensen, “Complete composition of GRINDSTED® SOFT-N-SAFE.” DANISCO research report.
- [23] F. V. Sparsø and T. F. Jensen, “In vivo og in vitro hydrolyse og omsætning af alternativ blødgører,” *Dansk Kemi*, vol. 88, no. 1, pp. 24–26, 2007.

- [24] C. Hansen, *Hansen solubility parameters : A users handbook*. CRC Press., 2nd edition ed., 2007.
- [25] D. W. van Krevelen, *Properties of polymers their correlation with chemical structure their numerical estimation and prediction from additive group contributions*. Elsevier (Amsterdam), 3rd edition ed., 1990.
- [26] E. Stefanis and C. Panayiotou, "Prediction of hansen solubility parameters with a new group-contribution method," *International Journal of Thermophysics*, vol. 29, no. 2, pp. 568–585, 2008.
- [27] C. Clarke, "Directive 2005/84/EC of the european parliament and of the council of 14 december 2005 amending for the 22nd time council directive 76/769/EC on the approximation of the laws, regulations and administrative provisions of the member states relating to restrictions on the marketing and use of certain dangerous substances and preparations (phthalates in toys and childcare articles)," *Official Journal of the European Union*, vol. 344, pp. 40–43, 2005.
- [28] R. Schenkel, "European union risk assessment report," Tech. Rep. 80, Institute for health and consumer protection, 2008. CAS 117-81-7, EINECS 204-211-2.
- [29] B.-g. Wang, H. Lv, and J.-c. Yang, "Estimation of solvent diffusion coefficient in amorphous polymers using the sanchez-lacombe equation-of-state," *Chemical Engineering Science*, vol. 62, no. 3, pp. 775–782, 2007.
- [30] P. B. Macedo and T. A. Litovitz, "On relative roles of free volume and activation energy in viscosity of liquids," *Journal Of Chemical Physics*, vol. 42, no. 1, pp. 245–256, 1965.
- [31] F. A. L. Dullien, "Predictive equations for self-diffusion in liquids - different approach," *AIChE Journal*, vol. 18, no. 1, pp. 62–70, 1972.
- [32] H. Vogel, "The temperature dependence law of the viscosity of fluids," *Physikalische Zeitschrift*, vol. 22, pp. 645–646, 1921.
- [33] J. S. Vrentas and J. L. Duda, "Diffusion in polymer-solvent systems. 2. predictive theory for dependence of diffusion-coefficients on temperature, concentration, and molecular-weight," *Journal of Polymer Science Part B-Polymer Physics*, vol. 15, no. 3, pp. 417–439, 1977.
- [34] J. Brandrup, E. Immergut, and E. Grulke, *Polymer handbook*. Wiley (New York), 4.th ed., 1999.
- [35] J. S. Vrentas and J. L. Duda, "Diffusion in polymer-solvent systems. 1. re-examination of free-volume theory," *Journal of Polymer Science Part B-Polymer Physics*, vol. 15, no. 3, pp. 403–416, 1977.
- [36] D. Lide, ed., *CRC Handbook of Chemistry and Physics*. CRC PRESS, 2000.

- [37] R. N. Haward, "Occupied volume of liquids and polymers," *Journal of macromolecular science-reviews in macromolecular chemistry*, vol. C4, no. 2, pp. 191–242, 1970.
- [38] J. Marrero and R. Gani, "Group-contribution based estimation of pure component properties," *Fluid Phase Equilibria*, vol. 183, pp. 183–208, July 2001.
- [39] T. Begley, L. Castle, A. Feigenbaum, R. Franz, K. Hinrichs, T. Lickly, P. Mercea, M. Milana, A. O'Brien, S. Rebre, R. Rijk, and O. Piringier, "Evaluation of migration models that might be used in support of regulations for food-contact plastics," *Food Additives and Contaminants*, vol. 22, no. 1, pp. 73–90, 2005.
- [40] E. Kondyli, M. Kontominas, and M. Kosmas, "The effect of stirring on the diffusion of small molecules from a polymer matrix into a solution," *Polymer*, vol. 34, no. 12, pp. 2592–2596, 1993.
- [41] J. Crank, *Mathematics of diffusion*. Clarendon press, Oxford, 1st ed., 1956.
- [42] "AKTS-SML[®]" <http://www.akts.com/>, September 2010.
- [43] "FABES-MIGRATEST[®] EXP" <http://www.fabes-online.de/>, September 2010.
- [44] "COMSOL Multiphysics[®] 3.4" <http://www.comsol.com/>, September 2010.
- [45] J. Danguillaume, "Investigation of antistatic mechanisms in polymer," special course, DTU Chemical and Biochemical engineering, June 2008.
- [46] G. Gillet, O. Vitrac, and S. Desobry, "Prediction of solute partition coefficients between polyolefins and alcohols using a generalized flory-huggins approach," *Industrial & Engineering Chemistry Research*, vol. 48, no. 11, pp. 5285–5301, 2009.
- [47] D. L. Beveridge and F. M. Dicapua, "Free energy via molecular simulation applications to chemical and biomolecular systems," *Annual Review Of Biophysics And Biophysical Chemistry*, vol. 18, pp. 431–492, 1989.
- [48] S. A. Best, K. M. Merz, and C. H. Reynolds, "Free energy perturbation study of octanol/water partition coefficients: Comparison with continuum gb/sa calculations," *Journal Of Physical Chemistry B*, vol. 103, pp. 714–726, Jan. 1999.
- [49] J. W. Essex, C. A. Reynolds, and W. G. Richards, "Relative partition-coefficients from partition-functions - a theoretical approach to drug transport," *Journal Of The Chemical Society-Chemical Communications*, pp. 1152–1154, Aug. 1989.
- [50] A. D. MacKerell, N. Banavali, and N. Foloppe, "Development and current status of the charmm force field for nucleic acids," *Biopolymers*, vol. 56, no. 4, pp. 257–265, 2000.
- [51] A. R. Leach, *Molecular Modeling - Principles and Applications*. Addison Wesley Longman Limited, 1996.

- [52] E. Commission, "Council directive of 19 december 1985 laying down the list of simulants to be used for testing migration of constituents of plastic materials and articles intended to come into contact with foodstuffs (85/572/EC)," *Official Journal of the European Union*, vol. 572, pp. 1–9, 1985.
- [53] C. Christophe and A. Pohorille, *Free Energy Calculations - Theory and Applications in Chemistry and Biology*. Springer Berlin, 2007.
- [54] D. Pearlman and P. Kollman, "The lag between the hamiltonian and the system configuration in free energy perturbation calculations," *Journal of Chemical Physics*, vol. 91, no. 12, pp. 7831–7839, 1989.
- [55] M. R. Shirts, J. W. Pitner, W. C. Swope, and V. S. Pande, "Extremely precise free energy calculations of amino acid side chain analogs: Comparison of common molecular mechanics force fields for proteins," *Journal Of Chemical Physics*, vol. 119, pp. 5740–5761, Sept. 2003.
- [56] C. Oostenbrink, A. Villa, A. E. Mark, and W. F. Van Gunsteren, "A biomolecular force field based on the free enthalpy of hydration and solvation: The gromos force-field parameter sets 53a5 and 53a6," *Journal Of Computational Chemistry*, vol. 25, pp. 1656–1676, Oct. 2004.
- [57] H. J. C. Berendsen, J. R. Grigera, and T. P. Straatsma, "The missing term in effective pair potentials," *Journal Of Physical Chemistry*, vol. 91, pp. 6269–6271, Nov. 1987.
- [58] A. Schüttelkopf and D. van Aalten, "ProDRG: a tool for high-throughput crystallography of protein-ligand complexes," *Acta Crystallographica, Section D (Biological Crystallography)*, vol. D60, pp. 1355–1363, 2004.
- [59] M. G. Martin and J. I. Siepmann, "Novel configurational-bias monte carlo method for branched molecules. transferable potentials for phase equilibria. 2. united-atom description of branched alkanes," *Journal Of Physical Chemistry B*, vol. 103, pp. 4508–4517, May 1999. Fejl i CH_n-CH₂-CH₂-CH_n ... skal være 355.03.
- [60] C. D. Wick, M. G. Martin, and J. I. Siepmann, "Transferable potentials for phase equilibria. 4. united-atom description of linear and branched alkenes and alkylbenzenes," *Journal Of Physical Chemistry B*, vol. 104, pp. 8008–8016, Aug. 2000.
- [61] B. Chen, J. J. Potoff, and J. I. Siepmann, "Monte carlo calculations for alcohols and their mixtures with alkanes. transferable potentials for phase equilibria. 5. united-atom description of primary, secondary, and tertiary alcohols," *Journal Of Physical Chemistry B*, vol. 105, pp. 3093–3104, Apr. 2001.
- [62] W. L. Jorgensen, J. Chandrasekhar, J. D. Madura, R. W. Impey, and M. L. Klein, "Comparison of simple potential functions for simulating liquid water," *Journal Of Chemical Physics*, vol. 79, no. 2, pp. 926–935, 1983.

- [63] H. W. Horn, W. C. Swope, J. W. Pitera, J. D. Madura, T. J. Dick, G. L. Hura, and T. Head-Gordon, "Development of an improved four-site water model for biomolecular simulations: TIP4P-ew," *The Journal of Chemical Physics*, vol. 120, no. 20, pp. 9665–9678, 2004.
- [64] J. L. F. Abascal and C. Vega, "A general purpose model for the condensed phases of water: TIP4P/2005," *Journal Of Chemical Physics*, vol. 123, p. 234505, Dec. 2005.
- [65] D. L. Mobley, E. Dumont, J. D. Chodera, and K. A. Dill, "Comparison of charge models for fixed-charge force fields: Small-molecule hydration free energies in explicit solvent," *Journal of Physical Chemistry B*, vol. 111, no. 9, p. 2242, 2007.
- [66] W. F. Van Gunsteren and H. J. C. Berendsen, "A leap-frog algorithm for stochastic dynamics," *Molecular Simulation*, vol. 1, no. 3, pp. 173–185, 1988.
- [67] F. Lee and A. Warshel, "A local reaction field method for fast evaluation of long-range electrostatic interactions in molecular simulations," *Journal of Chemical Physics*, vol. 97, no. 5, pp. 3100–3107, 1992.
- [68] H. J. C. Berendsen, J. P. M. Postma, W. F. van Gunsteren, A. DiNola, and J. R. Haak, "Molecular dynamics with coupling to an external bath," *The Journal of Chemical Physics*, vol. 81, no. 8, pp. 3684–3690, 1984.
- [69] T. C. Beutler, A. E. Mark, R. C. van Schaik, P. R. Gerber, and W. F. van Gunsteren, "Avoiding singularities and numerical instabilities in free energy calculations based on molecular simulations," *Chemical Physics Letters*, vol. 222, pp. 529–539, June 1994.
- [70] S. Cabani, P. Gianni, V. Mollica, and L. Lepori, "Group contributions to the thermodynamic properties of non-ionic organic solutes in dilute aqueous-solution," *Journal of Solution Chemistry*, vol. 10, no. 8, pp. 563–595, 1981. Ethy butyrate.
- [71] J. Kozinowski and O. Piringer, "The influence of partition processes between packaging and foodstuffs or cosmetics on the quality of packed products," *Verpackungs-Rundschau*, vol. 40, pp. 39–44, 1989.
- [72] K. Becker, J. Koszinowski, and O. Piringer, "Permeation of scenting and flavoring substances through polyolefins," *Deutsche Lebensmittel-Rundschau*, vol. 79, no. 8, pp. 257–266, 1983.
- [73] A. Baner, *partition coefficients of aroma compounds between polyethylene aqueous ethanol and their estimation using UNIFAC and GCFEOS*. PhD thesis, Michigan State University, East Lansing, 1992.
- [74] E. A. Tehrany and S. Desobry, "Partition coefficient of migrants in food simulants/polymers systems," *Food Chemistry*, vol. 101, no. 4, pp. 1714–1718, 2007.
- [75] E. A. Tehrany, C. Mouawad, and S. Desobry, "Determination of partition coefficient of migrants in food simulants by the prv method," *Food Chemistry*, vol. 105, no. 4, pp. 1571–1577, 2007.

- [76] J. Chocholousova, J. Vacek, and P. Hobza, "Acetic acid dimer in the gas phase, nonpolar solvent, microhydrated environment, and dilute and concentrated acetic acid: Ab initio quantum chemical and molecular dynamics simulations," *The Journal of Physical Chemistry A*, vol. 107, no. 17, pp. 3086–3092, 2003.
- [77] G. Kamath, F. Cao, and J. J. Potoff, "An improved force field for the prediction of the vapor-liquid equilibria for carboxylic acids," *The Journal of Physical Chemistry B*, vol. 108, no. 37, pp. 14130–14136, 2004.
- [78] Darden, York, and Pedersen, "Particle mesh ewald: an $n \cdot \log(n)$ method for ewald sums in large systems," *Journal of Chemical Physics*, vol. 98, no. 12, pp. 10089–10092, 1993.
- [79] M. A. Motin, M. H. Kabir, and E. M. Huque, "Densities and excess molar volumes of formic acid, acetic acid and propionic acid in pure water and in water + surf excel solutions at different temperatures," *Physics and Chemistry of Liquids: An International Journal*, vol. 43, no. 3, pp. 277–288, 2005. Density, Acetic Acid.
- [80] P. G. Kusalik and I. M. Svishchev, "The spatial structure in liquid water," *Science*, vol. 265, pp. 1219–1221, Aug. 1994.
- [81] R. L. Rowley, W. V. Wilding, J. L. Oscarson, Y. Yang, and N. F. Giles, *DIPPR® Data Compilation of Pure Chemical Properties, Design Institute for Physical Properties*. AIChE - New York, 2010.
- [82] E. Andereya and J. Chase, "Implications of carboxylic acid properties," *Chemical Engineering and Technology*, vol. 13, no. 5, pp. 304–312, 1990.
- [83] D. Wagman, W. Evans, V. Parker, R. Schumm, I. Halow, and S. Bailey, *Selected values of chemical thermodynamic properties. Tables for the first thirty-four elements in the standard order of arrangement 270-3*. National Bureau of Standards, 1968.
- [84] J. Konicek and I. Wadso, "Enthalpies of vaporization of organic compounds .7. some carboxylic acids," *Acta Chemica Scandinavica*, vol. 24, no. 7, pp. 2612–2616, 1970.
- [85] J. D. Chase, "Enthalpy data for saturated lower fatty acids.," *Chemical Engineering (New York)*, vol. 87, no. 6, pp. 107–112, 1980.
- [86] W. Weltner, "The vibrational spectrum, associative and thermodynamic properties of acetic acid vapor," *Journal of the American Chemical Society*, vol. 77, no. 15, pp. 3941–3950, 1955.
- [87] A. Jonasson, O. Persson, P. Rasmussen, and G. S. Soave, "Vapor-liquid equilibria of systems containing acetic acid and gaseous components. measurements and calculations by a cubic equation of state," *Fluid Phase Equilibria*, vol. 152, no. 1, p. 67, 1998.
- [88] N. Lebedeva and Y. Katin, "Heats of evaporation of a series of monocarboxylic acids," *Termodin Termokhim Konstanty (Russian)*, vol. 62, 1970.

- [89] R. Chalmers and R. Watts, "Studies on the quantitative freeze drying of aqueous solutions of some metabolically important aliphatic acids prior to gas-liquid chromatographic analysis," *Analyst*, vol. 97, p. 224, 1972.
- [90] J. Cox and G. Pilcher, *Thermochemistry of Organic and Organometallic Compounds*. Academic press, 1970.
- [91] H. Afeefy, J. Liebman, and S. Stein, *NIST Chemistry WebBook, NIST Standard Reference Database Number 69*. <http://webbook.nist.gov/chemistry>: National Institute of Standards and Technology, September 2010.
- [92] V. Majer and V. Svoboda, *Enthalpies of Vaporization of Organic Compounds: A Critical Review and Data Compilation*. Blackwell Scientific Publications, 1985.
- [93] A. D. H. Claugue and H. J. Bernstein, "Heat of dimerization of some carboxylic acids in the vapor phase determined by a spectroscopic method," *Spectrochimica Acta, Part A: Molecular and Biomolecular Spectroscopy*, vol. 25, pp. 593–, 1969.
- [94] "Matlab R2007b[®]" <http://www.mathworks.com/>, september 2010.
- [95] T. Nakabayashi, K. Kosugi, and N. Nishi, "Liquid structure of acetic acid studied by raman spectroscopy and ab initio molecular orbital calculations," *Journal of Physical Chemistry A*, vol. 103, pp. 8595–8603, Oct. 1999.
- [96] "Scienomics[®]" <http://www.scienomics.com/>, September 2010.
- [97] "Materials studio[®]" <http://accelrys.com/products/materials-studio/>, september 2010.

Appendix **A**

Article: Modeling of the Migration of
Glycerol Monoester Plasticizers in Highly
Plasticized Poly(vinyl chloride)

Modeling of the Migration of Glycerol Monoester Plasticizers in Highly Plasticized Poly(vinyl chloride)

Rasmus Lundsgaard,¹ Georgios M. Kontogeorgis,¹ Jørgen K. Kristiansen,² Torkil F. Jensen²

¹Department of Chemical and Biochemical Engineering, Center for Phase Equilibria and Separation Processes (IVC-SEP), Technical University of Denmark, Lyngby DK-2800, Denmark

²Danisco A/S, Brabrand DK-8220, Denmark

Different migration models were evaluated on the basis of data from migration experiments carried out by Danisco in 2005. The migration experiments were set up to investigate the behavior of the three plasticizers GRINDSTED[®]SOFT-N-SAFE (SNS), GRINDSTED[®]ACETEM 95 CO (Acetem), and epoxidized soybean oil (ESBO) with regard to their migration from three different types of poly(vinyl chloride) into isooctane at 20, 40, and 60°C. Diffusion coefficients derived from the experimental migration data were evaluated against diffusion coefficients estimated from a model based solely on the migration data for ESBO. The diffusion coefficient estimation model proved to be very good in estimating the diffusion coefficients at 20°C but overestimated them at 40°C and 60°C. By using a migration model originally derived by Kontominas [Kondyli et al., *Polymer*, 34, 2592 (1993)] and the estimated diffusion coefficients, it was possible to obtain a more satisfactory representation of the experimental migration data at 40°C than that obtained with the commonly used migration model of Crank [Crank, *Mathematics of diffusion*, (1956)] based on the experimental diffusion coefficients. *J. VINYL ADDIT. TECHNOL.*, 15:147–158, 2009. © 2009 Society of Plastics Engineers

INTRODUCTION AND MIGRATION MODELS

The most commonly used plasticizers for poly(vinyl chloride) (PVC) are the phthalates, especially, the plasticizer DEHP (di-2-ethylhexyl phthalate) [1]. Several of these phthalates are being suspected of having carcinogenic properties and are furthermore very slowly biodegradable. This means that there is a need to develop safe substitutes for these plasticizers. The Danish food-additive manufacturer Danisco A/S has recently developed such an alternative, the GRINDSTED[®]SOFT-N-SAFE plasticizer (SNS), which is based on a fully acetylated glycerol monoester on hardened oil from the castor bean. On the basis of a natural product, the composition of SNS can

exhibit small changes from batch to batch, but the two main components are the fully acetylated glycerol monoester based on 12-hydroxystearic acid (85%) and stearic acid (10%), as shown in Fig. 1 [2].

The product is now approved for use in the European market and moreover preliminary results show smaller migration to specific food simulants (aqueous acetic acid, water–ethanol, and sunflower oil) compared to standard plasticizers like di-2-ethylhexyl phthalate (DEHP) and diisononyl phthalate (DINP) [3]. In addition, SNS has been shown to be a nontoxic, fully biodegradable substitute, but is substantially more expensive than DEHP (3–4 times). As there has been great attention on the use of plasticizers in the later years, especially the use of phthalates, many new migration limit regulations have appeared, e.g., Commission directive 2005/79/EC [4] by the European Union (EU). The experimental tests needed to check whether the migration of the plasticizer is within the regulations are very time consuming or difficult to carry out. For this reason, in 2002, EU made it possible to use food simulants and even generally recognized migration models to estimate the complete migration into different foods [5].

The purpose of the current work was first to estimate diffusion coefficients of SNS at different temperatures. This was possible by utilizing the data from a migration experiment Danisco had conducted on this new plasticizer for other purposes [6]. In this experiment SNS was compared against epoxidized soybean oil (ESBO) and GRINDSTED[®]ACETEM 95 CO (Acetem), the latter was another plasticizer candidate at that time. Acetem is based on coconut oil instead of castor oil used in SNS. This means that the main components of Acetem are the fully acetylated glycerol monoester based on caprylic, capric, and lauric acid, as illustrated in Fig. 2.

In addition, the purpose of this work was to investigate whether it is possible to estimate the migration of SNS, in particular, from a polymer monolayer into a solvent utilizing the migration model generally recognized by EU [5] and originally derived by Crank [7]:

Correspondence to: Georgios M. Kontogeorgis; e-mail: gk@kt.dtu.dk
DOI 10.1002/vnl.20193
Published online in Wiley InterScience (www.interscience.wiley.com).
© 2009 Society of Plastics Engineers

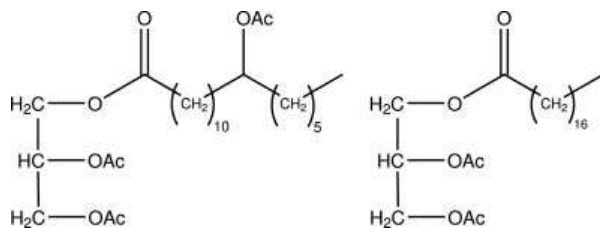


FIG. 1. Fully acetylated glycerol monoester based on 12-hydroxystearic acid (85%, left) and on stearic acid (10%, right), the two main components of GRINDSTED[®]SOFT-N-SAFE.

$$\frac{M_t}{M_\infty} = 1 - \sum_{n=1}^{\infty} \frac{2\alpha(1+\alpha)}{1+\alpha+\alpha^2q_n^2} \exp\left(\frac{-Dtq_n^2}{L^2}\right) \quad (1)$$

where M_t is the migration at time t , M_∞ is the migration at infinite time, D is the diffusion coefficient, L is the thickness of the polymer and q_n are the positive roots of $\tan q_n = -\alpha q_n$. α is a dimensionless quantity taking into account the solubility of the migrant in the solvent and the volume ratio of the polymer to the solvent. The parameter α is defined as: $\alpha = K^{-1}(V_s/V_p)$, where V_s/V_p is the volume ratio of the solvent over the polymer and K is the partition coefficient of the migrant in the polymer over the solvent, $K = C_{p,\infty}/C_{s,\infty}$. In this particular experimental setup, the partition coefficient K of the plasticizer is set to unity, as all the plasticizers have a very high solubility in isooctane which means that there will be no partition between polymer and solvent. This leads to an α -value of 700, as the volume ratio between polymer and solvent in this particular experiment was 700 ml (solvent) to 1 ml (polymer).

Another migration model (Eq. 2), originally derived by Kontominas in 1993 [8], has incorporated an agitation parameter “ u ” that can change the estimated migration from going towards a limit of 50% plasticizer migrated (static solvent, $u = 0$) to 100% plasticizer migrated ($u \gg 0$), which is almost the same as Crank’s model (Eq. 1) in this setup where α is set to 700.

$$\frac{M_t}{M_\infty} = \frac{ut}{2L} \operatorname{erf}\left(\frac{ut}{2\sqrt{Dt}}\right) + \frac{ut-L}{2L} \operatorname{erf}\left(\frac{L-ut}{2\sqrt{Dt}}\right) + \frac{\sqrt{Dt}}{L\sqrt{\pi}} \left[\exp\left(-\frac{(ut)^2}{4Dt}\right) - \exp\left(-\frac{(L-ut)^2}{4Dt}\right) \right] + \frac{1}{2} \quad (2)$$

All symbols have the same meaning as in Eq. 1. The Kontominas model was proposed as a solution for systems where the diffusion of the migrant in the solvent is so low that it affects the overall migration out from the polymer matrix. This is of course not the case for this particular system where isooctane is used as the solvent, but it can be argued that this particular analytical solution could be used to mimic the effect of slower overall migration due to fast depletion of plasticizer from the boundary area of the highly plasticized PVC. The fitting of the “ u ”

parameter to the migration data was done by the nonlinear least-squares solver (lsqnonlin) from Mathworks MatLab, using Eq. 3 as the objective function, where n is the number of samples, x_t is the migration datum at time t , M_t is the calculated migration at time t .

$$\frac{1}{n} \sum_{t=1}^n \left| \frac{x_t - M_t}{x_t} \right| \quad (3)$$

The dependence between temperature and diffusion coefficient is normally seen to follow an Arrhenius type equation (Eq. 4), where D_0 is the temperature independent diffusion constant, E_d is activation energy of diffusion, R is the ideal gas constant, and T is the temperature.

$$D = D_0 \exp\left(\frac{-E_d}{RT}\right) \quad (4)$$

Both the Crank and the Kontominas models require values of the diffusion coefficient. An empirical model for estimating the diffusion coefficient of additives in polymers has been suggested by Piringer and coworkers [9–11]. Using this model the diffusion coefficient can be estimated using only three parameters:

- T , Temperature (K)
- M_r , Molecular weight of the migrating additive (g/mol)
- A_p , Specific polymer matrix parameter (dimensionless)

$$D = 10^4 \exp\left(A_p + 0.01M_r - \frac{10454}{T}\right) \quad (5)$$

$$D = 10^4 \exp\left(\left(A_p^* - \frac{\tau}{T}\right) - 0.1351M_r^{2/3} + 0.003M_r - \frac{10454}{T}\right) \\ \Leftrightarrow D = 10^4 \exp\left(A_p^* - 0.1351M_r^{2/3} + 0.003M_r\right) \\ \times \exp\left(\frac{-(\tau R + 10454R)}{RT}\right) \quad (6)$$

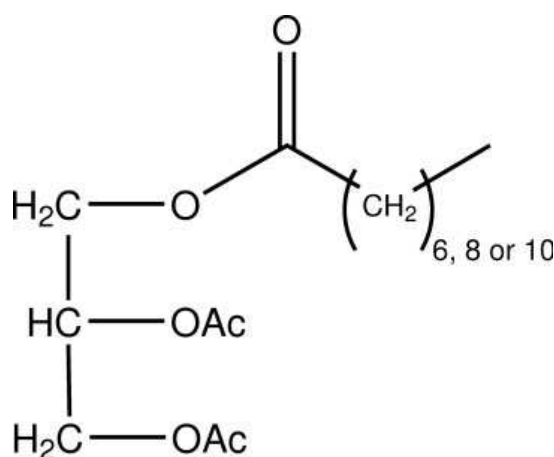


FIG. 2. The main components of Acetem, fully acetylated glycerol monoester based on coconut oil, which consists of caprylic (6), capric (8), and lauric acid (10).

TABLE 1. Migration data from the Danisco migration experiments on SNS, Acetem, and ESBO from three PVC types into isooctane at three temperatures.

$M_t/100(LC_{p0})$ (%)	Sampling time (h)							
	0.25	0.5	1	3	6	24	48	96
SNS at 20°C								
PVC 1		4.2	5.7	9.2	12.5	23.1	30.6	40.4
PVC 2		7.0	10.5	18.1	26.2	50.9	68.8	82.4
PVC 3		8.6	12.4	20.5	28.0	51.2	70.2	84.3
SNS at 40°C								
PVC 1		4.2	5.3	7.9	10.3	17.9	25.7	37.2
PVC 2		9.3	12.0	19.3	26.1	49.2	63.0	75.0
PVC 3		10.8	13.7	20.7	26.3	47.9	58.8	68.8
SNS at 60°C								
PVC 1	3.4	4.5	6.3	10.8	17.4			
PVC 2	4.7	5.7	7.3	11.6	16.9			
PVC 3	6.3	6.9	9.8	15.9	23.3			
Acetem at 20°C								
PVC 1		6.8	9.2	15.6	22.7	68.6	74.7	96.6
PVC 2		10.2	15.2	28.2	48.6	84.0	86.0	98.4
PVC 3		16.5	22.3	42.5	57.8	86.3	85.1	99.0
Acetem at 40°C								
PVC 1		10.5	12.6	19.3	24.7	52.6	53.6	69.7
PVC 2		16.0	24.5	42.0	61.2	71.3	79.1	99.2
PVC 3		27.2	37.7	62.4	82.0	75.2	72.9	103.7
Acetem at 60°C								
PVC 1	2.2	2.5	4.2	6.6	11.8			
PVC 2	4.1	4.3	5.6	9.2	12.0			
PVC 3	7.9	9.7	7.6	15.6	33.5			
ESBO at 20°C								
PVC 1		1.5	1.8	2.5	2.6	5.3	6.7	8.2
PVC 2		1.7	2.2	2.9	3.3	7.2	9.8	12.7
PVC 3		2.5	2.8	4.5	5.1	11.7	15.9	22.0
ESBO at 40°C								
PVC 1		1.9	2.2	3.4		9.1	14.0	19.8
PVC 2		2.9	3.8	4.6	7.8	15.5	27.8	31.0
PVC 3		3.6	4.7	7.1	10.3	20.2	28.3	41.8
ESBO at 60°C								
PVC 1	2.0	2.7	3.0	5.1	8.8			
PVC 2	2.2	2.5	3.5	7.2	17.2			
PVC 3	2.4		5.6	9.6	14.4			

M_t (mg/cm²) is the amount migrated per area at time t , C_{p0} (mg/cm³) is the starting concentration of the migrant in the polymer sheet and L (cm) is the thickness of the polymer sheet. $M_t/(LC_{p0})$ is the ratio of the amount migrated at time t to the total migrant amount.

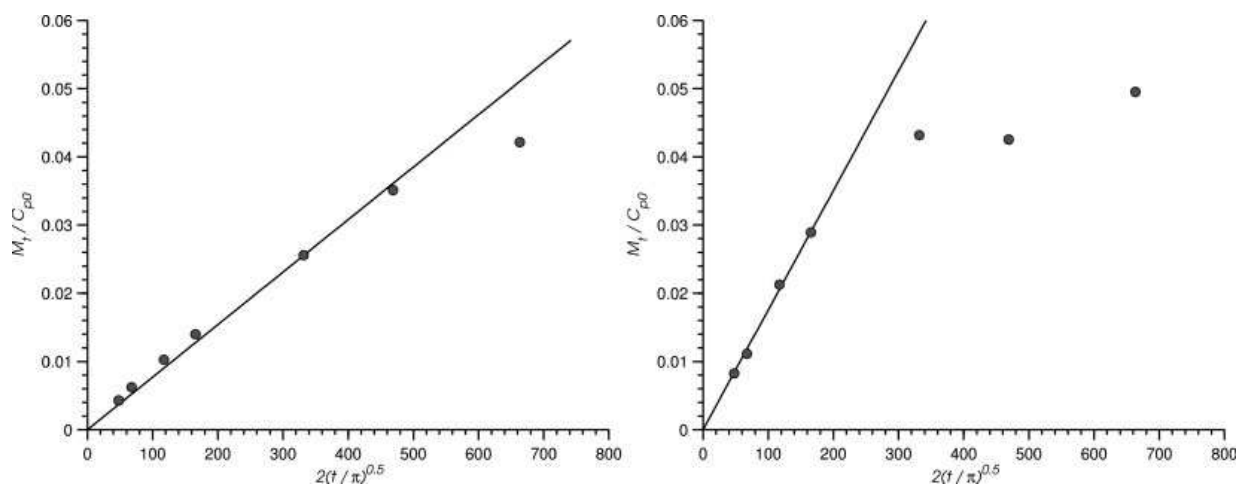


FIG. 3. Plot of the linear regression on the data points from the migration of SNS and Acetem from PVC 3 at 20°C into isooctane for estimating the diffusion coefficient using Eq. 8. Only the first four data points are used for the regression in the right figure (Acetem), whereas six out of the seven data points are used in the left figure (SNS).

TABLE 2. Estimated diffusion coefficients based on Eq. 8 from the Danisco migration experiments on SNS, Acetem, and ESBO from PVC into isoctane.

D (cm ² /s)	20°C (cm ² /s) (data points)	40°C (cm ² /s) (data points)	60°C (cm ² /s) (data points)
SNS			
PVC 1	1.30×10^{-9} (5/7)	1.10×10^{-9} (4/7)	2.49×10^{-9} (5/5)
PVC 2	5.95×10^{-9} (5/7)	5.84×10^{-9} (5/7)	2.67×10^{-9} (5/5)
PVC 3	5.93×10^{-9} (5/7)	5.81×10^{-9} (4/7)	4.95×10^{-9} (5/5)
Acetem			
PVC 1	6.17×10^{-9} (7/7)	6.42×10^{-9} (4/7)	1.07×10^{-9} (5/5)
PVC 2	16.66×10^{-9} (5/7)	33.04×10^{-9} (4/7)	1.49×10^{-9} (5/5)
PVC 3	30.74×10^{-9} (4/7)	66.29×10^{-9} (4/7)	7.67×10^{-9} (5/5)
ESBO			
PVC 1	0.07×10^{-9} (5/7)	0.24×10^{-9} (3/6)	0.62×10^{-9} (5/5)
PVC 2	0.13×10^{-9} (5/7)	0.73×10^{-9} (6/7)	0.86×10^{-9} (4/4)
PVC 3	0.31×10^{-9} (5/7)	0.95×10^{-9} (5/7)	1.78×10^{-9} (4/4)

Data points = data points used for linear regression/total number of data points in the experiment.

In Eqs. 5 and 6, D is expressed in cm²/s. Two versions of the model are currently suggested by Piringer (Eqs. 5 and 6). Equation 5 is the original version, where the polymer matrix parameter (A_p) is independent of temperature, and the equation is recommended for polymer additives with low molecular weights ($M_r < 1000$ g/mol) in an unplasticized polymer. The more recent model (Eq. 6) has two parameters for the polymer matrix ($A_p = A_p^* - \tau/T$). When Eq. 6 is compared with the standard Arrhenius type equation (Eq. 4), it is seen that:

$$D_0 = 10^4 \exp\left(A_p^* - 0.1351M_r^{2/3} + 0.003M_r\right) \quad \text{and} \\ E_d = \tau R + 10454R = \tau R + \langle E_d \rangle \quad (7)$$

It can now be seen from Eq. 7 that τ is the correction contribution to the mean activation energy term of the model ($E_d = \tau R + \langle E_d \rangle$).

EXPERIMENTAL DATA

A series of migration experiments was carried out by DANISCO A/S in 2005 for the migration of GRINDSTED[®] SOFT-N-SAFE (SNS), GRINDSTED[®] ACETEM 95 CO (Acetem), and epoxidized soybean oil (ESBO) from three different PVC types. These experiments were carried out for a possible customer of the key product, SNS. The migration experiments were carried out with the three different plasticizers, on the three different PVC types, at three different temperatures. This gave in all 18 migration experiments.

Plasticizers

GRINDSTED[®] SOFT-N-SAFE (SNS).
GRINDSTED[®] ACETEM 95 CO (Acetem).
Epoxidized soybean oil (ESBO).

Polymers

PVC 1:50 phr plasticizer, 2.5 phr surfactant, and stabilizer.

PVC 2:50 phr plasticizer, 7 phr lubricant, and 2.5 phr surfactant and stabilizer.

PVC 3:67 phr plasticizer, 2.5 phr surfactant, and stabilizer.

[phr = parts per hundred resin (by weight)].

Temperatures

20°C, 40°C, and 60°C.

Sampling

0.5 h, 1 h, 3 h, 6 h, 24 h, 48 h, and 96 h (for experiments at 60°C, sampling was started at 0.25 h and stopped after 6 h).

Each PVC sheet (2.5 cm × 4.0 cm × 0.1 cm) was accurately weighed and then put into 700 ml of isoctane in a closed container at the specified temperature under mild agitation; 1 ml samples were then taken according to the sampling times. The 1 ml sample was evaporated to

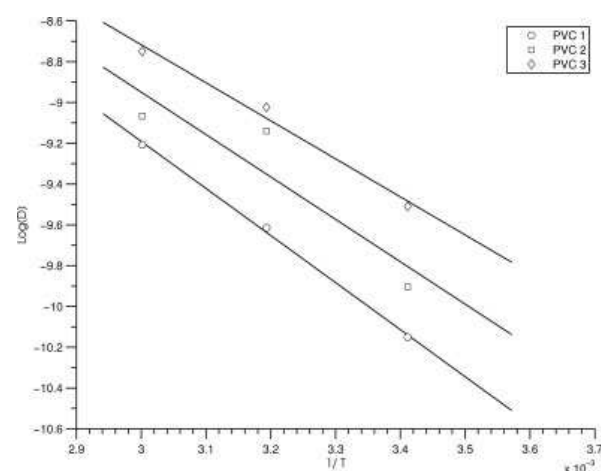


FIG. 4. The temperature dependence of ESBO diffusion coefficients from three different PVC types into isoctane.

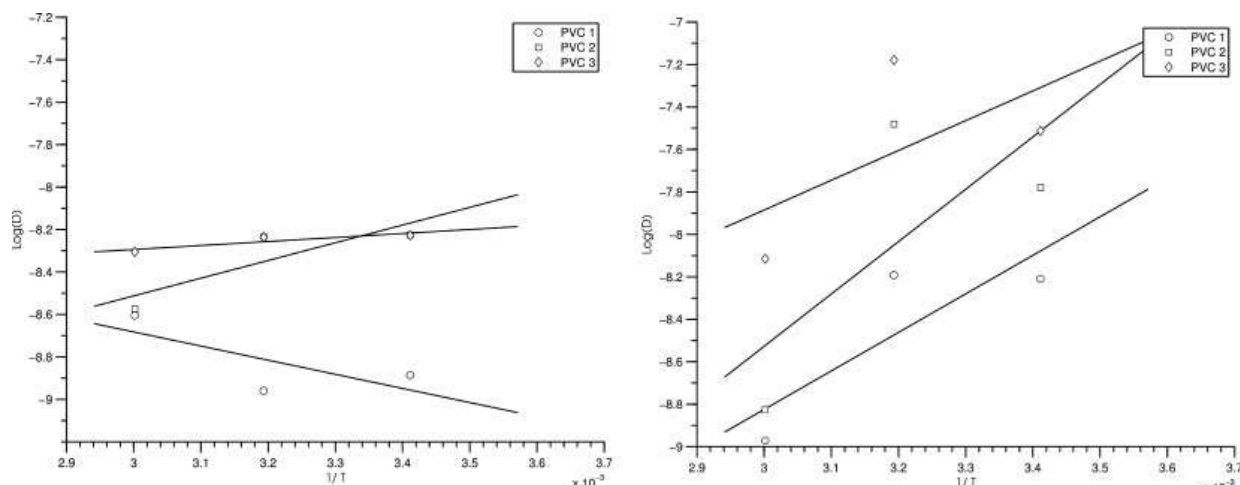


FIG. 5. The temperature dependence of diffusion coefficients for SNS (left) and Acetem (right) migrating from three different PVC types into isoctane.

TABLE 3. Experimentally derived A_p values for ESBO in PVC using Eq. 4.

	20°C	40°C	60°C	Mean A_p
PVC 1	12.13	11.09	10.02	11.08
PVC 2	12.70	12.18	10.34	11.74
PVC 3	13.60	12.44	11.07	12.37

dryness at 70°C under a stream of N₂. SNS and Acetem were analyzed by GC-FID and ESBO by GC-MS.

All the data from the migration experiments are collected in Table 1 and shown as the ratio of the amount migrated at time t over the total amount of plasticizer used in the experiment.

RESULTS AND DISCUSSION

In the first part of the migration, the concentration of the migrant in the solvent will be zero, and since the concentration in the solvent is very low compared to the concentration in the polymer, the migration will follow the simplified version of Crank's [7] migration model shown in Eq. 8 [9, 12].

$$M_t = 2C_{p0} \sqrt{\frac{Dt}{\pi}} \Leftrightarrow \frac{M_t}{C_{p0}} = \sqrt{D} \cdot 2\sqrt{\frac{t}{\pi}} \quad (8)$$

Following Eq. 8 it is possible to develop an expression of the migration (M_t) as a linear function of the square root of time (t), where the slope is the square root of the diffusion coefficient (D). By plotting M_t/C_{p0} against

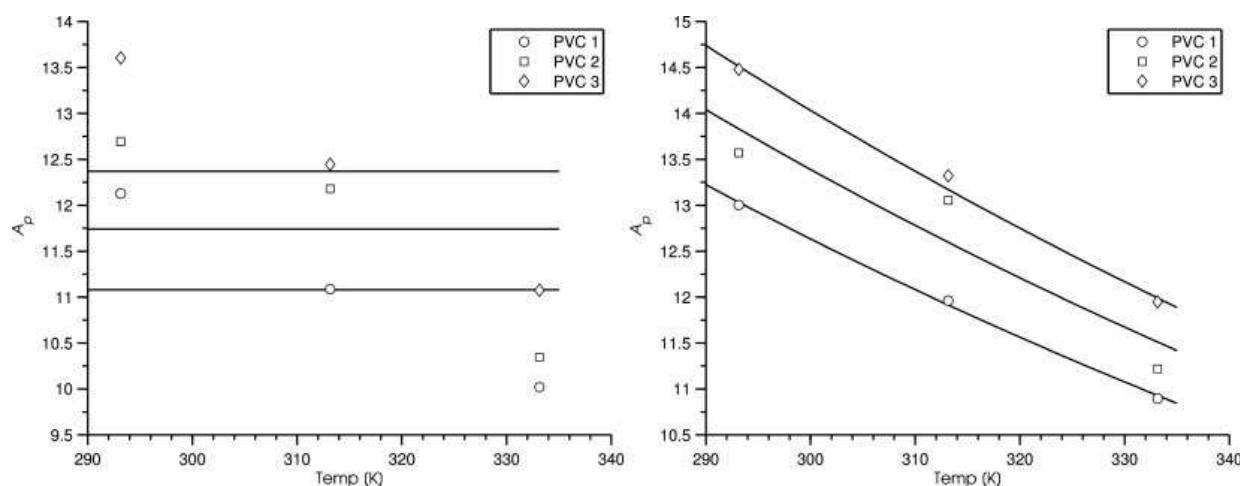


FIG. 6. Correlation between the calculated polymer parameter A_p and the mean parameter using Eq. 5 (refer Table 3) (left); and the correlation using Eq. 6 where A_p is dependent on temperature ($A_p = A_p^* - \tau/T$) (right).

TABLE 4. The fitted polymer parameters of Eq. 6, and the collective Arrhenius activation energy $E_d = (\tau + 10454)R$, according to Eq. 7.

	A_p^*	τ	E_d (kJ/mol)
PVC 1	-4.5	-5140	44.16
PVC 2	-5.5	-5667	39.78
PVC 3	-6.5	-6160	35.68

$2(t/\pi)^{1/2}$ it is possible to estimate the diffusion coefficient by linear regression from the experimentally measured migration data. The problem with this method for estimating the diffusion coefficient is that there must be a sufficient number of data points in this first part of the migration area where this simplified model is valid. The first four of the seven data points from the experiment with Acetem migrating from PVC 3 into isooctane at 20°C (Fig. 3, right), clearly lie in the linear part of the migration, whereas the last three data points break off from the linear model. For the same system, with SNS as the plasticizer, only the first six of the seven data points were used for the regression (Fig. 3, left).

Diffusion Coefficients from Experimental Data

One of the purposes of this project was to estimate the diffusion coefficients of SNS at different temperatures, based on the migration data from the Danisco A/S experiments. This was done with linear regression using Eq. 8. As the migration experiments also included the plasticizer candidate Acetem and the widely used plasticizer ESBO, the diffusion coefficients were calculated for these plasticizers as well. All the estimated diffusion coefficients are listed in Table 2 along with the number of datapoints that have been used for the regression.

As can be seen from the estimated diffusion coefficients in Table 2, ESBO has the lowest diffusion coefficient, thus the slowest migration. SNS has a diffusion coefficient approximately a factor of 10 higher and Acetem almost a factor of 50 higher on average, compared to ESBO. This means that it should be expected that SNS exhibits a slightly faster migration from PVC into isooctane compared to ESBO. As displayed in Fig. 4, there is good agreement between the estimated diffusion coefficients of ESBO and the temperature dependency suggested by the Arrhenius equation (Eq. 4).

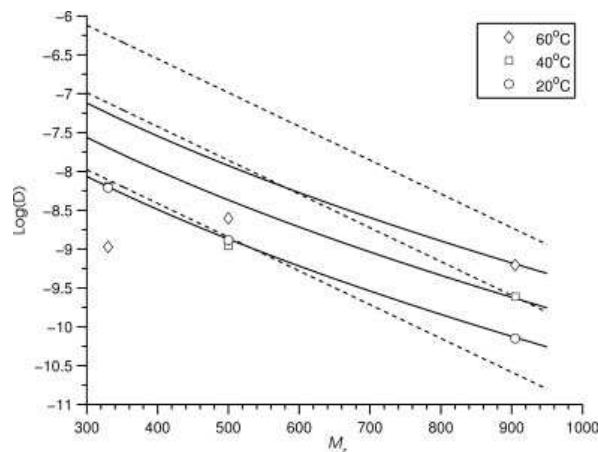


FIG. 7. The estimation of the diffusion coefficient for PVC 3. The dotted lines are estimations with Eq. 5 and the solid lines are estimations using Eq. 6, at the three temperatures 20°C (bottom), 40°C (middle), and 60°C (top). It can be seen that the estimated diffusion coefficients of Acetem ($M_r = 330$ g/mol) and SNS ($M_r = 500$ g/mol) are in good agreement with the results of experiments performed at 20°C (circled data points), but that as the temperature gets higher, the experimentally derived diffusion coefficient is too low compared to the model calculations.

The diffusion coefficients tend to reach higher values (faster migration) at higher temperatures, as expected. Unlike ESBO, the estimated diffusion coefficients of SNS

TABLE 5. Estimated diffusion coefficients (D_{calc} in cm^2/s) and the error % (Err) calculated by $100 \cdot \left(\frac{\log(D_{\text{calc}}) - \log(D_{\text{exp}})}{\log(D_{\text{exp}})} \right)$ for Acetem, SNS, and ESBO in all three PVC types at 20°C, 40°C, and 60°C.

	PVC 1		PVC 2		PVC 3		Mean Err	Mean Err
	D_{calc} (cm^2/s)	Err (%)	D_{calc} (cm^2/s)	Err (%)	D_{calc} (cm^2/s)	Err (%)		
20°C	$(\times 10^{-10})$							0.77
Ace	63.27	-0.14	140.49	0.93	277.78	0.58	0.55	
SNS	13.44	-0.16	29.84	3.65	59.01	0.02	1.28	
ESBO	0.73	-0.13	1.62	-1.14	3.20	-0.15	0.48	
40°C	$(\times 10^{-9})$							2.69
Ace	20.14	-6.06	39.86	-1.09	70.79	-0.40	2.52	
SNS	4.28	-6.60	8.47	-1.96	15.04	-5.01	4.52	
ESBO	0.23	0.21	0.46	2.17	0.82	0.72	1.03	
60°C	$(\times 10^{-8})$							9.6
Ace	5.58	-19.15	9.98	-20.68	16.13	-16.30	18.71	
SNS	1.18	-7.88	2.12	-10.50	3.43	-10.12	9.50	
ESBO	0.06	-0.16	0.11	-1.40	0.19	-0.21	0.59	
Mean Err		4.5		4.84		3.72		

The mean error is calculated as the mean absolute error.

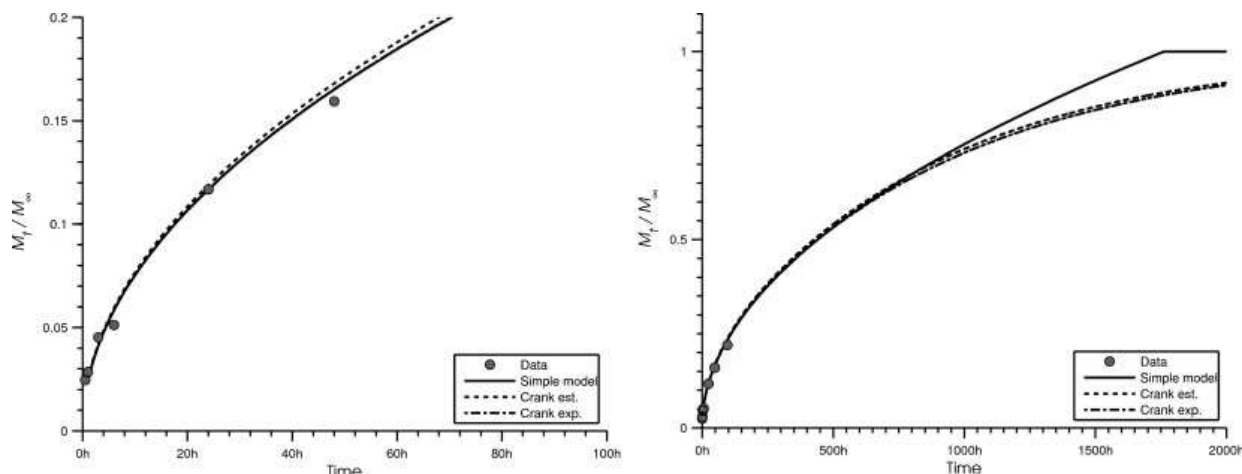


FIG. 8. The migration of ESBO from PVC 3 at 20°C estimated by the migration model of Crank (Eq. 1) using the experimentally derived diffusion coefficient (“Crank exp.”) and the estimated diffusion coefficient from Piringer’s model (Eq. 6) (“Crank est.”). All the data points from ESBO lie within the first part of the migration where the simplified migration model (Eq. 8, “Simple model”) can be used, as can be seen when the migration is estimated up to 2000 h (right graph).

(migration from PVC into isoctane) seem to be temperature independent (Fig. 5, left). It is difficult to explain this behavior, as higher temperatures imply faster Brownian movement of the molecules, thus the molecules will reach the lowest energy state of the system more quickly (equilibrium, $M_t = M_{\infty}$). One explanation for this unexpected behavior could be that the high solubility of SNS in isoctane combined with the high diffusion rate of SNS in the plasticized PVC may result in an extraction of SNS in the boundary area of the polymer. This almost empty part of the PVC will then have a much different physical character than the plasticized part of the PVC, and thus

lead to a much different diffusion rate of SNS in this area. This will lead to a much different overall mean diffusion coefficient for the total system, which is what is calculated by the method described in the start of this section (using Eq. 8). This could be an explanation of why the experimentally measured diffusion coefficients do not increase with temperature as would have been expected.

For Acetem there seem to be some correlation between temperature and diffusion, as the diffusion coefficients of all three PVC types behave in the same manner. But, as in the case of SNS, the temperature dependence does not

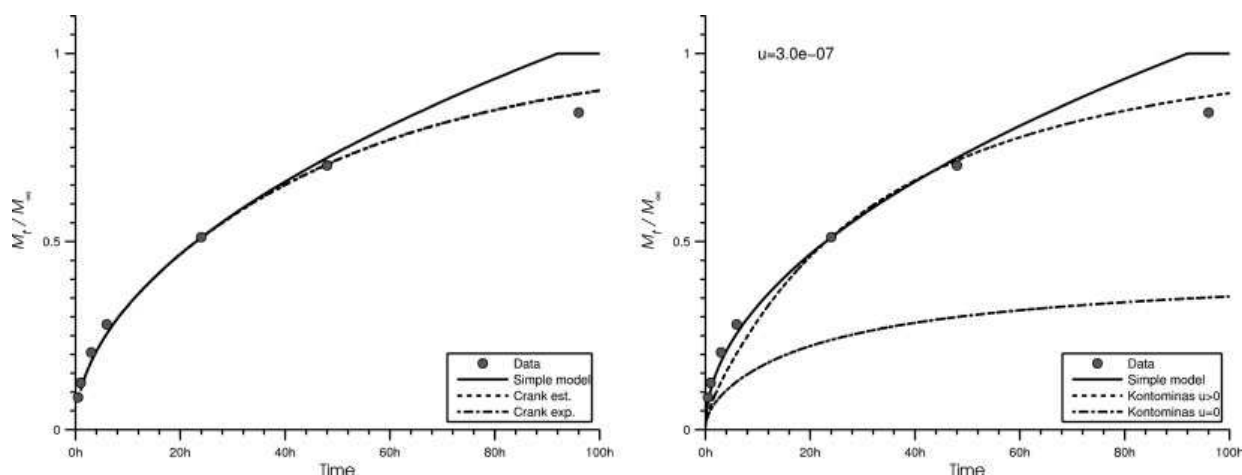


FIG. 9. The estimated migration at 20°C of SNS from PVC 3. The fully estimated migration (“Crank est.”) lies very close to the migration estimated from the experimental diffusion coefficient (“Crank exp.”) (left). Using the migration model of Kontominas (Eq. 2) and the estimated diffusion coefficient, it is also possible to make a satisfactory fit to the migration data when optimizing the agitation parameter “ u ,” here, $u = 3.0 \times 10^{-7}$ (right).

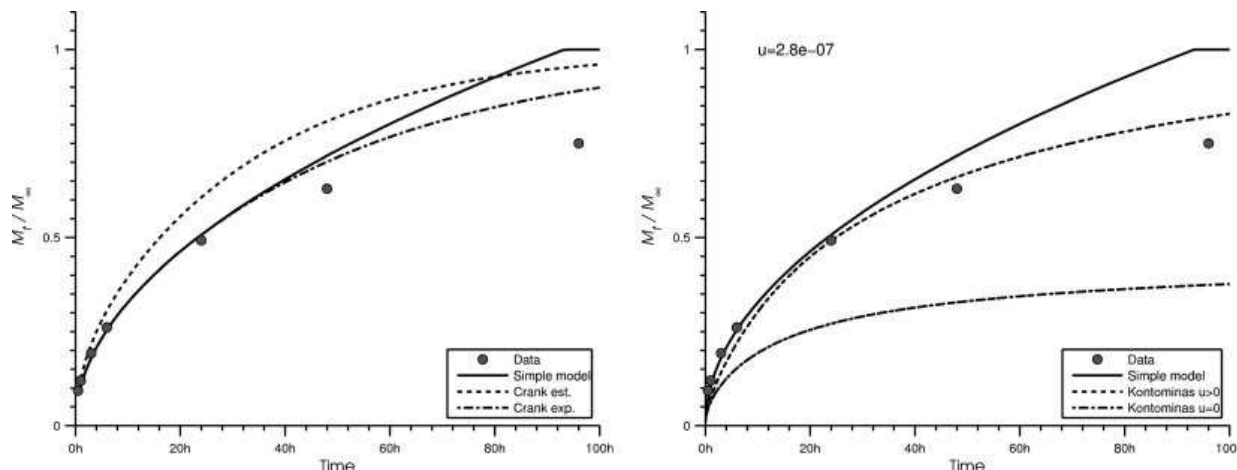


FIG. 10. The estimated migration at 40°C of SNS from PVC 2. A poor fit to the experimental data is obtained by the use of Crank's model with the estimated diffusion coefficient ("Crank est.") (left). By using the migration model of Kontominas (Eq. 2) with the estimated diffusion coefficient, it is possible to obtain a better fit to the data than with Crank's model using the experimentally derived diffusion coefficient ("Crank exp.") (right).

follow the Arrhenius equation. As Acetem has an even faster diffusion than SNS in the plasticized PVC, it is again likely that some sort of boundary layer of empty rigid PVC is built up on the rim of the polymer, thus resulting in an overall slower migration from the polymer to the solvent, and thus a lower diffusion coefficient for the total system calculated by this method.

Estimation of the Diffusion Coefficient

Since the experimentally derived diffusion coefficients of ESBO followed exactly the Arrhenius correlation, these data can be used to estimate the specific polymer parameters for each PVC type as proposed for the use of the Pir-

inger model [9] (Eq. 5). First, the A_p parameter for each experiment was calculated, using the molecular weight of ESBO and the temperature for each experiment. The mean value of the three calculated A_p parameters of each PVC type was taken as the specific A_p parameter and the results are shown in Table 3.

As seen from Table 3, it is clear that there is some temperature dependence of the A_p parameter, which is accounted for in Eq. 6. In the same way the A_p parameter was first calculated for each experiment when using Eq. 5, we can use Eq. 6 knowing that $A_p = A_p^* - \tau/T$. Afterwards the two polymer specific parameters (A_p^* and τ) were estimated by linear regression as illustrated in (Fig. 6, right).

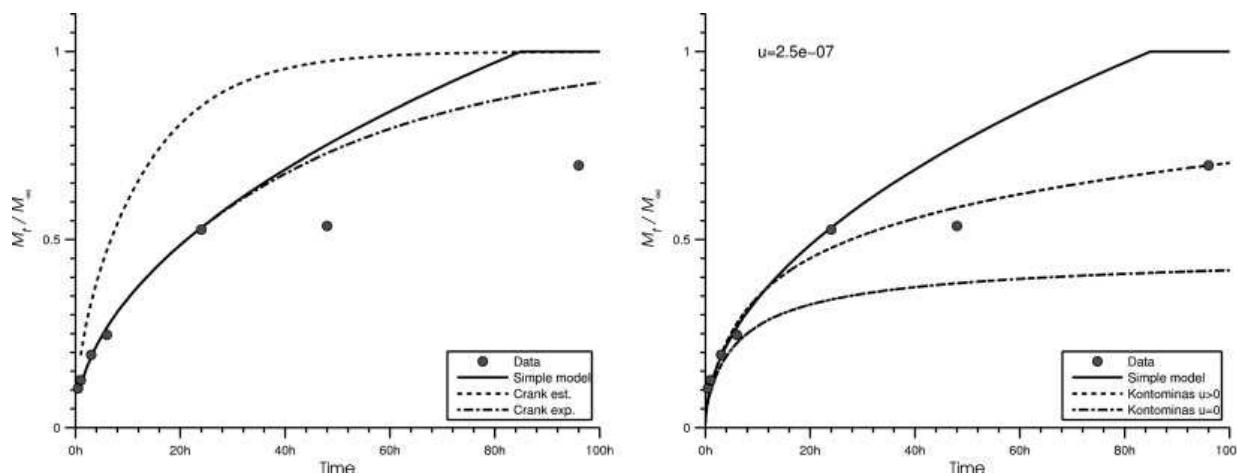


FIG. 11. The estimated migration at 40°C of Acetem from PVC 1. The fully estimated migration is in poor agreement with the experimental data (left). It is possible to obtain a satisfactory fit to the migration data by utilizing the migration model of Kontominas (Eq. 2) and fitting the agitation parameter "u," here, $u = 2.5 \times 10^{-7}$ (right).

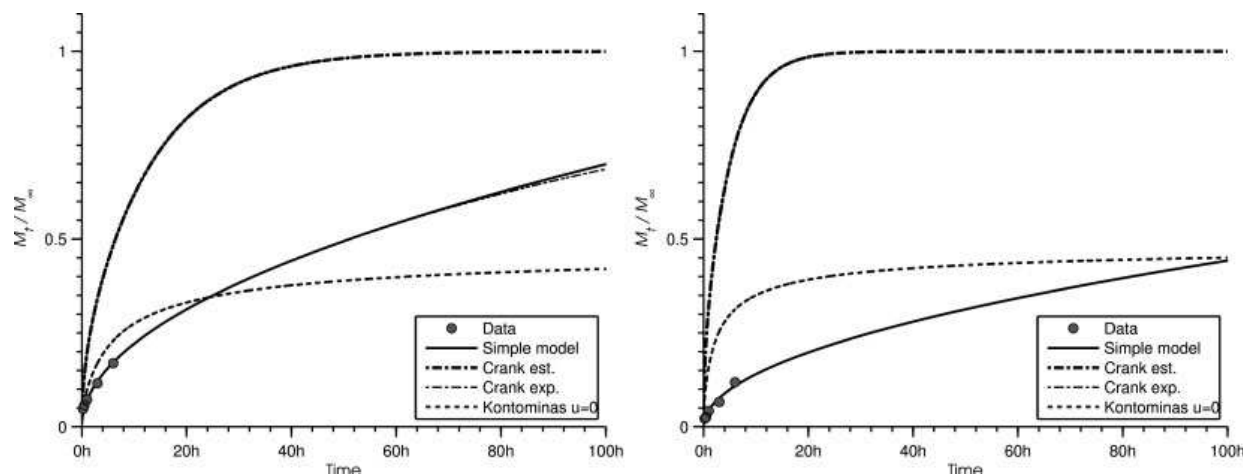


FIG. 12. The estimated migration at 60°C of SNS and Acetem from PVC 2. The diffusion coefficients are overestimated to such an extent that even the lower limit of the migration model of Kontominas ($u = 0$, Eq. 2) gives a faster migration compared to the experimental migration data.

As seen in Fig. 6, it is clear that the A_p parameter depends on temperature for these specific experiments, as was expected because of the highly plasticized PVC polymer matrix. All the calculated polymer specific parameters for the three PVC types for use with Eq. 6 are listed in Table 4.

Using these polymer specific parameters based solely on the data of ESBO migration, it should be possible to estimate the diffusion coefficients for the two other plasticizers (SNS and Acetem) in the three PVC types, knowing that ESBO has a molecular weight of 905 g/mol, SNS of 500 g/mol, and Acetem of 330 g/mol. The estimation for PVC 3 can be seen in Fig. 7.

All the estimated diffusion coefficients and the error compared to the experimentally measured diffusion coefficients are shown in Table 5. The error is calculated as the logarithmic error of the calculated diffusion coefficient compared to the experimental one. As can be seen the error of the estimated diffusion coefficients of SNS and Acetem at 20°C is in the area of 0–1%, whereas at 40°C, the error rises to 1–6% and at 60°C is as large as 10–20%. Both at 40°C and 60°C, the model overestimates the diffusion coefficients compared to the experimental data, which is also seen in Fig. 7. This is in very good agreement with the postulated buildup of a boundary layer in the polymer where diffusion into isooctane is very fast for SNS and Acetem at higher temperatures. This will almost give an extraction of the plasticizer in the boundary layer, and hence a much lower diffusion coefficient in this layer.

Estimation of Migration

As the polymer parameters of the diffusion coefficient estimation model (Eqs. 5 and 6) were determined by

using the ESBO migration data, we cannot draw a conclusion on the possibility of using the estimated diffusion coefficients to predict migration for this plasticizer. Furthermore, the migration of ESBO is so slow that all the data points lie within the first part of the migration where even the simplified migration model (Eq. 8) can be used, as shown in Fig. 8.

The estimation of migration for SNS and Acetem at 20°C is almost as good as for ESBO, as the deviation of the estimated diffusion coefficients from the experimental values is under 1% (see Table 5). This is shown by “Crank est.” \approx “Crank exp.” in Fig. 9. Even though a satisfactory representation is obtained with the migration model of Crank (Eq. 1) at 20°C, the migration model of Kontominas was also evaluated (Eq. 2; “Kontominas” in Fig. 9).

The deviations of the estimated diffusion coefficients of SNS and Acetem at 40°C lie in the area of 1–6%

TABLE 6. The fitted “ u ” parameters for SNS and Acetem at 20°C and 40°C.

u ($\times 10^{-7}$)	PVC 1	PVC 2	PVC 3		
SNS	20°C	D_{exp}	0.68	2.99	3.01
		D_{calc}	0.67	2.96	3.01
	40°C	D_{exp}	0.51	2.82	2.06
		D_{calc}	0	2.79	2.57
Acetem	20°C	D_{exp}	4.9	11.06	17.93
		D_{calc}	4.92	11.09	18.12
	40°C	D_{exp}	1.74	17.43	35.11
		D_{calc}	2.5	17.34	35.84

It was not possible to tune the model of Kontominas (Eq. 2) to fit the migration data at 60°C. There seems to be a tendency towards a correlation of parameters for each PVC type and plasticizer, independently of temperature.

TABLE 7. The mean absolute error (MAE) for the two migration models and the experimental data using the purely estimated diffusion coefficient (D_{calc}) and the diffusion coefficient fitted to the migration data (D_{exp}).

MAE ($\times 10^{-2}$)		PVC 1		PVC 2		PVC 3	
		Crank	Kontominas	Crank	Kontominas	Crank	Kontominas
SNS							
20°C	D_{exp}	2.05	3.81	1.47	3.81	1.92	4.51
	D_{calc}	2.23	3.74	8.86	6.80	1.93	4.53
40°C	D_{exp}	2.69	2.56	4.03	6.01	6.35	6.56
	D_{calc}	18.48	1.66	8.22	4.11	17.40	2.71
Acetem							
20°C	D_{exp}	4.91	3.41	3.78	3.56	3.79	5.49
	D_{calc}	4.74	3.38	3.94	3.96	4.03	5.88
40°C	D_{exp}	6.86	6.00	6.96	7.79	9.25	9.75
	D_{calc}	21.86	2.58	8.91	7.11	8.48	9.62

The error is calculated by $\text{MAE} = \frac{1}{n} \sum_{i=1}^n |x_i - M_i|$, where n is the number of samples, x_i is the migration datum at time t , M_i is the calculated migration at time t with either equation 1 or 2 for the Crank and Kontominas models, respectively.

(Table 5), which means that a poor fit to the experimental migration data is obtained by the use of Crank’s model with estimated diffusion coefficients (“Crank est.” in Figs. 10 and 11). However, with Crank’s model and experimental diffusion coefficients, the migration is in good agreement with experimental data. A very good fit to the experimental data is made possible by using the migration model of Kontominas (Eq. 2) when adjusting the agitation parameter “ u ” to the data. This migration model yields in some of the cases an even better fit to the data than Crank’s model using the experimentally derived diffusion coefficient (“Crank exp.”) as illustrated in Fig. 10.

At 60°C, the error of the estimated diffusion coefficients of SNS and Acetem is 10–20% (Table 5), and even the lower limit value of the migration model of Kontominas (when $u = 0$ in Eq. 2) is too high compared to the measured migration (Fig. 12).

When all the fitted “ u ” parameters are listed together (Table 6) it seems as if there is almost a specific “ u ”

parameter for each PVC type with each plasticizer independent of temperature. Unfortunately, the deviation of the estimated and experimental data at 60°C is so large that it is not possible to use the migration model of Kontominas (Eq. 2), and no unique “ u ” parameters could then be fitted. This “ u ” parameter was fitted only to the data at 20°C and 40°C.

The final result of the fitted “ u ” parameters for the use of the Kontominas migration model was compared to the original migration model of Crank by calculating the mean absolute error ($\text{MAE} = \frac{1}{n} \sum_{i=1}^n |x_i - M_i|$) and the mean

absolute percentage error ($\text{MAPE} = \frac{100\%}{n} \sum_{i=1}^n \left| \frac{x_i - M_i}{x_i} \right|$) for the two models. The overall statistical errors can be seen in Tables 7 and 8. At 20°C, there is no gain overall in using the Kontominas model with an optimized “ u ” parameter. At 40°C, there are even some cases where the error for the Kontominas model with the fully estimated

TABLE 8. The mean absolute percentage error (MAPE) for the two migration models and the experimental data using the purely estimated diffusion coefficient (D_{calc}) and the diffusion coefficient fitted to the migration data (D_{exp}).

MAPE (%)		PVC 1		PVC 2		PVC 3	
		Crank	Kontominas	Crank	Kontominas	Crank	Kontominas
SNS							
20°C	D_{exp}	10.90	33.15	2.98	22.31	8.16	27.40
	D_{calc}	10.84	33.35	26.11	27.48	8.26	12.04
40°C	D_{exp}	15.64	31.28	11.05	28.63	18.21	32.06
	D_{calc}	103.04	21.90	16.76	15.22	41.52	15.03
Acetem							
20°C	D_{exp}	13.45	12.95	10.26	8.52	5.56	11.64
	D_{calc}	13.94	12.69	8.00	10.45	5.99	12.67
40°C	D_{exp}	16.91	30.81	10.49	15.16	13.72	17.07
	D_{calc}	61.86	11.28	16.02	14.13	12.14	16.52

The error is calculated by $\text{MAPE} = \frac{100\%}{n} \sum_{i=1}^n \left| \frac{x_i - M_i}{x_i} \right|$, where n is the number of samples, x_i is the migration datum at time t , M_i is the calculated migration at time t with either equation 1 or 2 for the Crank and Kontominas models, respectively.

diffusion coefficient (D_{calc}) is lower than that obtained by using Crank's model with the experimental diffusion coefficient (D_{exp}). But in all cases, at 40°C, the Kontominas model (Eq. 2) with the estimated diffusion coefficient (D_{calc}) is at least as good as the Crank model (Eq. 1) with the experimentally derived diffusion coefficient (D_{exp}).

CONCLUSIONS

By using the simplified version of the migration model of Crank [7] (Eq. 8) it was possible to estimate diffusion coefficients for various PVC-plasticizer systems using the experimental migration data. A very good agreement with the expected Arrhenius temperature dependency of the diffusion coefficients was seen for ESBO, whereas the diffusion coefficients of SNS seemed temperature independent. A buildup of a boundary layer because of the fast migration of the plasticizer is suggested as an explanation for this odd behavior. By using the data for ESBO alone, polymer specific parameters were estimated for the diffusion coefficient estimation model of Piring (Eqs. 5 and 6). From this model it was possible to estimate the diffusion coefficients of SNS and Acetem at 20°C in good agreement with the experimentally derived coefficients. The overestimation of the diffusion coefficients at 40°C and 60°C can also be explained by using the postulated mechanism of a buildup of a boundary layer because of the fast migration.

The migration model of Crank [7] (Eq. 1) performed very well in estimating migration data at 20°C, but did not succeed equally well for the data at 40°C and 60°C even when using the experimentally based diffusion coefficients. The migration model of Crank works only for systems where the migrant is evenly distributed in the polymer matrix and the diffusion coefficient can be seen as concentration independent. For this particular system, at higher temperatures, the migration is so fast that this condition no longer applies.

By using a migration model originally derived by Kontominas and coworkers[8] (Eq. 2) and the estimated diffusion coefficient, it was possible to get an even better fit to the experimental migration data at 40°C than that obtained with the migration model of Crank using the experimentally derived diffusion coefficient. The fitted agitation parameter “ u ” from the migration model of Kontominas seemed to be specific to the polymer and plasticizer independently of temperature, especially for SNS. Since the deviation of the estimated diffusion coefficients from the experimentally derived values at 60°C was too large to be compensated for by the migration model of Kontominas, no fit of the “ u ” parameters could be done at this temperature.

The migration model of Crank is very useful for systems where the migration is so slow that the migrant concentration in the polymer matrix can be seen as uniform. For systems where a small boundary layer is built up it is possible to use the migration model of Kontominas when

fitting the “ u ” parameter, but when the depletion of the plasticizer from the polymer is too fast this model is no longer applicable either, as was seen for the systems at 60°C.

ACKNOWLEDGMENTS

The authors acknowledge Danisco for making this project possible. We also thank Bjarne Nielsen and Ulrik Aunskjær of Danisco for providing fund for the continuation of this project as a Ph. D. study.

NOMENCLATURE

Abbreviations

Acetem	GRINDSTED [®] ACETEM 95 CO
DEHP	di-2-ethylhexyl phthalate
DINP	diisononyl phthalate
ESBO	epoxidized soybean oil
phr	Parts per hundred resin
PVC	poly(vinyl chloride)
SNS	GRINDSTED [®] SOFT-N-SAFE

List of Symbols

α	Ratio of solvent volume over polymer volume and the partition coefficient of the migrant in the two, $\alpha = K^{-1}(V_s/V_p)$
C_{p0}	Initial concentration of plasticizer in polymer (mg/cm ³)
D_0	Temperature independent diffusion constant (cm ² /s)
D	Diffusion coefficient (cm ² /s)
E_d	Activation energy of diffusion (J/mol)
erf	Error function, $\text{erf}(x) = \frac{2}{\sqrt{\pi}} \int_0^x e^{-t^2} dt$
K	Partition coefficient of the migrant polymer/solvent, $K = C_{p,\infty}/C_{s,\infty}$
L	Thickness of polymer (cm)
M_∞	Migration at infinite time (mg/cm ²)
M_r	Molecular weight of the migrating additive (g/mol)
M_t	Migration at time t (mg/cm ²)
n	Integer used in Eq. 1
q_n	Positive roots of $\tan q_n = -\alpha q_n$
t	Time (s)
u	Agitation parameter (cm/s)

REFERENCES

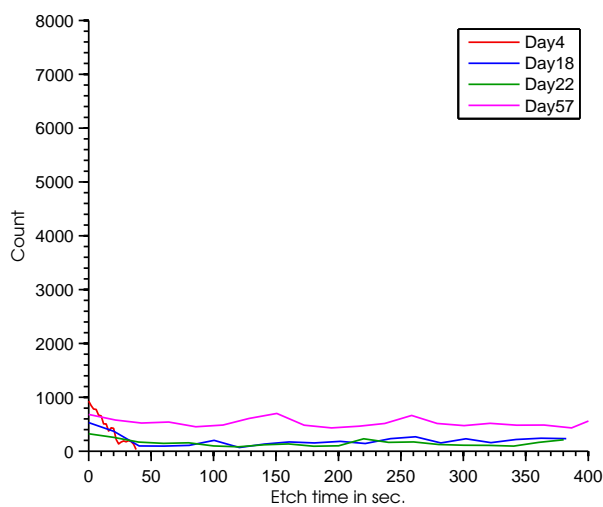
1. S. Braucks, “Green Paper: Environmental Issues of PVC,” in *The Commission of the European Communities*, July (2000).
2. T.F. Jensen, *Complete Composition of GRINDSTED[®] SOFT-N-SAFE*, Danisco Research Report.

3. Danisco, *GRINDSTED[®]SOFT-N-SAFE—The Sustainable Plasticiser for PVC*, Danisco, August (2006).
4. M. Kyprianou, *Off. J. Eur. Union*, **91**, 17 (2007).
5. D. Byrne, *Off. J. Eur. Union*, **220**, 18 (2002).
6. T.F. Jensen, *Migration of Plasticizers from PVC to iso-octane*, Danisco Research Report.
7. J. Crank, *Mathematics of Diffusion*, 1st ed., Clarendon press, Oxford (1956).
8. E. Kondyli, M. Kontominas, and M. Kosmas, *Polymer*, **34**, 2592 (1993).
9. O.-G. Piringer and A.L. Baner, *Plastic Packaging Materials for Food Barrier Function, Mass Transport, Quality Assurance and Legislation*, Wiley-VCH, Weinheim (2000).
10. O.-G. Piringer, *Food Addit. Contam.*, **11**, 221 (1994).
11. T. Begley, L. Castle, A. Feigenbaum, R. Franz, K. Hinrichs, T. Lickly, P. Mercea, M. Milana, A. O'Brien, S. Rebre, R. Rijk, and O. Piringer, *Food Addit. Contam.*, **22**, 73 (2005).
12. P. Zygoura, A. Goulas, K. Riganakos, and M. Kontominas, *J. Food Eng.*, **78**, 870 (2007).

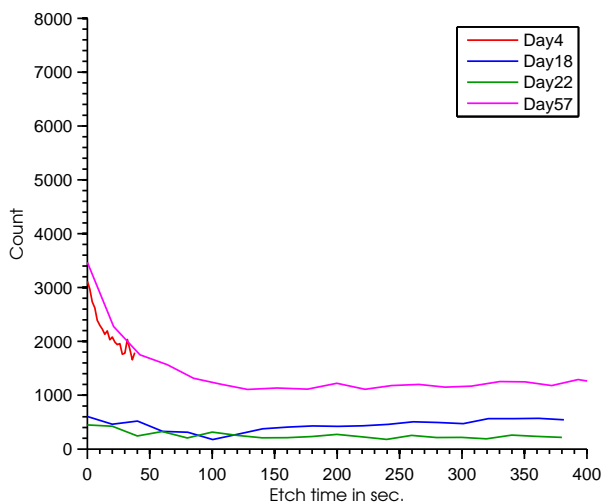
XPS measurements

Plots from the X-ray photo-electron spectroscopy (XPS) measurements of antistatic additive concentration at the polymer surface. The XPS measures the specific oxygen concentration in the top surface layer. Between each measurement is then etched away a thin layer of the surface of the polymer. This method then gives a concentration profile of oxygen down into the polymer from the surface. The etching time at the first sampling day (day 2, 3 or 4) was only 2 seconds, which showed to be too short, so the rest of the measurements are with an etching time of 20 seconds (giving a deeper profile into the polymer). For each polymer was a control measurement with a polymer with no antistatic agent in it also made. Unfortunately the XPS equipment at DTU-RISØ suffered from a lot of breakdowns in the 60 days test period, so oxygen surface concentration values measured were strongly deviating.

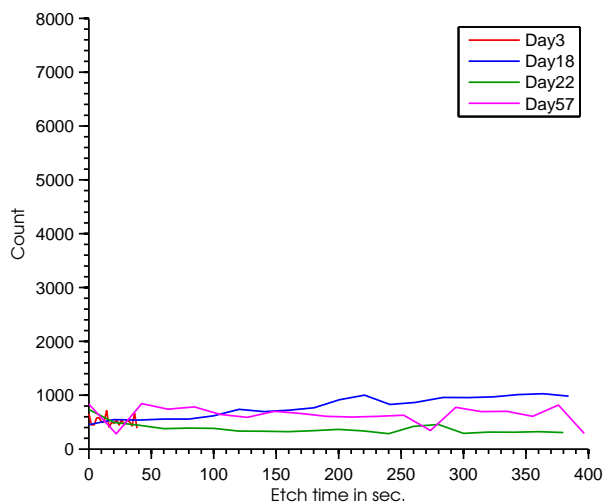
B.1 Impact Poly Propylene



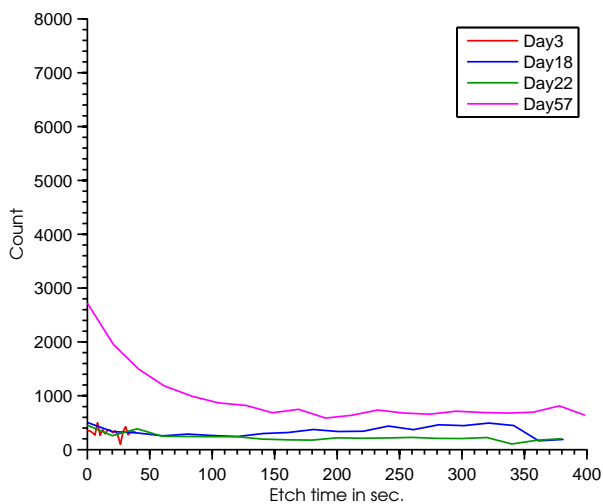
(a) Control



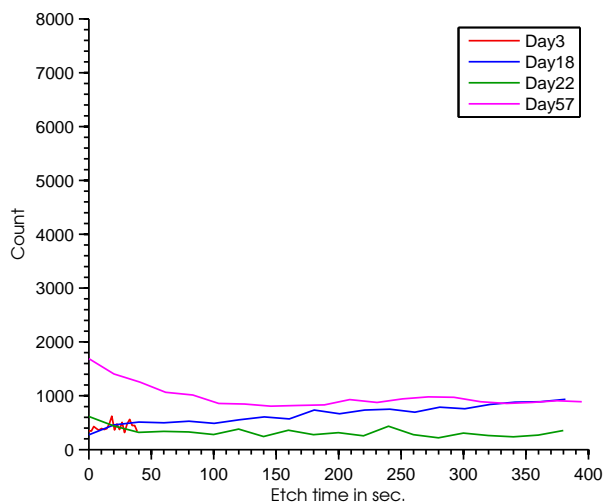
(b) Dimodan HPL70 0.4%



(c) Dimodan HPL70 0.8%

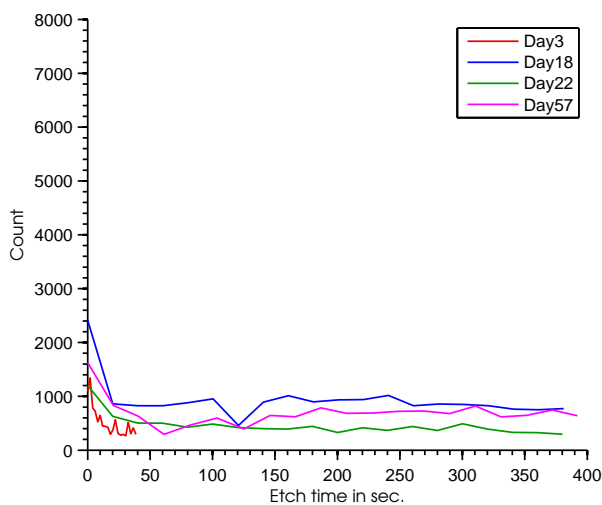


(d) Dimodan HP 0.4%

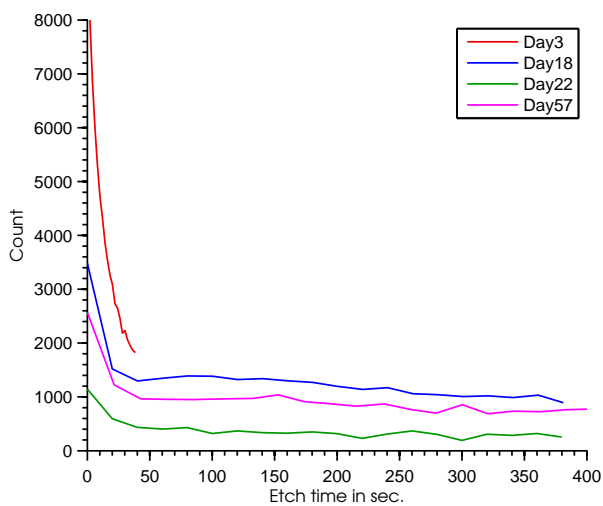


(e) Dimodan HP 0.8%

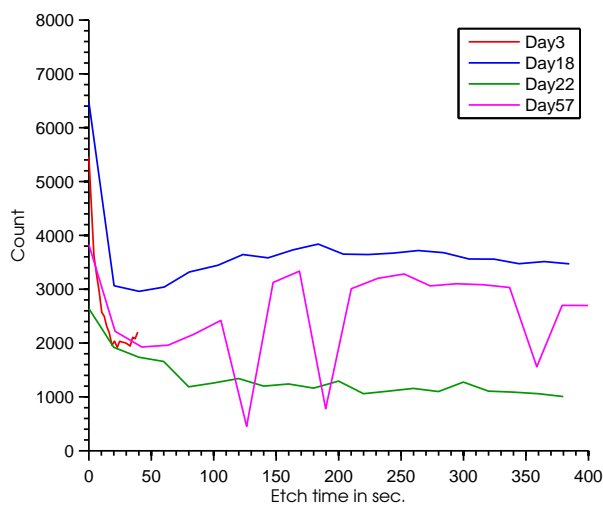
B.2 Poly Propylene (RB 707)



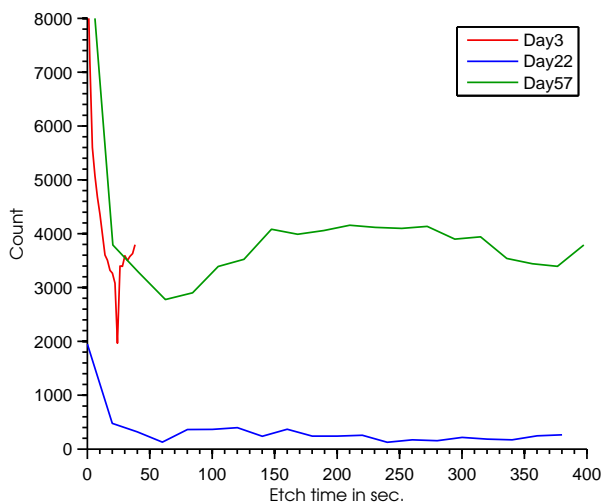
(a) Control



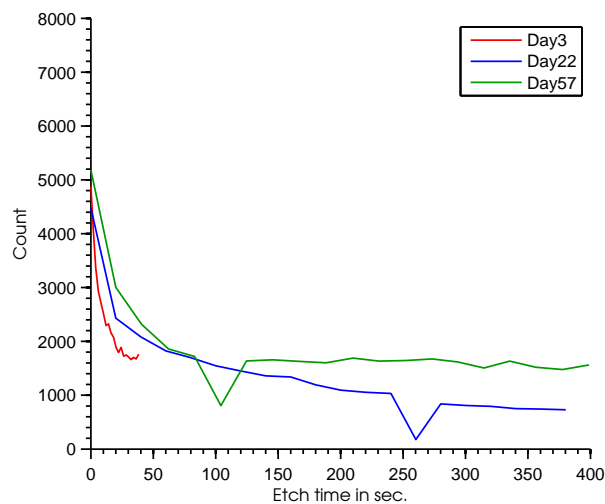
(b) PGE308 1.5%



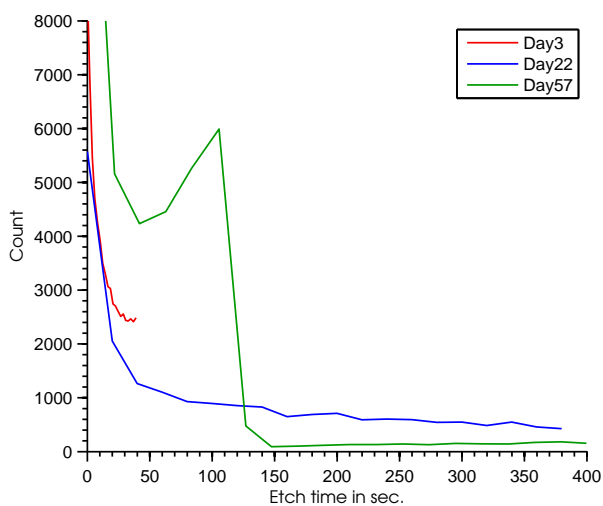
(c) PGE308 2.0%



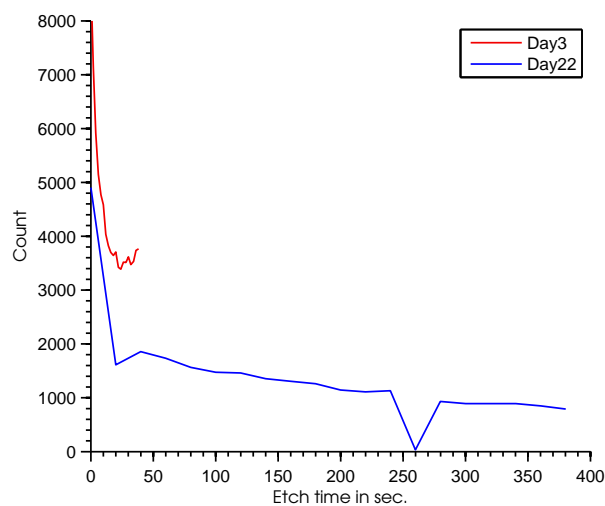
(d) Coconut oil (pure Mono glyceride) 1.5%



(e) Coconut oil (pure Mono glyceride) 2.0%

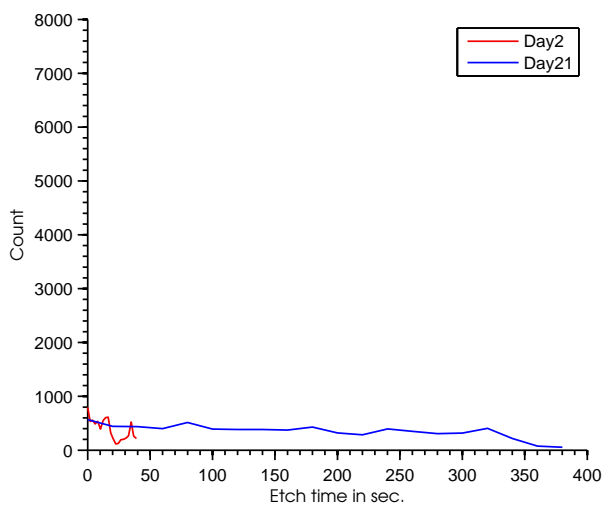


(f) Coconut oil (Mono/Di glyceride mixture) 1.5%

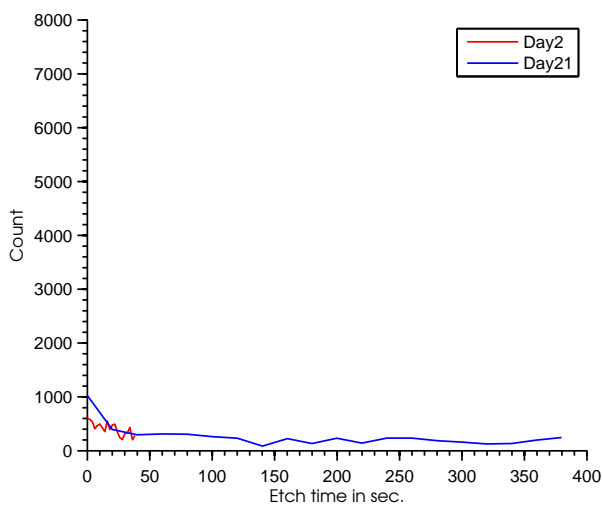


(g) Coconut oil (Mono/Di glyceride mixture) 2.0%

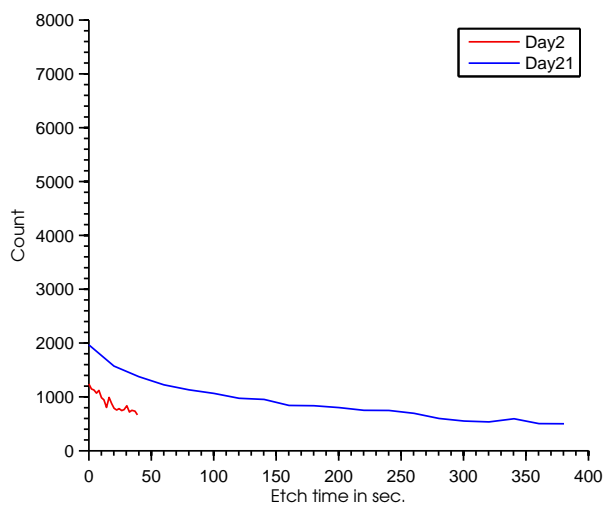
B.3 Poly Propylene (RD 226)



(a) Control

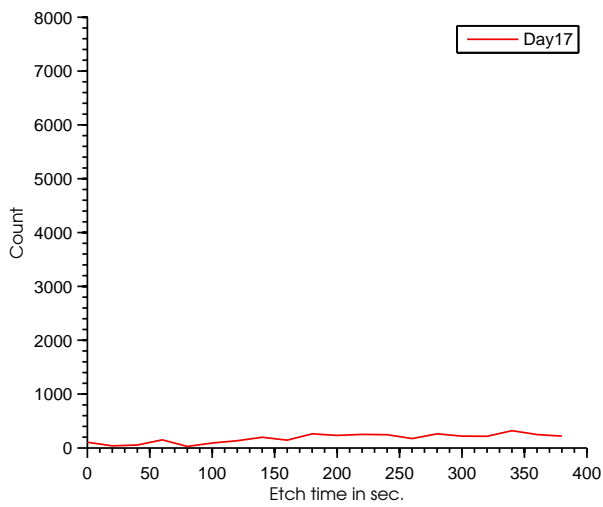


(b) Dimodan HP 0.6%

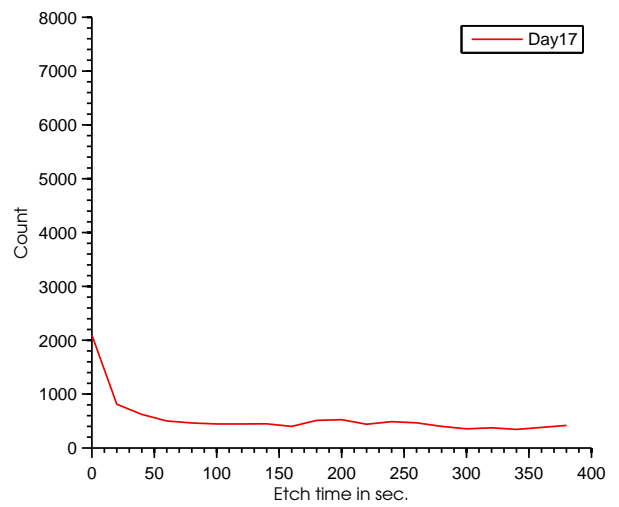


(c) PGE308 0.6%

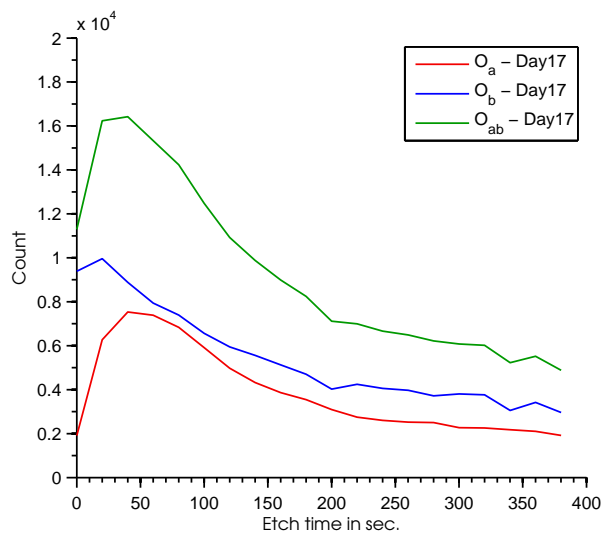
B.4 Low Density Poly Ethylene



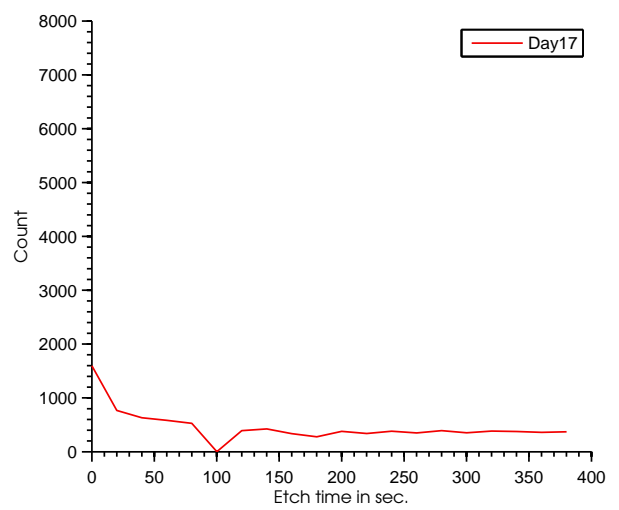
(a) Control



(b) Dimodan HP 0.30%



(c) PGE308 0.15%



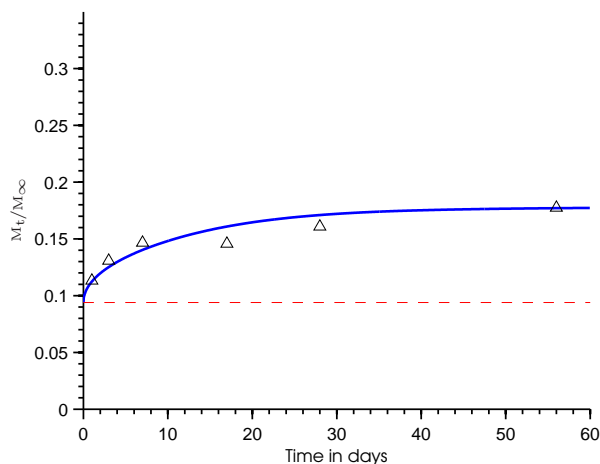
(d) PGE308 0.30%

Appendix C

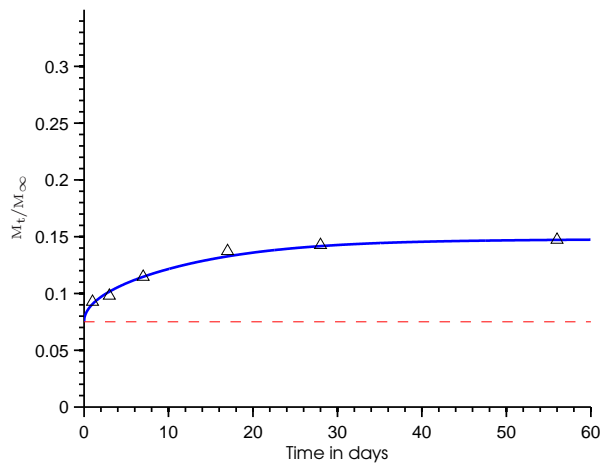
Migration of antistatic additive

The estimated migration of antistatic additive components to the surface of low density polyethylene and polypropylene. All the estimated migrations are done using the fitted partition coefficients listed in table 4.5 and the estimated surface start concentrations from table 4.4 (the dotted red line in the plots). The triangles show the experimentally measured concentrations at the surface of the polymer.

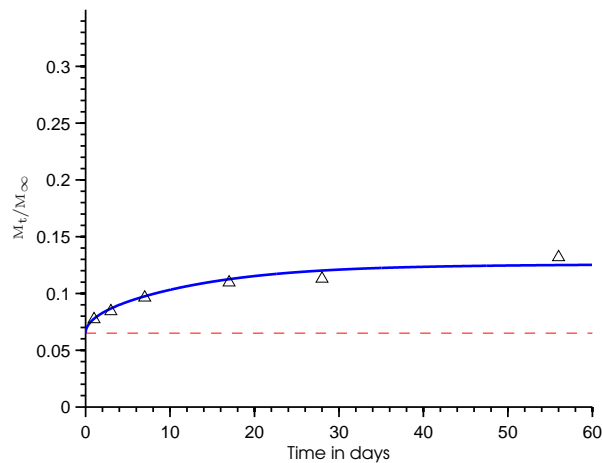
C.1 Low Density Poly Ethylene



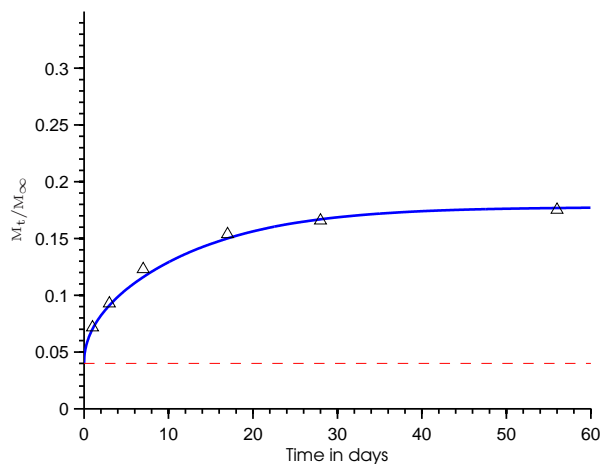
(a) Dimodan HP 0.30%



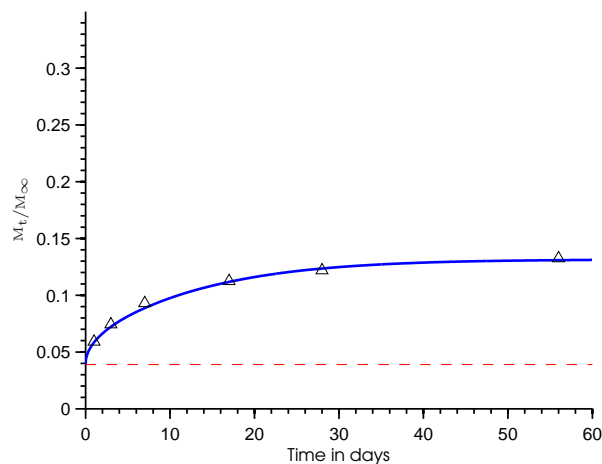
(b) PGE308 (C₁₂ monoglyceride) 0.15%



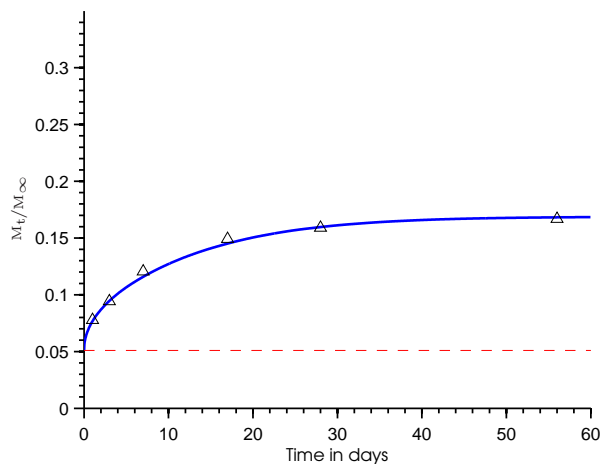
(c) PGE308 (C₁₂ monoglyceride) 0.30%



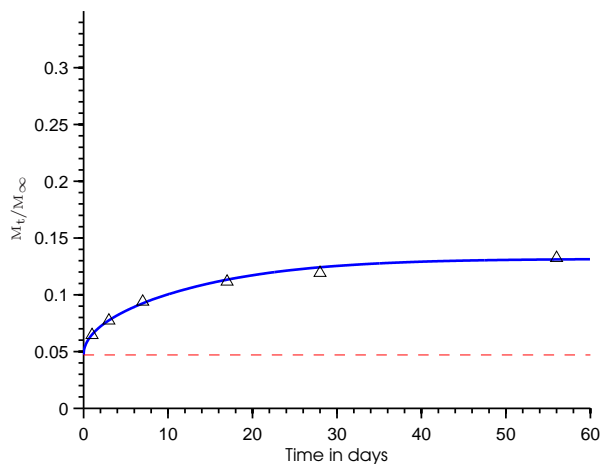
(d) PGE308 (Diglycerole monoester) 0.15%



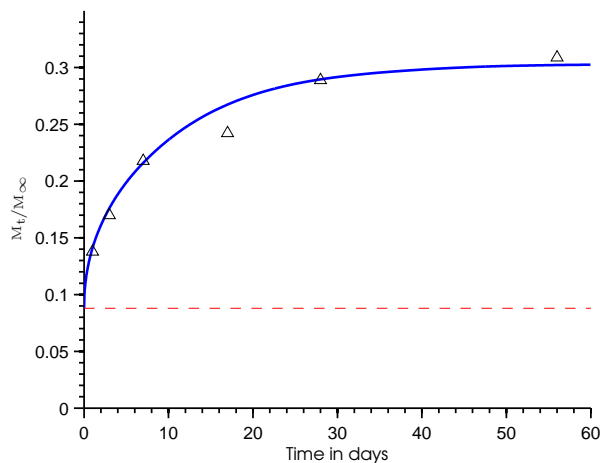
(e) PGE308 (Diglycerole monoester) 0.30%



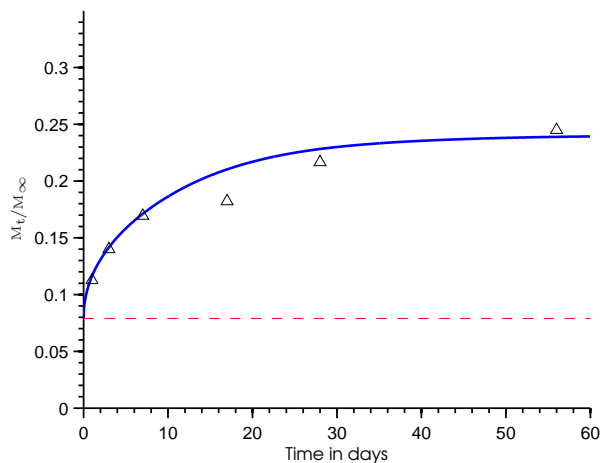
(f) PGE308 (Main components) 0.15%



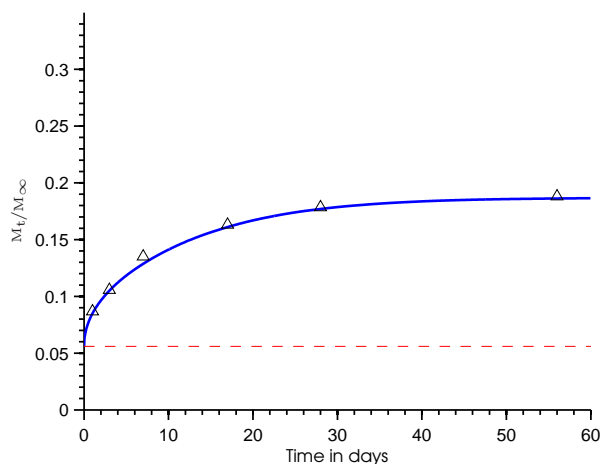
(g) PGE308 (Main components) 0.30%



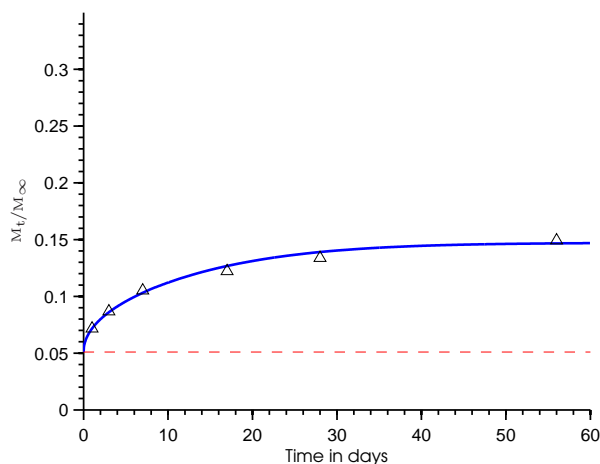
(h) PGE308 (Minor components) 0.15%



(i) PGE308 (Minor components) 0.30%

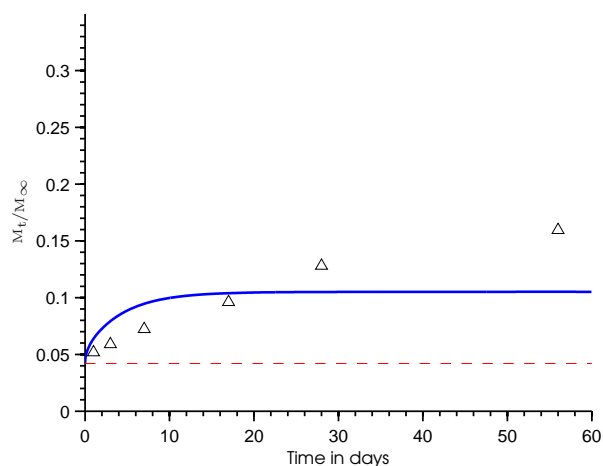


(j) PGE308 (All components) 0.15%

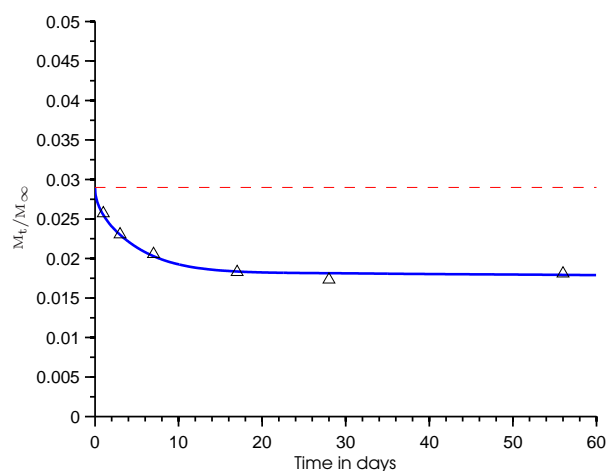
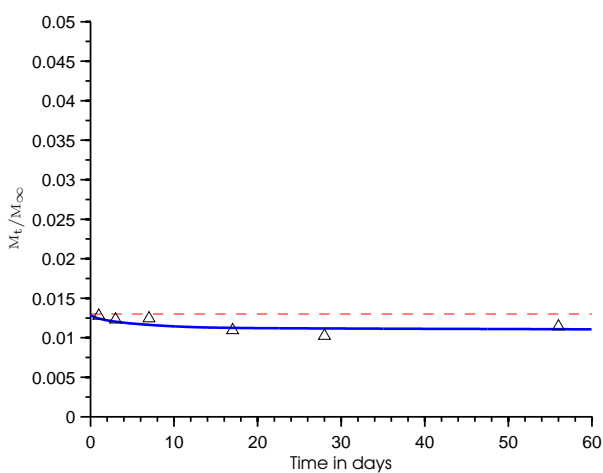


(k) PGE308 (All components) 0.30%

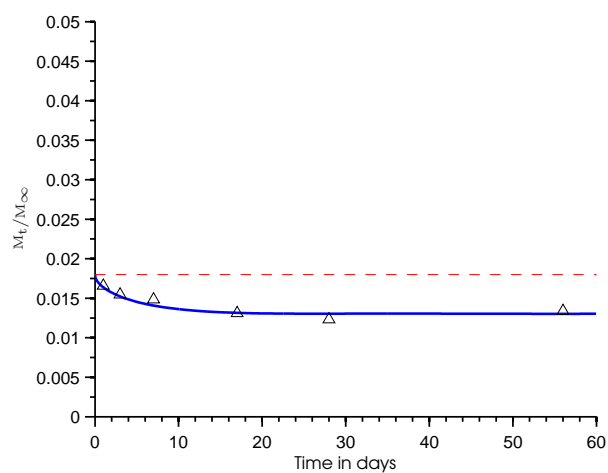
C.2 Poly Propylene



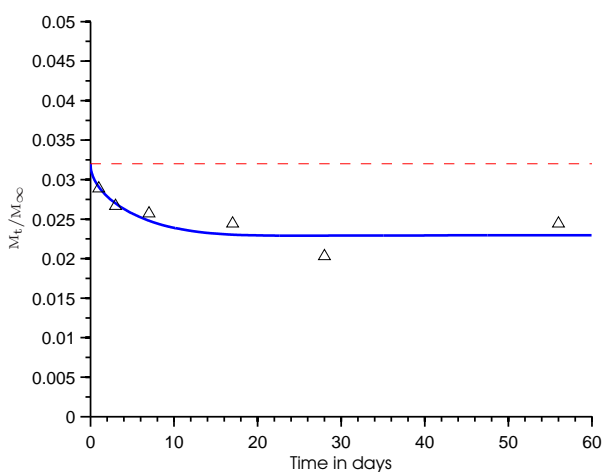
(a) Dimodan HP 0.60%

(b) PGE308 (C_{12} monoglyceride) 0.60%

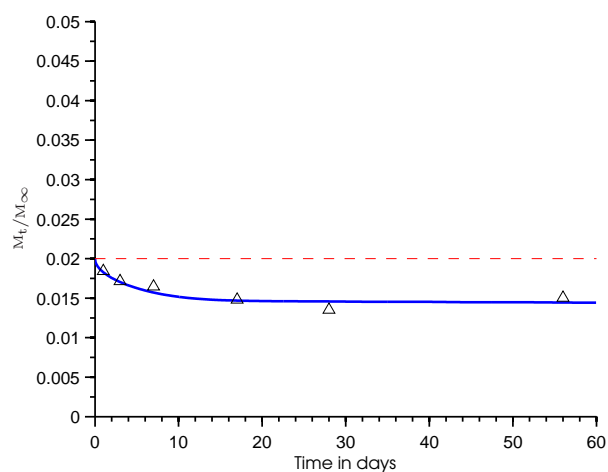
(c) PGE308 (Diglycerole monoester) 0.60%



(d) PGE308 (Main components) 0.60%



(e) PGE308 (Minor components) 0.60%



(f) PGE308 (All components) 0.60%

Appendix D

Hydrogen bond clustering counting code in Matlab

D.1 Bash script to convert Gromacs output files

Using the Gromacs program **g_hbond** with the parameters **-hbn -hbm** will give to output files: **hbond.ndx** and **hbmap.xpm**. This files needs to be converted for easier import by the Matlab script. This conversion is done by the **hb-dat.sh** bash script:

```
1 #!/bin/bash
2 sed '/*/ d; s/\(.*\)../\1/; s/.\(.*\)\/\1/' hbmap.xpm > hbmap.dat
3 sed '1,/\[ hbonds/ d' hbond.ndx > hbond.dat
```

D.2 Matlab algorithm - Hydrogen_bond_wrap.m

The Hydrogen bond clustering counting algorithm is divided into three files. The main program **Hydrogen_bond_wrap.m**, the cluster search algorithm **make_clusters.m** and the specific dimer search algorithm **find_dimers.m**.

```
1 %%%%%%%%%%%%%%%%%%%%%%%%%%%%%%%%%%%%%%%%%%%%%%%%%%%%%%%%%%%%%%%%%%%%%%%%%%
2 %                               — Hydrogen_bond_wrap —                               %
3 %                               ver. 0.3                                             %
4 %                               10/12-2009                                          %
5 %                                                                              %
6 %                               Search for Dimer, Pure Dimer and Cluster           %
7 %                               structures from hydrogen bond connectivity           %
8 %                               using the GROMACS hydrogen bond map(xpm)           %
9 %                               and hydrogen bond index(ndx) output files.         %
```

```

10 %                                                                 %
11 %           Made by Rasmus Lundsgaard at CERE, KT, DTU, Denmark %
12 %%%%%%%%%%%%%%%%%%%%%%%%%%%%%%%%%%%%%%%%%%%%%%%%%%%%%%%%%%%%%%%%%%%%%%%%%%
13 function y = Hydrogen_bond_wrap(Natom, Nmols) % Nmols = Number of molecules
    in box; Natom = Number of atomes in molecule
14
15 % **** read files ****
16 fid = fopen('hbmap.dat','r');
17 hbmap=[];hbond=[];H1=[];
18 header=str2num(fgetl(fid));
19 hbmap=fread(fid, header(1:2), strcat(num2str(header(1)),'*uchar'), 1);
20 fclose(fid);
21 hbmap=flipud(hbmap');
22
23 hbond = importdata('hbond.dat');
24 bond=111;histogram=[];
25 % *****
26
27 t_stop=header(1); % Timestep to stop if not all (header(1))
28
29 mkdir ndx;
30 fnpath='ndx/';
31 fnoutext='.ndx';
32
33 % ***** WRAP ***** WRAP *****
34 fprintf(1,'\n Timestep: ');
35 for n = 1:(ceil(log10(t_stop+1))-1), fprintf(1,' '); end
36
37     for t_step=1:t_stop
38         H1=[];
39         for i=1:size(hbmap,1) % make hydrogen bond list
40             for t=t_step
41                 if hbmap(i,t_step)==bond;
42                     H1(end+1,:)=[fix((hbond(i,1)-1)/Natom)+1,fix((hbond(
43                         i,3)-1)/Natom)+1];
44                 end
45             end
46
47         % ***** Cluster search *****
48         fnout = strcat(fnpath,'clusters_',num2str(t_step), fnoutext);
49         [hist_out, histogram] = make_clusters(H1, Natom, Nmols, t_step,
50             t_stop, fnout, histogram);
51         % ***** Dimers*****

```

```

52     dimers = find_dimers ( H1 , Nmols, fnpath, t_step, fnoutext ,
53                          Natom);          % Find Dimers and Pure Dimers
54
55     Dimer_hist(t_step,:)=[size(dimers{1},1) size(dimers{2},1)
56                          ].*200./Nmols;
57
58     % *****
59     % ***** Progress counter in command window *****
60     if t_step~=1;
61         for n = 1:(ceil(log10(t_step+1))+ceil(log10(t_stop+1))+3),
62             fprintf(1,'\b'); end
63         end
64         fprintf(1,'%d / %d',t_step, t_stop);
65     % *****
66     end
67     fprintf('\n')
68 %***** WRAP END ***** WRAP END *****
69
70 %***** Statistics By Molecule *****
71 for i=1:500
72     don(i,:)=sum(hbmap( fix ( hbond (:,1) /Natom+1)==i ,:)==bond,1);
73     acc(i,:)=sum(hbmap( fix ( hbond (:,3) /Natom+1)==i ,:)==bond,1);
74 end
75 allbnd=don+acc;
76 res (:,1:2)=[mean(don>=1,2).*100,mean(acc>=1,2).*100];
77 res (:,3:4)=[mean(don>=2,2).*100,mean(acc>=2,2).*100];
78 res (:,5:6)=[mean(allbnd>=1,2).*100,mean(allbnd>=2,2).*100];
79 statout{1}=[mean(res,1); std(res,1)];
80
81 fid=fopen('Occupancy_mol.txt','w');
82 fprintf(fid,'%s\n%s\n\n%s\n%s\n\n', 'The Occupancy in percent of each
83 molecule as donor, acceptor', 'or with any bond over all timesteps.',
84 '[b>=1] means molecule has 1 or more bonds', '[b>=2] means molecule has
85 2 or more bonds');
86
87 for n = 1:65, fprintf(fid,'='); end; fprintf(fid,'\n');
88 fprintf(fid,'%18s%18s%15s%9s\n', '[b>=1]', '[b>=2]', '[b>=1]', '[b
89 >=2]');
90
91 fprintf(fid,'%12s%9s%9s%9s%11s%9s\n', 'don', 'acc', 'don', 'acc', 'all
92 ', 'all');
93
94 for n = 1:65, fprintf(fid,'-'); end; fprintf(fid,'\n');
95
96 fprintf(fid,'%4s %8.2f %8.2f %8.2f %8.2f %10.2f %8.2f\n', 'Ave',
97 statout{1}(1,:));
98
99 fprintf(fid,'%4s %8.2f %8.2f %8.2f %8.2f %10.2f %8.2f\n', 'Std',
100 statout{1}(2,:));
101
102 for n = 1:65, fprintf(fid,'='); end; fprintf(fid,'\n\n');
103
104 for imol = 1:Nmols;

```

```

88     fprintf(fid, '%4.0f %8.2f %8.2f %8.2f %8.2f %10.2f %8.2f\n', [imol
89         res(imol,:)]);
90     end
91     fclose(fid);
92     % *****
93     %***** Statistics By Hydrogen bond *****
94     spebond(:,1:2)=[fix((hbond(:,1)-1)/Natom+1), fix((hbond(:,3)-1)/Natom+1)];
95     spebond(:,3)=(mean(hbmap==bond,2)).*100;
96     spebond=sortrows(spebond,-3);
97     if sum(spebond(:,3)>=10)<100
98         spebond=spebond(1:100,:);
99     else
100         spebond=spebond(spebond(:,3)>=10,:);
101     end
102
103     fid=fopen('Occupancy_bnd.txt','w');
104     fprintf(fid, '%s\n%s\n\n', 'The Occupancy in percent of each hydrogen
105         bond over all timesteps.', 'The list is sorted after Occupancy, and
106         values less than 10% are not listed beyond the first 100 values. ');
107     fprintf(fid, '%8s%9s%9s\n', 'mol1', 'mol2', ' [%] ');
108     for n = 1:30, fprintf(fid, '- '); end; fprintf(fid, '\n');
109     for ibnd = 1:length(spebond);
110         fprintf(fid, '%8.0f %8.0f %8.2f\n', spebond(ibnd,:));
111     end
112     fclose(fid);
113     % *****
114     %***** Statistics by number of Hydrogen bonds **
115     for hbnd=0:max(max(allbnd))
116         hbndmat(hbnd+1,:)=((sum(allbnd==hbnd,1)).*100)./Nmols;
117     end
118     statout{2}=[mean(hbndmat(1:5,:),2)', mean(Dimer_hist,1); std(hbndmat(1:5,:),
119         ,0,2)', std(Dimer_hist,1)];
120
121     fid=fopen('Bonds_mol_time.txt','w');
122     fprintf(fid, '%s\n%s\n\n', 'The ratio of molecules with 0 to 4 bonds (
123         plus dimer and pure dimer)', 'over all molecules. All ratios are given
124         as percentage [%]. ');
125     for n = 1:75, fprintf(fid, '= '); end; fprintf(fid, '\n');
126     fprintf(fid, '%8s %8.2f %8.2f %8.2f %8.2f %8.2f %8.2f %8.2f\n', 'Ave',
127         statout{2}(1,:));
128     fprintf(fid, '%8s %8.2f %8.2f %8.2f %8.2f %8.2f %8.2f %8.2f\n', 'Std',
129         statout{2}(2,:));
130     for n = 1:75, fprintf(fid, '- '); end; fprintf(fid, '\n');

```

```

126     fprintf(fid, '%8s%9s\n', 't_step ', 'bonds ');
127     fprintf(fid, '%17s%9s%9s%9s%9s%10s%12s\n', '0', '1', '2', '3', '4', '
Dimer', 'PureDimer ');
128     for n = 1:75, fprintf(fid, '-'); end; fprintf(fid, '\n');
129     for i_t_step = 1:t_stop;
130         fprintf(fid, '%8.0f %8.0f %8.0f %8.0f %8.0f %8.0f %8.0f %8.0f\n', [
i_t_step hbndmat(1:5, i_t_step) ' Dimer_hist(i_t_step, :)]);
131     end
132     fclose(fid);
133     % *****
134     statout{3}=hist_out;
135     save statout.mat statout
136     end

```

D.3 Matlab algorithm - make_clusters.m

```

1  %%%%%%%%%%%%%%%%%%%%%%%%%%%%%%%%%%%%%%%%%%%%%%%%%%%%%%%%%%%%%%%%%%%%%%%%%%
2  %                               — make_clusters —                               %
3  %                               sub program for Hydrogen_bond_wrap                %
4  %                               ver. 0.3                                         %
5  %                               10/12-2009                                       %
6  %                                                                              %
7  %                               Search for Dimer, Pure Dimer and Cluster         %
8  %                               structures from hydrogen bond connectivity        %
9  %                               using the GROMACS hydrogen bond map(xpm)         %
10 %                               and hydrogen bond index(ndx) output files.      %
11 %                                                                              %
12 %                               Made by Rasmus Lundsgaard at CERE, KT, DTU, Denmark %
13 %%%%%%%%%%%%%%%%%%%%%%%%%%%%%%%%%%%%%%%%%%%%%%%%%%%%%%%%%%%%%%%%%%%%%%%%%%
14
15
16 function [hist_out, histogram] = make_clusters(H1, Natom, Nmols, t_step,
t_stop, fn, histogram)
17 hist_out = [];
18 Ncluster=0;
19 if sum(size(H1)) ~= 0
20     m1list=1:Nmols;
21
22     while ~isempty(m1list)
23
24         meros1=m1list(1);
25         cl_x=meros1;
26         cl_size=1;
27         m2list1=H1(H1(:,1)==meros1,2)';

```

```

28     m2list2=H1(H1(:,2)==meros1,1)';
29     m2list=[m2list1 m2list2];
30
31     nextm2_list = [];
32     % ***** Find members in current cluster *****
33     while ~isempty(m2list)
34
35         for i=1:length(m2list)
36
37             if sum(cl_x==m2list(i))==0           %if none
38                 of the entries in cl_x is equal to m2list(i)..
39                 cl_x(end+1)=m2list(i);         % add new
40                 entry to cl_x list
41                 cl_size=cl_size+1;
42                 m1list=m1list(m1list~=m2list(i)); % create
43                 new m1list which consists of all entries in m1list
44                 which are not equal to m2list(i)
45                 nextm2_1=H1(H1(:,1)==m2list(i),2)'; % find
46                 out who m2list(i) connects to
47                 nextm2_2=H1(H1(:,2)==m2list(i),1)'; % find
48                 out who connects to m2list(i)
49                 nextm2_list=[nextm2_list nextm2_1 nextm2_2]; % add
50                 these lists to the list of molecules not treated yet..
51
52             end
53         end
54         m2list=nextm2_list;
55         nextm2_list = [];
56     end
57     %*****
58     m1list=m1list(m1list~=meros1);
59
60     clustermap{Ncluster+1}=sort(cl_x);
61     cl_hist(Ncluster+1)=cl_size;
62     Ncluster=Ncluster+1;
63 end
64
65 else
66     Ncluster=Nmols;
67     for imol=1:Nmols
68         icluster=imol;
69         clustermap{icluster}=imol;
70         cl_hist(icluster)=1;
71     end
72 end
73
74 write_clusters_Natom( clustermap, Ncluster, fn, Natom )

```

```

67     for k=1:max(cl_hist)
68         histogram(k,t_step)=sum(cl_hist==k);
69     end
70     if t_step==t_stop
71         dlmwrite('clusterhist_all.txt',histogram,'delimiter','\t');
72
73         final_hist=[sum(histogram,2) mean(histogram,2) , std(histogram,0,2)
74         ];
75
76         fid=fopen('clusterhist_final.txt','w');
77         fprintf(fid,'%s\n%s\n\n','Cluster histogram over all time
78         steps.','The values in percent is the ratio: [mean amount]*[
79         molecules in cluster] / [number of all molecules]');
80
81         for n = 1:60, fprintf(fid,'='); end; fprintf(fid,'\n');
82         fprintf(fid,'%8s%9s%9s%9s%12s%9s\n','Cluster', '', 'Amount',
83         '', ' [%]', '');
84         fprintf(fid,'%8s%9s%9s%9s%12s%9s\n','size', 'Sum', 'Mean', '
85         Std', 'Mean', 'Std');
86
87         for n = 1:60, fprintf(fid,'-'); end; fprintf(fid,'\n');
88         for iclu = 1:size(final_hist,1);
89             ratio(iclu,:)=(final_hist(iclu,2:3).*iclu.*100)./Nmols;
90             fprintf(fid,'%8.0f %8.0f %8.2f %8.2f %11.2f %8.2f\n',[iclu
91             final_hist(iclu,:) ratio(iclu,:)]);
92         end
93         for n = 1:60, fprintf(fid,'='); end; fprintf(fid,'\n');
94         fprintf(fid,'%26.2f %20.2f\n',[sum(final_hist(:,2)) sum(ratio
95         (:,1)) ]);
96         fclose(fid);
97         hist_out=[final_hist ratio ];
98     end
99
100 %*****write_clusters_Natom*****
101 function y = write_clusters_Natom( clustermap, Ncluster, fn, Natom )
102
103 fid=fopen( fn, 'w' );
104
105     formatstr='%d';
106     for i=2:Natom
107         formatstr=strcat(formatstr, ' %d');
108     end
109     formatstr=strcat(formatstr,'\n');
110
111     for icluster = 1:Ncluster;

```

```

106     fprintf(fid, '%s%d%s\n', '[ cluster_ ', icluster, ' ]');
107
108     arr=zeros(Natom, cl_hist(icluster));
109
110     for imol=1:cl_hist(icluster)
111         arr(1:Natom, imol)=(clustermap{icluster}(imol)-1)*Natom+(1:Natom
112         );
113     end
114     fprintf(fid, formatstr, arr);
115     fprintf(fid, '\n');
116
117 end
118
119 for icluster = 1:Ncluster;
120
121     fprintf(fid, '%s%d%s\n', '[ mol1_ ', icluster, ' ]');
122
123     arr=zeros(Natom, 1);
124     arr(1:Natom)=(clustermap{icluster}(1)-1)*Natom+(1:Natom);
125
126     fprintf(fid, formatstr, arr);
127     fprintf(fid, '\n');
128
129 end
130 fclose(fid);
131 end
132 %*****

```

D.4 Matlab algorithm - find_dimers.m

```

1  %%%%%%%%%%%%%%%%%%%%%%%%%%%%%%%%%%%%%%%%%%%%%%%%%%%%%%%%%%%%%%%%%%%%%%%%%%
2  %                               — find_dimers —                               %
3  %                               sub program for Hydrogen_bond_wrap              %
4  %                               ver. 0.3                                       %
5  %                               10/12-2009                                     %
6  %                                                                                               %
7  %                               Search for Dimer, Pure Dimer and Cluster      %
8  %                               structures from hydrogen bond connectivity      %
9  %                               using the GROMACS hydrogen bond map(xpm)      %
10 %                               and hydrogen bond index(ndx) output files.    %
11 %                                                                                               %
12 %                               Made by Rasmus Lundsgaard at CERE, KT, DTU, Denmark %
13 %%%%%%%%%%%%%%%%%%%%%%%%%%%%%%%%%%%%%%%%%%%%%%%%%%%%%%%%%%%%%%%%%%%%%%%%%%
14

```

```

15 function dimers = find_dimers ( H1 , Nmols, fnpath , t_step , fnouttext , Natom
16 )
17 % ***** search Dimer *****
18 Dimer ( 1 , : ) = [ 0 , 0 ] ; Pure_Dimer ( 1 , : ) = [ 0 , 0 ] ;
19 for i = 1 : Nmols
20     if sum ( Dimer ( : , 2 ) == i ) == 0 && sum ( size ( H1 ) ) ~ = 0
21         H2 = H1 ( H1 ( : , 1 ) == i , 2 ) ;
22
23         for j = 1 : length ( H2 )
24             H2rev = H1 ( H1 ( : , 1 ) == H2 ( j ) , 2 ) ;
25
26             for k = 1 : length ( H2rev )
27                 if H2rev ( k ) == i
28                     Dimer ( end + 1 , : ) = [ i , H2 ( j ) ] ;
29
30                     if sum ( sum ( H1 ( : , : ) == i ) ) == 2 && sum ( sum ( H1 ( : , : ) == H2 ( j ) ) ) == 2
31                         Pure_Dimer ( end + 1 , : ) = [ i , H2 ( j ) ] ;
32                     end
33
34                 end
35             end
36
37         end
38
39     end
40 end
41 Dimer ( 1 , : ) = [] ; Pure_Dimer ( 1 , : ) = [] ;
42
43 dimers = { Dimer ; Pure_Dimer } ;
44
45 fnout = strcat ( fnpath , ' dimers_ ' , num2str ( t_step ) , fnouttext ) ;
46 write_dimer ( Dimer , fnout , Natom ) ; % write the Dimers
47
48 fnout = strcat ( fnpath , ' puredimers_ ' , num2str ( t_step ) , fnouttext ) ;
49 write_dimer ( Pure_Dimer , fnout , Natom ) ; % write the Pure Dimers
50 % *****
51
52
53
54 % ***** Write_dimers *****
55 function y = write_dimer ( dimer , fnout , Natom )
56
57 fid = fopen ( fnout , ' w ' ) ;
58
59 formatstr = '% d ' ;

```

```
60 for i=2:Natom
61     formatstr=strcat(formatstr, ' %d');
62 end
63 formatstr=strcat(formatstr, '\n');
64
65 for ipd = 1:size(dimer,1);
66
67     fprintf(fid, '%s%d%s\n', '[ dimer_', ipd, ' ]');
68
69     arr=zeros(Natom,2);
70     for imol=1:size(arr,2)
71
72         arr(1:Natom,imol)=(dimer(ipd,imol)-1)*Natom+(1:Natom);
73     end
74     fprintf(fid, formatstr, arr);
75     fprintf(fid, '\n');
76 end
77
78
79 for ipd = 1:size(dimer,1);
80     fprintf(fid, '%s%d%s\n', '[ molNo_', ipd, ' ]');
81
82     fprintf(fid, '%d %d\n', dimer(ipd,1:2));
83     fprintf(fid, '\n');
84 end
85
86 fclose(fid);
87 end
88 % *****
89
90 end
```